

Towards a complete classification of symmetry-protected topological phases for interacting fermions in three dimensions and a general group super-cohomology theory

Qing-Rui Wang¹ and Zheng-Cheng Gu^{1,*}

¹*Department of Physics, The Chinese University of Hong Kong, Shatin, New Territories, Hong Kong, China*
(Dated: April 5, 2018)

The classification and construction of symmetry-protected topological (SPT) phases in interacting boson and fermion systems have become a fascinating theoretical direction in recent years. It has been shown that (generalized) group cohomology theory or cobordism theory gives rise to a complete classification of SPT phases in interacting boson/spin systems. The construction and classification of SPT phases in interacting fermion systems are much more complicated, especially in three dimensions. In this work, we revisit this problem based on an equivalence class of fermionic symmetric local unitary (FSLU) transformations. We construct very general fixed-point SPT wavefunctions for interacting fermion systems. We naturally reproduce the partial classifications given by special group super-cohomology theory, and we show that with an additional $\tilde{B}H^2(G_b, \mathbb{Z}_2)$ structure (the so-called obstruction-free subgroup of $H^2(G_b, \mathbb{Z}_2)$), a complete classification of SPT phases for three-dimensional interacting fermion systems with a total symmetry group $G_f = G_b \times \mathbb{Z}_2^f$ can be obtained for unitary symmetry group G_b . We also discuss the procedure for deriving a general group super-cohomology theory in arbitrary dimensions.

CONTENTS

I. Introduction	2
A. Classify FSPT phases via equivalence classes of fermionic symmetric local unitary transformations	3
B. Summary of main results	4
C. Organization of the paper	5
II. Fixed-point wavefunctions of FSPT phases	6
A. Constructing fixed-point wavefunction and classification for FSPT phases in 1D	6
1. Fermionic symmetric local unitary transformation	6
2. Consistent equations and equivalence classes	7
B. Constructing fixed-point wavefunction for FSPT phases in 2D and 3D	8
III. Constructions and classifications for FSPT states in 2D	10
A. Discrete spin structure and Kasteleyn orientations	10
1. Discrete Stiefel–Whitney homology class w_0	11
2. Kasteleyn orientations and gauge transformations	12
3. Kasteleyn orientations under retriangulations	14
B. FSLU transformations and consistent conditions for fixed-point states	15
1. Decoration of Kitaev’s Majorana chains	15
2. Fermionic pentagon equations	17
IV. Constructions and classifications for FSPT states in 3D	18
A. Discrete spin structure in 3D and local Kasteleyn orientations	18
1. Discrete Stiefel–Whitney homology class w_1	18
2. Local Kasteleyn orientations and gauge transformations	18
3. Local Kasteleyn orientations under retriangulations	20
B. FSLU transformations and consistent conditions for fixed-point states	22
1. Fermion parity conservation and the obstruction of Kitaev’s Majorana chain decoration	22
2. Fermionic symmetric local unitary transformations	23
3. Fermionic hexagon equations	25
V. Discussion and conclusions	30

* zcgu@phy.cuhk.edu.hk

Acknowledgments	30
A. Kitaev’s Majorana chain, fermion parity and Kasteleyn orientation	31
1. Ground states	31
2. Excited states and the appearance of phase factor $\pm i$	31
3. Fermion parity and Kasteleyn orientation	32
B. 2D Pachner moves	33
1. (2-2) moves	33
2. (1-3) moves	34
C. 3D Pachner moves and fermion parity changes	36
1. (2-0) moves	36
2. (1-4) moves	36
3. (2-3) moves	38
D. Abelian group structure of the general group super-cohomology solutions	43
1. Explicit construction of $\theta[n_3, n'_3, \tilde{n}_2, \tilde{n}'_2]$	44
2. Solving system of linear equations in $\mathbb{R}/4\mathbb{Z}$	44
References	46

I. INTRODUCTION

In recent years, a new type of topological order—symmetry-protected topological (SPT) order [1–3]—has been proposed and intensively studied in interacting boson and fermion systems. Two-dimensional (2D) and three-dimensional (3D) topological insulators (TIs) [4, 5] are the simplest examples of SPT phases, which are protected by time-reversal and charge-conservation symmetries. Although TIs were initially proposed and experimentally realized in essentially non-interacting electron systems, very recent studies have established their existence and stability even in the presence of strong interactions, by identifying non-perturbative quantum anomalies on various manifolds [6]. The first attempt to systematically understand SPT phases in interacting systems was proposed in Ref. 1, in which the author pointed out that the well-known spin-1 Haldane chain [7] was actually an SPT phase. Later, a systematic classification of SPT phases for interacting bosonic systems in arbitrary dimensions with arbitrary global symmetry was achieved using generalized group cohomology theory [2, 3, 8] or cobordism theory [9]. This systematic classification essentially classifies the quantum anomalies associated with the corresponding global symmetries in interacting bosonic systems. In terms of the physical picture, it has been further pointed out that by gauging the global symmetry G , different SPT phases can be characterized by different types of braiding statistics of G -flux/flux lines in 2D/3D [10–17]. Anomalous surface topological order has also been proposed as another very powerful way to identify and characterize different 3D SPT phases in interacting boson and fermion systems [18–27].

From the quantum information perspective, intrinsic topological phases are gapped quantum states that can be defined and classified by an equivalence class of finite depth local unitary transformations [28], which leads to the novel concept of long-range entanglement. However, in contrast to those intrinsic topological phases, all SPT phases can be adiabatically connected to a trivial disordered phase or to an atomic insulator without symmetry protection. Therefore, SPT phases contain only short-range entanglement, and can be constructed by applying local unitary transformations on a trivial product state. In particular, Refs. 2 and 3 introduced a systematic way of constructing fixed-point ground-state wavefunctions for bosonic SPT phases on arbitrary triangulations in arbitrary dimensions. Such a construction is fairly complete for bosonic SPT phases protected by unitary symmetry groups (up to 3D). So far, the only known example beyond this construction is the so-called *efmf* SPT state [18], which is protected by time-reversal symmetry in 3D. Later, it was shown that such an exotic bosonic SPT state could be realized by the Walker–Wang model [29, 30].

The classification and systematic understanding of SPT phases in interacting fermion systems are much more complicated. One obvious way to achieve fruitful results is to study the reduction of the free-fermion classifications [31, 32] under the effect of interactions [33–39]. However, this approach misses those fermionic SPT (FSPT) phases that cannot be realized in free-fermion systems [12, 40]. A slightly general way to understand FSPT in interacting fermion systems is to stack some additional bosonic SPT states onto a free-fermion SPT state [26]. An arguably fairly complete classification of TIs in interacting electron systems [41] can be constructed in such a way. However, there is no natural reason to believe that all FSPT phases in interacting systems can be realized by the abovementioned stacking constructions, and counterexamples can be constructed explicitly. Moreover, it has been shown that certain

bosonic SPT phases become “trivial” (adiabatically connected to a product state) [26, 42] when embedded into interacting fermion systems. Apparently, the stacking construction cannot explain all of these subtle issues. Therefore, a systematic understanding and the construction of interacting FSPT phases are very desirable.

The first attempt to classify interacting FSPT phases in general dimensions was proposed in Ref. 42, in which a class of FSPT phases was constructed systematically by generalizing the usual group cohomology theory into the so-called special group super-cohomology theory. However, it turns out that such a construction cannot give rise to all FSPT phases except in one dimension, where the obtained classification of FSPT phases perfectly agrees with previous results [43, 44]). On the other hand, quantum anomalies characterized by spin cobordism [45] or invertible spin topological quantum field theory (TQFT) [46–48] suggest a rich diversity of FSPT phases, although it is not clear how to construct these FSPT states in an explicit and systematic way.

Alternatively, the idea of gauging fermion parity [37, 49–52] provides another way to understand FSPT. In 2D, a fairly complete classification of FSPT can be obtained in this way, which also agrees with the anomaly classification given by spin cobordism and invertible spin TQFT [45, 46, 48, 53, 54]. It has been shown that the mathematical objects that classify 2D FSPT phases with a total symmetry $G_f = G_b \times \mathbb{Z}_2^f$ (where G_b is the bosonic global symmetry and \mathbb{Z}_2^f is the fermion parity conservation symmetry), can be summarized as three group cohomologies of the symmetry group G_b [48, 50]: $H^1(G_b, \mathbb{Z}_2)$, $BH^2(G_b, \mathbb{Z}_2)$, and $H^3(G_b, U_T(1))$. $H^1(G_b, \mathbb{Z}_2)$, which corresponds one-to-one to the \mathbb{Z}_2 subgroups of G_b , classifies FSPT phases with Majorana edge modes. $BH^2(G_b, \mathbb{Z}_2)$, the obstruction-free subgroup of $H^2(G_b, \mathbb{Z}_2)$, is formed by elements $n_2 \in H^2(G_b, \mathbb{Z}_2)$ that satisfy $Sq^2(n_2) = 0$ in $H^4(G_b, U_T(1))$, where Sq^2 is the Steenrod square, $Sq^2 : H^d(G_b, \mathbb{Z}_2) \rightarrow H^{d+2}(G_b, \mathbb{Z}_2) \subset H^{d+2}[G_b, U_T(1)]$. $H^3(G_b, U_T(1))$ is the well-known classification of bosonic SPT phases. Physically, the $H^1(G_b, \mathbb{Z}_2)$ layer can be constructed by decorating a Majorana chain [55], which is a one-dimensional (1D) invertible fermionic TQFT, onto the domain walls of symmetry group G_b . The $BH^2(G_b, \mathbb{Z}_2)$ layer can be constructed by decorating complex fermions, which are zero-dimensional (0D) invertible TQFT, onto the intersection points of G_b -symmetry domain walls. Nevertheless, the decoration scheme can suffer from obstructions, and only subgroup $BH^2(G_b, \mathbb{Z}_2)$ classifies valid and inequivalent 2D FSPT phases. Some interesting examples of SPT phases have been studied in 3D based on a Walker–Wang model construction [56], e.g., DIII-class topological superconductors [24, 57–59]. Unfortunately, it is impossible to construct all FSPT phases using the Walker–Wang model. It is even unclear how to reproduce all of the special group super-cohomology constructions in this way. Very recently, some new interacting FSPT phases beyond special group super-cohomology were formally proposed by using spin TQFT [60]. However, a general principle and lattice model realization are still lacking.

A. Classify FSPT phases via equivalence classes of fermionic symmetric local unitary transformations

In this paper, we propose a general physical principle to construct all FSPT phases in 3D with the total symmetry group $G_f = G_b \times \mathbb{Z}_2^f$. A previous work showed that in the presence of global symmetry, symmetry-enriched topological (SET) phases can be defined and classified by equivalence classes of symmetric local unitary transformations [61, 62]. In particular, SPT phases can be realized as a special class of SET phases whose bulk excitations are trivial and can be adiabatically connected to a product state in the absence of global symmetry.

In Ref. 63, it was shown that fermionic local unitary (FLU) transformations can be used to define and classify intrinsic topological phases for interacting fermion systems. The Fock space structure and fermion parity conservation symmetry of fermion systems can be naturally encoded into FLU transformations. Let us first briefly review the definition of FLU transformation. Similar to the local bosonic systems, the finite-time evolution generated by a local fermion Hamiltonian defines an equivalence relation between gapped states in interacting fermion systems:

$$|\psi(1)\rangle \sim |\psi(0)\rangle \text{ iff } |\psi(1)\rangle = \mathcal{T} \left[e^{-i \int_0^1 d\lambda \tilde{H}_f(\lambda)} \right] |\psi(0)\rangle \quad (1)$$

where \mathcal{T} is the path-ordering operator and $\tilde{H}_f(\lambda)$ is a local fermionic Hamiltonian defined in Fock space. We will call $\mathcal{T} \left[e^{-i \int_0^1 d\lambda \tilde{H}_f(\lambda)} \right]$ a FLU evolution. It is well-known that the finite-time FLU evolution is closely related to fermionic quantum circuits with finite depth, which is defined through piecewise FLU operators. A piecewise FLU operator has the form $U_{pwl} = \prod_{\mathbf{i}} e^{-i H_f(\mathbf{i})} \equiv \prod_{\mathbf{i}} U(\mathbf{i})$, where $H_f(\mathbf{i})$ is a fermionic Hermitian operator and $U(\mathbf{i})$ is the corresponding fermionic unitary operator defined in Fock space that preserve fermion parity (e.g., contains even number of fermion creation and annihilation operators) and act on a region labeled by \mathbf{i} . Note that regions labeled by different \mathbf{i} 's are not overlapping. We further require that the size of each region is less than some finite number l . The unitary operator U_{pwl} defined in this way is called a piecewise fermionic local unitary operator with range l . A fermion quantum circuit with depth M is given by the product of M piecewise fermionic local unitary operators: $U_{circ}^M = U_{pwl}^{(1)} U_{pwl}^{(2)} \dots U_{pwl}^{(M)}$. It is believed that any FLU evolution can be simulated with a constant depth fermionic quantum circuit and vice

versa. Therefore, the equivalence relation between gapped states in interacting fermion systems can be rewritten in terms of constant depth fermionic quantum circuits:

$$|\psi(1)\rangle \sim |\psi(0)\rangle \text{ iff } |\psi(1)\rangle = U_{\text{circ}}^M |\psi(0)\rangle \quad (2)$$

Thus, we can use the term FLU transformation to refer to both FLU evolution and constant depth fermionic quantum circuit. From the definition of FSPT state, it is easy to see that (in the absence of global symmetry):

$$|\text{FSPT}\rangle = U_{\text{circ}}^M |\text{Trivial}\rangle \quad (3)$$

Namely, a FSPT state can be connected to a trivial state (e.g., a product state) via FLU transformation (in the absence of global symmetry). Now let us consider the entanglement density matrix ρ_A of for a FSPT state in region A . ρ_A may act on a subspace of the Hilbert space in region A , and the subspace is called the support space \tilde{V}_A of region A . Clearly, Eq.(3) implies that the support space of any FSPT in region A must be one dimensional. This is simply because a trivial state (e.g., a product state) has a one dimensional support space, and any FSPT state will become a product state via a proper local basis change (induced by a FLU transformation).

In the presence of global symmetry, we can further introduce the notion of fermionic symmetric local unitary (FSLU) transformations to define and classify fermionic SET (FSET) phases in interacting fermion systems. By FSLU transformation, we mean the corresponding piecewise FLU operator is invariant under symmetry G_b . More precisely, we have $U_{\text{pwl}} = \prod_{\mathbf{i}} e^{-iH_f(g_{i0}, g_{i1}, g_{i2}, \dots)} \equiv \prod_{\mathbf{i}} U(g_{i0}, g_{i1}, g_{i2}, \dots)$ and $U(gg_{i0}, gg_{i2}, gg_{i3}, \dots) = U(g_{i0}, g_{i1}, g_{i2}, \dots)$ for any $g \in G_b$. (We note that here we choose the group element basis $g_{i0}, g_{i1}, g_{i2}, \dots$ to represent fermionic symmetric unitary operator acting on a region labeled by \mathbf{i} .) Again, FSPT phases are a special class of FSET phases that have trivial bulk excitation and can be adiabatically connected to a product state in the absence of global symmetry. Thus, we need only to enforce the FSLU transformations to be one dimensional (when acting on the support space ρ_A for any region A) to classify all FSPT states.

B. Summary of main results

It turns out that the novel concept of FSLU transformation allows us to construct very general fixed-point FSPT states of 2D and 3D FSPT phases. All of these fixed-point wavefunctions admit exactly solvable parent Hamiltonians consisting of commuting projectors on an arbitrary triangulation with an arbitrary branching structure. We begin with the 2D case, in which the discrete spin structure can be implemented by Kasteleyn orientations [64–66], allowing us to decorate Majorana chains onto G_b -symmetry domain walls [67, 68]. We then show how to implement the discrete spin structure on a triangulation of a 3D orientable spin manifold, which is a nontrivial generalization of 2D Kasteleyn orientation. The discrete spin structure allows us to decorate the Majorana chains onto the intersection lines of G_b -symmetry domain walls in a self-consistent and topologically invariant way. The fundamental mathematical data describing such a decoration scheme belong to $H^2(G_b, \mathbb{Z}_2)$, subjected to an obstruction on $H^4(G_b, \mathbb{Z}_2)$. The obstruction can be understood through the following physical picture. As Kasteleyn orientation is not always possible for a large loop (the 3D discrete spin structure can be used to construct *local* Kasteleyn orientations of small loops), complex fermion decoration on the intersection points of G_b -symmetry domain walls is typically required, and this is only possible when the $H^4(G_b, \mathbb{Z}_2)$ obstruction vanishes. Furthermore, another obstruction on $H^5(G_b, U_T(1))$ is generated by wavefunction renormalization to finally determine whether the entire decoration scheme of Majorana chains is valid for a fixed-point wavefunction in 3D.

The precise mathematical objects that classify 3D FSPT phases with a total symmetry $G_f = G_b \times \mathbb{Z}_2^f$ can also be summarized as three group cohomologies of the symmetry group G_b : $\tilde{B}H^2(G_b, \mathbb{Z}_2)$, $BH^3(G_b, \mathbb{Z}_2)$, and $H_{\text{rigid}}^4(G_b, U_T(1))$. $\tilde{B}H^2(G_b, \mathbb{Z}_2)$, the obstruction-free subgroup of $H^2(G_b, \mathbb{Z}_2)$, is formed by elements $\tilde{n}_2 \in H^2(G_b, \mathbb{Z}_2)$ that simultaneously satisfy $Sq^2(\tilde{n}_2) = 0$ in $H^4(G_b, \mathbb{Z}_2)$ and $\mathcal{O}(\tilde{n}_2) = 0$ in $H^5(G_b, U_T(1))$, where \mathcal{O} is some unknown cohomology operation (to the best of our knowledge) that maps \tilde{n}_2 satisfying $Sq^2(\tilde{n}_2) = 0$ in $H^2(G_b, \mathbb{Z}_2)$ into an element in $H^5(G_b, \mathbb{Z}_8) \subset H^5[G_b, U_T(1)]$. The explicit expression of \mathcal{O} is very complicated, and it is computed in a physical way in section IV B. $BH^3(G_b, \mathbb{Z}_2)$, the obstruction-free subgroup of $H^3(G_b, \mathbb{Z}_2)$, is formed by elements $n_3 \in H^3(G_b, \mathbb{Z}_2)$ that satisfy $Sq^2(n_3) = 0$ in $H^4(G_b, U_T(1))$. We note that $BH^3(G_b, \mathbb{Z}_2)$ and $H_{\text{rigid}}^4(G_b, U_T(1)) \equiv H^4(G_b, \mathbb{Z}_2)/\Gamma$ were derived in the special group super-cohomology classification. Recall that $H^4(G_b, U_T(1))$ is the well-known classification of bosonic SPT phases and Γ is a normal subgroup of $H^4(G_b, U_T(1))$ generated by $Sq^2(n_2)$, where $n_2 \in H^2(G_b, \mathbb{Z}_2)$ and $Sq^2(n_2)$ are viewed as elements of $H^4[G_b, U_T(1)]$. Physically, Γ describes those trivialized bosonic SPT phases when embedded into interacting fermion systems.

Together with several previous works [42, 50], we conjecture that up to spacial dimension $d_{sp} = 3$, FSPT with symmetry $G_f = G_b \times \mathbb{Z}_2^f$ can be classified by the general group super-cohomology class $H_f^{d_{sp}+1}[G_f, U_T(1)]$ defined

d_{sp}	short exact sequence
0	$0 \rightarrow H^1[G_b, U_T(1)] \rightarrow H_f^1[G_f, U_T(1)] \rightarrow \mathbb{Z}_2 \rightarrow 0$
1	$0 \rightarrow H^2[G_b, U_T(1)] \rightarrow H_f^2[G_f, U_T(1)] \rightarrow H^1(G_b, \mathbb{Z}_2) \rightarrow 0$
2	$0 \rightarrow H^3[G_b, U_T(1)] \rightarrow \mathcal{H}^3[G_f, U_T(1)] \rightarrow BH^2(G_b, \mathbb{Z}_2) \rightarrow 0$ $0 \rightarrow \mathcal{H}^3[G_f, U_T(1)] \rightarrow H_f^3[G_f, U_T(1)] \rightarrow H^1(G_b, \mathbb{Z}_2) \rightarrow 0$
3	$0 \rightarrow H_{\text{rigid}}^4[G_b, U_T(1)] \rightarrow \mathcal{H}^4[G_f, U_T(1)] \rightarrow BH^3(G_b, \mathbb{Z}_2) \rightarrow 0$ $0 \rightarrow \mathcal{H}^4[G_f, U_T(1)] \rightarrow H_f^4[G_f, U_T(1)] \rightarrow \tilde{B}H^2(G_b, \mathbb{Z}_2) \rightarrow 0$

TABLE I: Classifying FSPT phases up to spacial dimension $d_{sp} = 3$ with a total symmetry $G_f = G_b \times \mathbb{Z}_2^f$ using a general group super-cohomology class computed from short exact sequences. Note that $\mathcal{H}^{d_{sp}+1}[G_f, U_T(1)]$ is the so-called special group super-cohomology proposed in Ref. 42 and that in lower dimensions with $d_{sp} = 0, 1$, we have

$$H_f^{d_{sp}+1}[G_f, U_T(1)] \equiv \mathcal{H}^{d_{sp}+1}[G_f, U_T(1)].$$

$G_b \setminus d_{sp}$	0	1	2	3
\mathbb{Z}_2	\mathbb{Z}_2^2	\mathbb{Z}_2	\mathbb{Z}_8	\mathbb{Z}_1
\mathbb{Z}_{2k+1}	\mathbb{Z}_{4k+2}	\mathbb{Z}_1	\mathbb{Z}_{2k+1}	\mathbb{Z}_1
\mathbb{Z}_{2k}	$\mathbb{Z}_{2k} \times \mathbb{Z}_2$	\mathbb{Z}_2	$\begin{cases} \mathbb{Z}_{4k} \times \mathbb{Z}_2, & k \text{ even} \\ \mathbb{Z}_{8k}, & k \text{ odd} \end{cases}$	\mathbb{Z}_1
$\mathbb{Z}_2 \times \mathbb{Z}_2$	$(\mathbb{Z}_2)^3$	$(\mathbb{Z}_2)^3$	$(\mathbb{Z}_8)^2 \times \mathbb{Z}_4$	$(\mathbb{Z}_2)^2$
$\mathbb{Z}_2 \times \mathbb{Z}_4$	$\mathbb{Z}_4 \times (\mathbb{Z}_2)^2$	$(\mathbb{Z}_2)^3$	$(\mathbb{Z}_8)^2 \times (\mathbb{Z}_2)^3$	$\mathbb{Z}_4 \times \mathbb{Z}_2$
$\mathbb{Z}_4 \times \mathbb{Z}_4$	$(\mathbb{Z}_4)^2 \times \mathbb{Z}_2$	$(\mathbb{Z}_2)^2 \times \mathbb{Z}_4$	$(\mathbb{Z}_8)^2 \times \mathbb{Z}_4 \times (\mathbb{Z}_2)^3$	$(\mathbb{Z}_4)^2 \times \mathbb{Z}_2$
$\mathbb{Z}_2 \times \mathbb{Z}_8$	$\mathbb{Z}_8 \times (\mathbb{Z}_2)^2$	$(\mathbb{Z}_2)^3$	$\mathbb{Z}_{16} \times \mathbb{Z}_8 \times (\mathbb{Z}_2)^3$	$\mathbb{Z}_8 \times \mathbb{Z}_2$

TABLE II: Classification of FSPT phases with a total symmetry $G_f = G_b \times \mathbb{Z}_2^f$ in d_{sp} -spatial dimensions constructed using general group super-cohomology for some simple symmetries (represented by the bosonic symmetry groups G_b). Here \mathbb{Z}_1 means that our construction only gives rise to the trivial phase. \mathbb{Z}_n means that the constructed non-trivial SPT phases plus the trivial phase are labeled by the elements in \mathbb{Z}_n .

by the exact sequences summarized in Table I. We note that for spacial dimension $d_{sp} > 1$, general group super-cohomology theory is defined by two short exact sequences. The first short exact sequence can be understood as decoration of complex fermions onto the intersection points of the G_b -symmetry domain walls, which was first derived by special group super-cohomology theory. The second exact sequence can be understood as decoration of Kitaev's Majorana chains onto the intersection lines of G_b -symmetry domain walls, and our construction gives rise to a general scheme to compute $\tilde{B}H^{d_{sp}-1}(G_b, \mathbb{Z}_2)$ (the obstruction-free subgroup of $H^{d_{sp}-1}(G_b, \mathbb{Z}_2)$) in arbitrary dimensions. As an application, we also illustrate the classification results of FSPT phases for some simple symmetry group G_b in all physical dimensions in Table II.

Finally, regarding the completeness of general group super-cohomology classification for 3D FSPT phases, we present some physical arguments. Although the decoration of complex fermions on the intersection points of G_b -symmetry domain walls and the decoration of Majorana chains on G_b -symmetry domain walls give rise to a complete classification of 2D FSPT phases, this does not necessarily imply that this is also true in 3D. In fact, it has been pointed out [8] that the decoration of invertible TQFT on the G_b -symmetry domain walls may also give rise to new SPT states. For bosonic SPT states, decoration of the so-called E_8 state on the G_b -symmetry domain walls indeed produces the *efmf* SPT state beyond group cohomology classification. It has also been pointed out that $H^1(G_b, \mathbb{Z})$ classifies these additional bosonic SPT states. As $H^1(G_b, \mathbb{Z})$ is trivial for the unitary symmetry group G_b and $H^1(\mathbb{Z}_2^T, \mathbb{Z}) = \mathbb{Z}_2$ for the anti-unitary time-reversal symmetry, we understand why the *efmf* state is the only non-trivial root state of bosonic SPT states beyond group cohomology classification with time-reversal symmetry. For interacting fermion systems, in principle, we can decorate a $p + ip$ state (the root state of 2D fermionic invertible TQFT) onto the G_b -symmetry domain walls. However, as $H^1(G_b, \mathbb{Z})$ is trivial for the unitary symmetry group G_b , there are no new FSPT states with unitary symmetry group G_b . For time-reversal symmetry, it is possible to generate new FSPT states in this way, and we discuss this possibility in our future work.

C. Organization of the paper

The remainder of this paper is organized as follows. We begin with the definition of Hilbert space and the basic structure of fixed-point wavefunctions for FSPT states with total symmetry $G_f = G_b \times \mathbb{Z}_2^f$ in 1D, 2D and 3D in

section II. In section III A, we give a brief review of discrete spin structures and Kasteleyn orientations in 2D. In section III B, we derive the fixed-point conditions for FSLU transformations under wavefunction renormalization and re-derive the classifications of 2D FSPT phases. In section IV A, we discuss how to generalize the discrete spin structure and *local* Kasteleyn orientation in 3D. In section IV B, we use the concept of equivalence class of FSLU transformations and wavefunction renormalization to obtain the construction and classification of 3D FSPT phases. Finally, we offer conclusions and discussions for possible future directions.

Readers less interested in the detailed mathematical construction of (local) Kasteleyn orientations are invited to skip some part of section III A and IV A, and read directly section III B and IV B of constructing FSPT states. The only prerequisites are some terminology conventions and the conclusion that we can construct (local) Kasteleyn orientations systematically and rigorously on the resolved dual lattice of arbitrary triangulations of spin manifolds in arbitrary dimensions.

II. FIXED-POINT WAVEFUNCTIONS OF FSPT PHASES

A. Constructing fixed-point wavefunction and classification for FSPT phases in 1D

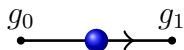


FIG. 1: Bosonic and fermionic degrees of freedoms for 1D fixed-point FSPT states on a link. The black dots are bosonic degrees of freedom labelled by $g_i \in G$ on sites. The blue ball represents the complex fermion $c_{(ij)}$ at the center of the link $\langle ij \rangle$. The arrow represents the local order of two sites.

As a warm up, let us begin with fixed-point wavefunction in 1D and use FSLU transformation to re-derive the well know classification result of 1D FSPT phases. The building block of bosonic and fermionic degrees of freedom in the 1D FSPT model is shown in Fig. 1. Similar to the bosonic SPT phase, every (locally ordered) vertex i of the 1D lattice has bosonic degrees of freedom labeled by a group element $g_i \in G_b$. (Recall that the FSPT phases have a total symmetry $G_f = G_b \times \mathbb{Z}_2^f$.) A spinless complex fermion $c_{(ij)}$ is at the center of each link $\langle ij \rangle$ (see the blue ball in Fig. 1), and the fermion occupation number $n_1(g_i, g_j)$ is either 0 or 1. Let $|0\rangle$ be the ground state of no fermions on any of the links; then, a generating set of the Fock space is given by $\prod_{(ij) \in l} c_{(ij)}^\dagger |0\rangle$, where $l \subset L$ is a subset of all links L , including the empty set. Thus, the full local Hilbert space for our 1D model on a fixed lattice \mathcal{T} (triangulation of 1D spacial manifold) is:

$$L_{\mathcal{T}}^{1D} = \bigoplus_{l \subset L} \left(\prod_{(ij) \in l} c_{(ij)}^\dagger |0\rangle \otimes \prod_{v \in V(\mathcal{T})} \mathbb{C}^{|G_b|} \right). \quad (4)$$

Here, $|G_b|$ is the order of the bosonic symmetry group G_b . As a vector space, the fermionic Hilbert space on the links is the same as the tensor product $\bigotimes_{L(\mathcal{T})} \mathbb{C}^2$; however, the Fock space structure means that a local Hamiltonian for a fermion system is non-local when regarded as one for a boson system. We note that the structure of total bosonic and fermionic Hilbert space on arbitrary triangulations is the same as the 1D case of Ref. 42, although the latter is considering the spacetime picture.

Our 1D fixed-point state is a superposition of those basis states with all possible triangulations \mathcal{T} :

$$|\Psi\rangle = \sum_{\text{all conf.}} \Psi (\text{---} \circ \text{---} \circ \text{---} \bullet \text{---} \circ \text{---} \bullet \text{---}) | \text{---} \circ \text{---} \circ \text{---} \bullet \text{---} \circ \text{---} \bullet \text{---} \rangle. \quad (5)$$

In the following, we will derive the rules of wavefunction renormalization generated by FSLU transformations for the above wavefunction. We will obtain the conditions for fixed-point wavefunction and show how to construct all FSPT states with total symmetry $G_f = G_b \times \mathbb{Z}_2^f$ in 1D.

1. Fermionic symmetric local unitary transformation

To obtain a fixed-point wavefunction for Eq. (5), we need to understand the changes of the wavefunction under renormalization. In 1D, renormalization can be understood as removing some bosonic or fermionic degrees of freedom

by reducing the number of vertices. The basic renormalization process is known as (2-1) Pachner move of triangulation of 1D manifold. Since we have a bosonic degree of freedom at each vertex and a fermionic degree of freedom at each link, the (2-1) move effectively reduces the Hilbert space of one bosonic mode and one fermionic mode.

To be more precise, the (2-1) move is a FSLU transformation between the fermionic Fock spaces on two different triangulations:

$$\Psi \left(\begin{array}{c} 0 \quad c_{(01)} \quad 1 \quad c_{(12)} \quad 2 \\ \bullet \xrightarrow{\quad} \circ \xrightarrow{\quad} \bullet \xrightarrow{\quad} \circ \xrightarrow{\quad} \bullet \end{array} \right) = F(g_0, g_1, g_2) \Psi \left(\begin{array}{c} 0 \quad c_{(02)} \quad 2 \\ \bullet \xrightarrow{\quad} \circ \xrightarrow{\quad} \bullet \end{array} \right), \quad (6)$$

where the F operator is defined as

$$F(g_0, g_1, g_2) = \frac{1}{|G_b|^{1/2}} \nu_2(g_0, g_1, g_2) c_{(12)}^{\dagger n_1(g_1, g_2)} c_{(01)}^{\dagger n_1(g_0, g_1)} c_{(02)}^{n_1(g_0, g_2)}. \quad (7)$$

We note that the $|G_b|$ is the order of the group G_b and we introduce the normalization factor $1/|G_b|^{1/2}$ in the above expression due to the change of vertex number. Here, $\nu_2(g_0, g_1, g_2)$ is a $U_T(1)$ -valued function with variables $g_i \in G_b$ and $c_{(ij)}^{\dagger}$ is the creation operator for c fermions at link $\langle ij \rangle$, etc. $n_1(g_i, g_j) \in \{0, 1\}$ is a \mathbb{Z}_2 -valued function indicating whether there is a c fermion at link $\langle ij \rangle$ or not. Since we are constructing symmetric state, both ν_2 and n_1 should be symmetric under the action of G_b (We note that $\nu_2(gg_0, gg_1, gg_2) = \nu_2^*(g_0, g_1, g_2)$ if g is anti-unitary). So they are $U_T(1)$ -valued 2-cochain and \mathbb{Z}_2 -valued 1-cochain respectively. Because the renormalization process (2-1) move should preserve the fermion parity, we have $dn_1(g_0, g_1, g_2) = n_1(g_1, g_2) + n_1(g_0, g_2) + n_1(g_0, g_1) = 0 \pmod{2}$. Therefore n_1 is in fact a \mathbb{Z}_2 -valued 1-cocycle.

2. Consistent equations and equivalence classes

Since we are constructing fixed-point wavefunction, Eq. (5) should be invariant under renormalization. For instance, we can use two different sequences of F moves Eq. (6) to connect a fixed initial state and a fixed final state. Different approaches should give rise to the same wavefunction. These constraints give us the consistent equations for ν_2 .

The simplest example is the following two paths between two fixed states:

$$\begin{aligned} \Psi \left(\begin{array}{c} 0 \quad c_{(01)} \quad 1 \quad c_{(12)} \quad 2 \quad c_{(23)} \quad 3 \\ \bullet \xrightarrow{\quad} \circ \xrightarrow{\quad} \bullet \xrightarrow{\quad} \circ \xrightarrow{\quad} \bullet \xrightarrow{\quad} \circ \xrightarrow{\quad} \bullet \end{array} \right) &= F(g_1, g_2, g_3) \Psi \left(\begin{array}{c} 0 \quad c_{(01)} \quad 1 \quad c_{(13)} \quad 3 \\ \bullet \xrightarrow{\quad} \circ \xrightarrow{\quad} \bullet \xrightarrow{\quad} \circ \xrightarrow{\quad} \bullet \end{array} \right), \\ &= F(g_1, g_2, g_3) F(g_0, g_1, g_3) \Psi \left(\begin{array}{c} 0 \quad c_{(03)} \quad 3 \\ \bullet \xrightarrow{\quad} \circ \xrightarrow{\quad} \bullet \end{array} \right), \end{aligned} \quad (8)$$

$$\begin{aligned} \Psi \left(\begin{array}{c} 0 \quad c_{(01)} \quad 1 \quad c_{(12)} \quad 2 \quad c_{(23)} \quad 3 \\ \bullet \xrightarrow{\quad} \circ \xrightarrow{\quad} \bullet \xrightarrow{\quad} \circ \xrightarrow{\quad} \bullet \xrightarrow{\quad} \circ \xrightarrow{\quad} \bullet \end{array} \right) &= F(g_0, g_1, g_2) \Psi \left(\begin{array}{c} 0 \quad c_{(02)} \quad 2 \quad c_{(23)} \quad 3 \\ \bullet \xrightarrow{\quad} \circ \xrightarrow{\quad} \bullet \xrightarrow{\quad} \circ \xrightarrow{\quad} \bullet \end{array} \right), \\ &= F(g_0, g_1, g_2) F(g_0, g_2, g_3) \Psi \left(\begin{array}{c} 0 \quad c_{(03)} \quad 3 \\ \bullet \xrightarrow{\quad} \circ \xrightarrow{\quad} \bullet \end{array} \right). \end{aligned} \quad (9)$$

The constraint is that the product of F moves for the above two processes equal to each other:

$$F(g_0, g_1, g_3) F(g_1, g_2, g_3) = F(g_0, g_2, g_3) F(g_0, g_1, g_2). \quad (10)$$

Substituting the expression of F move Eq. (7) into this equation and using the fact $dn_1 = 0 \pmod{2}$, we find that the above equation for fermionic operators is equivalent to a purely bosonic one without any fermion sign:

$$d\nu_2(g_0, g_1, g_2, g_3) = \frac{\nu_2(g_1, g_2, g_3) \nu_2(g_0, g_1, g_3)}{\nu_2(g_0, g_2, g_3) \nu_2(g_0, g_1, g_2)} = 1. \quad (11)$$

That means ν_2 should be a $U_T(1)$ -valued 2-cocycle, provided that the wavefunction Eq. (5) is a fix-point wavefunction. This ν_2 data is the same as the construction of bosonic SPT states.

Using a FSLU transformation, we can redefine the basis state $|\{g_l\}\rangle$ as

$$|\{g_l\}\rangle' = U_{\mu_1, m_0} |\{g_l\}\rangle = \prod_{\langle ij \rangle} \mu_1(g_i, g_j) \prod_{\langle i \rangle} \left[f_{iA}^{m_0(g_i)} f_{iB}^{m_0(g_i)} \right] \prod_{\langle ij \rangle} \left[f_{jA}^{\dagger m_0(g_j)} f_{iB}^{\dagger m_0(g_i)} \right] |\{g_l\}\rangle, \quad (12)$$

where we first create two complex fermions f_{jA} and f_{iB} near the two ends of the link $\langle ij \rangle$ ($i < j$), and then annihilate the two fermions f_{iA} and f_{iB} near the vertex i when gluing the two links sharing vertex i . To preserve the fermion

parity and be symmetric, m_0 should be a 0-cocycle (with \mathbb{Z}_2 coefficient): $m_0(gg_i) = m_0(g_i)$ and $dm_0(g_i, g_j) = m_0(g_j) + m_0(g_i) = 0$. $\mu_1(g_i, g_j)$ is a phase factor associated with link $\langle ij \rangle$. In this new basis, the fermionic F move is $F' = U_{\mu_1, m_0} F U_{\mu_1, m_0}^\dagger$. After eliminating all f fermions (all the fermion signs are cancelled), one find that the phase factor in Eq. (7) becomes

$$\nu'_2(g_0, g_1, g_2) = \nu_2(g_0, g_1, g_2) \frac{\mu_1(g_1, g_2)\mu_1(g_0, g_1)}{\mu_1(g_0, g_2)}. \quad (13)$$

Since our gapped phases are defined by FSLU transformations, ν'_2 and ν_2 belong to the same phase. In general, the elements ν_2 in the same group cohomology class in $H^2(G_b, U_T(1))$ correspond to the same 1D FSPT phase. This is consistent with the general result obtained from the path-integral formalism in Ref. 42 that ν_{d+1} can be gauge transformed to

$$\nu'_{d+1} = \nu_{d+1} \cdot d\mu_d \cdot (-1)^{Sq^2(m_{d-1})}, \quad (14)$$

for $Sq^2(m_0)$ is trivial in the 1D FSPT case.

In summary, 1D FSPT is characterized by $n_1 \in H^1(G_b, \mathbb{Z}_2)$ and $\nu_2 \in H^2(G_b, U_T(1))$. This is consistent with the previous result [42].

B. Constructing fixed-point wavefunction for FSPT phases in 2D and 3D

The fixed-point wavefucitons for FSPT phases in 2D and 3D are much more complicated. We will describe all the details and explain the corresponding physical meanings below.

Similar to the wavefunction renormalization scheme for 2D bosonic SET phases, we consider the quantum state defined on an arbitrary triangulation for 2D and 3D FSPT phases. The triangulation admits a branching structure that can be labeled by a set of local arrows on all links (edges) with no oriented loop for any triangle. Mathematically, the branching structure can be regarded as a discrete version of a spin^c structure and can be consistently defined on arbitrary triangulations of 2D and 3D orientable manifolds.

We begin with the construction of fixed-point wavefunction in 2D; then, the generalization to 3D becomes straightforward. As any 2D FSPT state can be naturally mapped to a 2D bosonic SET state by gauging the fermion parity symmetry, our construction for fixed-point wavefunctions is greatly inspired by such connections. In particular, an FSPT state with total symmetry $G_f = G_b \times \mathbb{Z}_2^f$ can be mapped to a G_b symmetry-enriched toric code model. As a simple example, fixed-point wavefunctions and commuting projector parent Hamiltonians on an arbitrary trivalent graph (due to triangulation) with $G_b = \mathbb{Z}_2$ were constructed in Ref. 61. It has also been shown that all of these SET states can be obtained by gauging fermion parity from FSPT states with total symmetry $G_f = \mathbb{Z}_2 \times \mathbb{Z}_2^f$.

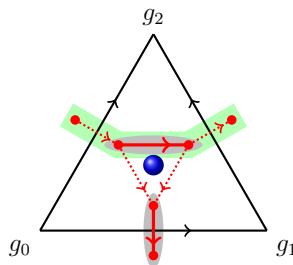


FIG. 2: Fermionic degrees of freedom in a triangle. The red dots represent Majorana fermions at the two sides of each link. The blue ball represents the complex fermion of the special group super-cohomology model at the center of the triangle. The green strip is the decorated Kitaev's Majorana chain onto the dual lattice \mathcal{P} .

The building block of bosonic and fermionic degrees of freedom in our 2D FSPT model is shown in Fig. 2. Exactly as in the bosonic SET phase, every vertex i of the space triangulation has bosonic degrees of freedom labeled by a group element $g_i \in G_b$. (Recall that the FSPT phases have a total symmetry $G_f = G_b \times \mathbb{Z}_2^f$.) A spinless complex fermion c is at the center of each triangle/face (see the blue ball in Fig. 2), and the fermion occupation number is either 0 or 1. Let $|0\rangle$ be the ground state of no fermions on any of the triangles; then, a generating set of the Fock space is given by $\prod_{(ijk) \in f} c_{(ijk)}^\dagger |0\rangle$, where $f \subset F$ is a subset of all triangles F , including the empty set. In addition, each link has two Majorana fermions on its two sides, an arrangement that is equivalent to spinless complex fermion

a. Similar to the c fermion on each triangle, let $|\tilde{0}\rangle$ be the ground state of no fermions on any of the links; then, a generating set of the Fock space is given by $\prod_{(ij)\in l} a_{(ij)}^\dagger |\tilde{0}\rangle$, where $l \subset L$ is a subset of all links L , including the empty set. Thus, the full local Hilbert space for our 2D model on a fixed triangulation \mathcal{T} is

$$L_{\mathcal{T}}^{2D} = \bigoplus_{f \subset F} \bigoplus_{l \subset L} \left(\prod_{(ijk) \in f} c_{(ijk)}^\dagger |0\rangle \otimes \prod_{(ij) \in l} a_{(ij)}^\dagger |\tilde{0}\rangle \otimes \prod_{v \in V(\mathcal{T})} \mathbb{C}^{|G_b|} \right). \quad (15)$$

Here, $|G_b|$ is the order of the bosonic symmetry group G_b . As a vector space, the fermionic Hilbert space on the triangles and links is the same as the tensor product $\bigotimes_{F(\mathcal{T})} \mathbb{C}^2 \otimes \bigotimes_{L(\mathcal{T})} \mathbb{C}^2$; however, the Fock space structure means that a local Hamiltonian for a fermion system is non-local when regarded as one for a boson system. We note that the structure of total fermionic Hilbert space on arbitrary triangulations is slightly more general than that given in Ref. 63; this allows us to construct very general FSET states in 2D. However, the construction of general FSET states is beyond the scope of this paper.

As mentioned above, for FSPT states, the support space of FSLU transformations must be one-dimensional such that it can adiabatically connect to a product state in the absence of global symmetry. Therefore, the fermionic states of c and a fermions on the triangles and edges are completely fixed by the configuration of group elements $\{g_i\}$ on the vertices. In particular, the equivalence classes of complex fermion occupation number of c fermions are uniquely determined by the elements in $BH^2(G_b, \mathbb{Z}_2)$ (the obstruction-free subgroup of $H^2(G_b, \mathbb{Z}_2)$), which was first proposed by the special group super-cohomology construction of FSPT phases. Essentially, the complex fermion c can be regarded as a decoration on the intersection points of G_b -symmetry domain walls. Ref. 50, 67, and 68 pointed out that a Majorana chain can be decorated onto the G_b -symmetry domain walls to generate a complete set of FSPT states in 2D. This layer of decoration is uniquely determined by the elements in $H^1(G_b, \mathbb{Z}_2)$. The Majorana fermions must be paired (see the gray ellipse in Fig. 2) to form Kitaev's Majorana chains on the G_b symmetry domain walls (see the green strip in Fig. 2). This requires a discrete spin structure—the Kasteleyn orientations on the dual trivalent lattice (with proper resolution for the lattice sites, as seen in Fig. 2)—such that the total fermion parity of the a fermion is always even on any closed loop. We review all of the details in section III A. An example of triangulation of the torus and decoration of Kitaev's Majorana chains is given in Fig. 4. The full details are discussed in section III B.

Thus, our 2D fixed-point state is a superposition of those basis states with all possible triangulations \mathcal{T} .

$$|\Psi\rangle = \sum_{\text{all conf.}} \Psi \left(\left(\begin{array}{c} \text{Diagram 1} \\ \text{Diagram 2} \end{array} \right) \right) \quad (16)$$

In section III B, we derive the rules of wavefunction renormalization generated by FSLU transformations. We also obtain the conditions for fixed-point wavefunctions and show how to construct all FSPT states with total symmetry $G_f = G_b \times \mathbb{Z}_2^f$ on arbitrary triangulations in 2D.

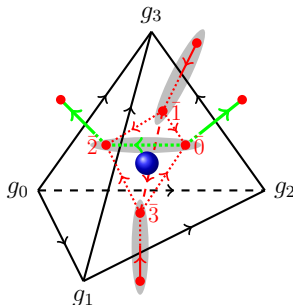


FIG. 3: Fermionic degrees of freedom in a tetrahedron. The red dots represent Majorana fermions on the two sides of each triangle. The blue ball represents the complex fermion of the (special) group super-cohomology model at the center of the tetrahedron. The green line is the decorated Kitaev's Majorana chain on the dual lattice \mathcal{P} .

In the following, we generalize all of the above constructions to 3D. The building block of bosonic and fermionic degrees of freedom is shown in Fig. 3. Again, every vertex i of the 3D space triangulation has a bosonic degree of freedom labeled by a group element $g_i \in G_b$. However, the spinless complex fermion c introduced by special group super-cohomology theory now resides on each tetrahedron (see the blue ball in Fig. 3). In addition, each triangle of

the space tetrahedron has two Majorana fermions on its two sides, which is again equivalent to a spinless complex fermion a . Similar to the 2D case, let $|0\rangle$ and $|\tilde{0}\rangle$ be the ground states of no fermions on any tetrahedron and triangle; then, a generating set of the Fock space is given by $\prod_{(ijkl)\in t} c_{(ijkl)}^\dagger |0\rangle \otimes \prod_{(ijk)\in f} a_{(ijk)}^\dagger |\tilde{0}\rangle$, where $t \subset T$ is a subset of all tetrahedra T , including the empty set, and $f \subset F$ is a subset of all triangles F , including the empty set. Thus, the full local Hilbert space of our 3D model on a fixed triangulation \mathcal{T} is

$$L_{\mathcal{T}}^{3D} = \bigoplus_{t \subset T} \bigoplus_{f \subset F} \left(\prod_{(ijkl)\in t} c_{(ijkl)}^\dagger |0\rangle \otimes \prod_{(ijk)\in f} a_{(ijk)}^\dagger |\tilde{0}\rangle \otimes \prod_{v \in V(\mathcal{T})} \mathbb{C}^{|G_b|} \right). \quad (17)$$

Similar to the 2D case, the fermionic states of c and a fermions on the tetrahedra and triangles are also completely fixed by the configuration of group elements $\{g_i\}$ on the vertices. The equivalence classes of complex fermion occupation number of the c fermion are uniquely determined by the elements in $BH^3(G_b, \mathbb{Z}_2)$ (the obstruction-free subgroup of $H^3(G_b, \mathbb{Z}_2)$), which was also first proposed by the special group super-cohomology construction of FSPT states. It is not a surprise that in 3D, the complex fermion c can also be regarded as a decoration (subjected to obstructions) onto the intersection points of G_b -symmetry domain walls. The most interesting new feature here is that a Majorana chain can also be decorated onto the intersection lines of G_b -symmetry domain walls, and such a construction generates a new set of FSPT states in 3D. As expected, this layer of decoration also requires a discrete spin structure on the dual trivalent lattice (with a proper resolution for the lattice sites as well, as seen in Fig. 3), and the Majorana fermions must also be paired to form Kitaev's Majorana chains (see the green line in Fig. 3). However, such decorations are subjected to a fundamental obstruction on $H^4(G_b, \mathbb{Z}_2)$ due to fermion parity conservation. We discuss all of the details in section IV A. Furthermore, the fixed-point condition of wavefunction renormalization gives rise to a secondary obstruction on $H^5(G_b, U_T(1))$, which is explored in full in section IV B.

Finally, our 3D fixed-point state is a superposition of those basis states with all possible triangulations \mathcal{T} .

$$|\Psi\rangle = \sum_{\text{all conf.}} \Psi \left(\left(\begin{array}{c} \text{Diagram 1} \\ \text{Diagram 2} \end{array} \right) \right). \quad (18)$$

In section IV B, we derive the rules of wavefunction renormalization generated by FSLU transformations. We also obtain the conditions for fixed-point wavefunction and show how to construct all FSPT states with total symmetry $G_f = G_b \times \mathbb{Z}_2^f$ on arbitrary triangulations in 3D.

III. CONSTRUCTIONS AND CLASSIFICATIONS FOR FSPT STATES IN 2D

Ref. 67 pointed out that discrete spin structures and Kasteleyn orientation played an essential role in constructing FSPT phases decorated with Kitaev's Majorana chains on G_b -symmetry domain walls. In this section, we give a brief review of the essential idea and generalize the construction to arbitrary triangulations in 2D (see Fig. 4). In particular, we use Poincaré dual to show how to implement discrete spin structures and Kasteleyn orientation for an arbitrary triangulation with a branching structure in 2D. Essentially, the Poincaré dual enables us to define discrete spin structures in arbitrary dimensions and gives rise to the notion of *local* Kasteleyn orientation, which serves as the key step toward decorating Kitaev's Majorana chains onto the intersection lines of G_b -symmetry domain walls in 3D.

In the following, we start by defining spin structures in terms of the second Stiefel–Whitney class. Then, we clarify the relation between the discrete spin structures and the Kasteleyn orientation in 2D. Finally, we make use of the novel concept of equivalence classes of FSLU transformations (with a one-dimensional support space) to obtain the full classification of FSPT states with total symmetry $G_f = G_b \times \mathbb{Z}_2^f$ in 2D.

A. Discrete spin structure and Kasteleyn orientations

In this subsection, we construct the zeroth Stiefel–Whitney homology class on arbitrary 2D triangulation lattice and relate it to the Kasteleyn orientations on the resolved dual lattice. The general procedures of constructing Kasteleyn orientations are summarized as follows:

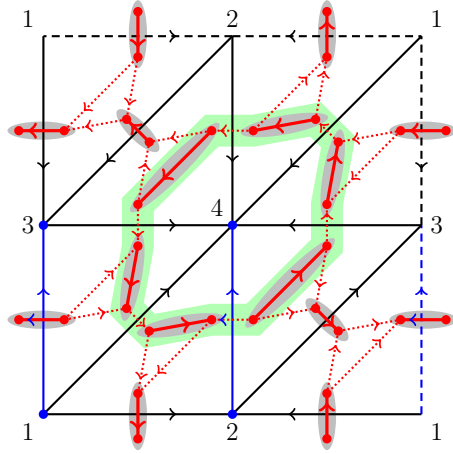


FIG. 4: Example of triangulation \mathcal{T} of torus and Kitaev chain decoration. All vertices $\langle 1 \rangle$, $\langle 2 \rangle$, $\langle 3 \rangle$, and $\langle 4 \rangle$ (blue dots) are singular vertices, i.e., $w_0 = \langle 1 \rangle + \langle 2 \rangle + \langle 3 \rangle + \langle 4 \rangle$. We choose link $\langle 13 \rangle$ and $\langle 24 \rangle$ (blue lines) to be singular lines, i.e., $w_0 = \partial(\langle 13 \rangle + \langle 24 \rangle)$. The direction of the red links dual to $\langle 13 \rangle$ and $\langle 24 \rangle$ are changed. Vertices $i = 1, 2, 3$, and 4 of \mathcal{T} are labelled by group elements $g_i \in G$. Majorana fermions (red dots) reside on the vertices of the resolved dual lattice $\tilde{\mathcal{P}}$ (solid and dashed red links). The solid red links and gray ellipses indicate that the two Majorana fermions at their two ends are paired with respect to the link direction. The green strip is the \mathbb{Z}_2 domain wall of the “spin” configuration $\{g_i\}$ and is decorated by a Kitaev’s Majorana chain (Majorana fermions along the domain wall are paired differently from the “vacuum”).

1. Given a (black) triangulation lattice \mathcal{T} with branching structure for a 2D spin manifold;
2. Construct the (red) resolved dual lattice $\tilde{\mathcal{P}}$ and (red) link orientations using convention Fig. 6. At this stage, some of the vertices in \mathcal{T} are non-Kasteleyn-oriented;
3. Find the expression of w_0 in Eq. (20) as a formal summation of singular vertices of \mathcal{T} (i.e., non-Kasteleyn-oriented vertices in step-2);
4. Connect singular vertices in \mathcal{T} by (blue) lines S (i.e., $\partial S = w_0$);
5. Using convention Fig. 7b, reverse the orientations of (red) links dual to (blue) links belonging to S ;
6. Now all the vertices in \mathcal{T} are Kasteleyn-oriented.

After all the above steps, the resolved dual lattice $\tilde{\mathcal{P}}$ now has Kasteleyn orientations. In this way, any decorations of Kitaev’s Majorana chains will have the same fermion parity. We will use them to construct generic FSPT states in section III B.

1. Discrete Stiefel–Whitney homology class w_0

It is well known that an oriented manifold M (with dimension n) admits spin structures if and only if its second Stiefel–Whitney class $[w^2] \in H^2(M, \mathbb{Z}_2)$ vanishes. In the construction of the lattice models upon triangulation of M , we found it more convenient to use the $(n-2)$ -th Stiefel–Whitney homology class $[w_{n-2}]$, which is the Poincaré dual of $[w^2]$.

In this subsection, we consider only the 2D case. For a spatial manifold M ($n = 2$) with triangulation \mathcal{T} , the Stiefel–Whitney homology class $[w_0]$ has a representative that is the summation of all vertices v with some (mod 2) coefficients as follows [69] [70]

$$w_0 = \sum_{v \in \mathcal{T}} \#\{\sigma | v \subseteq \sigma \text{ is regular}\} \cdot v. \quad (19)$$

Here, $v \subseteq \sigma$ means that v is a sub-simplex of simplex σ . $v \subseteq \sigma$ is called regular if v and σ have one of the three relative positions shown in Fig. 5. $\#\{\sigma | v \subseteq \sigma \text{ is regular}\} \cdot v$ denotes the formal product of the (mod 2) number of regular pairs $v \subseteq \sigma$ and the vertex v . We call vertex v singular if $\#\{\sigma | v \subseteq \sigma \text{ is regular}\}$ is odd. In this language, w_0

in Eq. (19) is the formal summation of all singular vertices. w_0 is a vector (0-th singular chain) in the vector space (of 0-th singular chains) spanned by the formal bases of all vertices with \mathbb{Z}_2 coefficients.

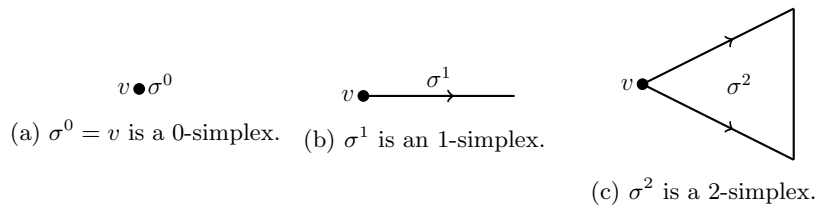


FIG. 5: Regular pair $v \subseteq \sigma^i$ ($i = 0, 1, 2$) for vertex v .

On the other hand, it is known that all oriented 2D surfaces admit spin structures. Thus, the second Stiefel–Whitney class $[w^2]$ or the zeroth Stiefel–Whitney homology class $[w_0]$ of any oriented surface is (co)homologically trivial. As a result, the collection of singular vertices w_0 in Eq. (19) can be viewed as a boundary ∂S for some lines S (we call them singular lines). The singular lines S are colored blue in the following figures.

For a fixed collection of singular vertices (a fixed representative w_0 for $[w_0]$), different inequivalent choices of singular lines S correspond to different spin structures that are isomorphic to $H^1(M, \mathbb{Z}_2)$ non-canonically. This can be seen as follows. We first choose arbitrary fixed S_0 such that $w_0 = \partial S_0$. Then for any other choice S with also $w_0 = \partial S$, we can add S_0 and S formally. The summation $S_0 + S$ is a collection of closed loops on the manifold (recall that lines in S_0 and S have the same end points). We can ask whether $S_0 + S$ is in the trivial class of $H_1(M, \mathbb{Z}_2)$ or not. If it is, we say S_0 and S are equivalent. In this way, with the fixed S_0 , we have a one-to-one correspondence between equivalence classes of singular lines S and $H_1(M, \mathbb{Z}_2)$. In other words, the set of equivalence classes of singular lines S is an affine $H_1(M, \mathbb{Z}_2)$ -space. This is also one of the most important properties of spin structures of a manifold. As a result, we have a one-to-one correspondence between 2^{2g} equivalence classes of singular lines S and 2^{2g} spin structures of the manifold with genus g .

2. Kasteleyn orientations and gauge transformations

To decorate Kitaev chains onto domain walls of a 2D spin model, it is useful to determine the Kasteleyn orientation [64] for the edges of the lattice [67, 68]. In this section, we relate the existence of discrete spin structures (the vanishing of $[w_0]$) of a triangulation \mathcal{T} to the existence of Kasteleyn orientation of the resolved dual lattice. Then, in the next section, we use FSLU transformations [28, 63] to classify FSPT states and define exactly solvable models on arbitrary triangulations in 2D.

Our set up begins with a fixed triangulation \mathcal{T} of the surface M . The first step is to construct a polyhedral decomposition \mathcal{P} of M that is a trivalent graph dual to \mathcal{T} . We add a spinless fermionic degree of freedom to every link of \mathcal{T} and split it into two Majorana fermions on the two sides of this link for convenience. Equivalently, we can resolve the triangulation \mathcal{T} by adding a new vertex to each triangle center and obtain a new triangulation $\tilde{\mathcal{T}}$. The Majorana fermions reside on the vertices of the resolved dual lattice $\tilde{\mathcal{P}}$, which is a trivalent graph dual to $\tilde{\mathcal{T}}$ (see Fig. 6 and Fig. 4 for this construction on a torus).

The second step is adding directions to links in \mathcal{T} and $\tilde{\mathcal{P}}$. We order all of the vertices in \mathcal{T} and use the convention that all links are from vertices of smaller number to vertices of larger number. This is a branching structure of \mathcal{T} such that there is no cycle for any triangle. The dual-link direction in \mathcal{P} is obtained from \mathcal{T} using the convention shown in Fig. 7a. The directions of the new links in $\tilde{\mathcal{P}}$ are also obtained from triangulation \mathcal{T} by using the conventions in Fig. 6.

The essential point of the aforementioned link orientation conventions can be explained as follows. When traveling along the smallest red loop in $\tilde{\mathcal{P}}$ around vertex $v \in \mathcal{T}$ counterclockwise, we encounter even numbers of red links (due to the resolution) with the direction along or opposite to our direction (for example, the red loop inside the green strip around vertex 4 in Fig. 4). Using the conventions in Fig. 6, the red link direction is opposite the counterclockwise direction if and only if (1) the red link is dual to a black link in \mathcal{T} such that v is the initial point of this black link (this corresponds to the case in Fig. 5b) or (2) the red link is resolved to a new link inside a triangle in \mathcal{T} such that v is the first point of this triangle, i.e., the 0 point of triangle $\langle 012 \rangle$ (this is the case in Fig. 5c). If the total number of red links with opposite directions is odd, the vertex v is considered Kasteleyn-oriented. As the smallest loop in $\tilde{\mathcal{P}}$ around v has an even number of red links, it does not matter whether we use counterclockwise or clockwise conventions. Under the above construction, we relate the zeroth Stiefel–Whitney homology class w_0 in Eq. (19) and the orientation of links

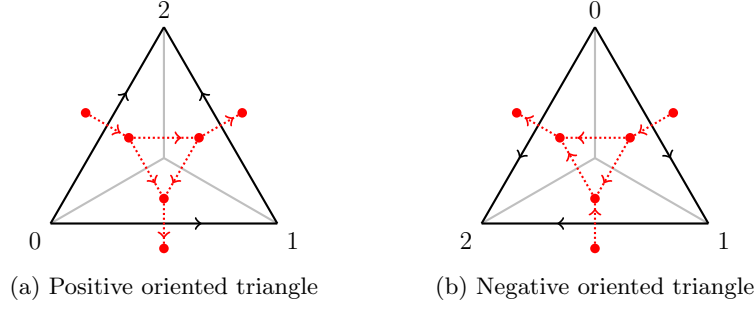


FIG. 6: Triangulation \mathcal{T} (black line), resolved triangulation $\tilde{\mathcal{T}}$ (black and gray line), and resolved dual lattice $\tilde{\mathcal{P}}$ (dashed red line). The resolved triangulation $\tilde{\mathcal{T}}$ was obtained from the original \mathcal{T} by adding a new vertex to the center of each triangle. The links of $\tilde{\mathcal{P}}$ have orientations induced from the link orientations of \mathcal{T} according to the conventions shown in Fig. 7a. Red dots on the vertices of $\tilde{\mathcal{P}}$ represent Majorana fermions that split from the complex fermions on each link of \mathcal{T} (see the discussion in section III B).

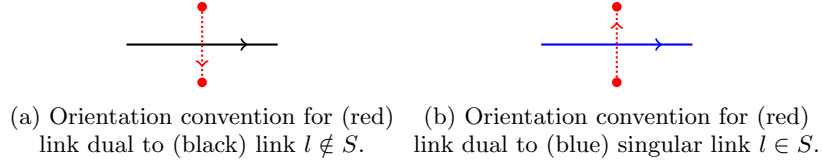


FIG. 7: Conventions for the orientation of links in $\tilde{\mathcal{P}}$ (dotted red line) from branching structure of triangulation \mathcal{T} (solid black line). Non-singular (singular) black (blue) links $l \notin S$ ($l \in S$) induce orientation conventions for the dual link in $\tilde{\mathcal{P}}$. We introduce a spinless fermion on each (black/blue) link in \mathcal{T} and split it into two Majorana fermions on the two sides of this link or vertices of $\tilde{\mathcal{P}}$ (red dots).

in $\tilde{\mathcal{P}}$, i.e., w_0 is the summation of all non-Kasteleyn-oriented vertices.

$$\begin{aligned}
 w_0 &= \sum_{v \in \mathcal{T}} (1 + \#\{\sigma^1 | v \subseteq \sigma^1 \text{ is regular}\} + \#\{\sigma^2 | v \subseteq \sigma^2 \text{ is regular}\}) \cdot v \\
 &= \sum_{v \in \mathcal{T}} v \text{ (} v \text{ is non-Kasteleyn-oriented)}.
 \end{aligned} \tag{20}$$

As the zeroth Stiefel–Whitney homology class $[w_0]$ for any oriented surface is trivial, we have $w_0 = \partial S$ for some singular line S . If we further reverse the direction of the links in $\tilde{\mathcal{P}}$, thus crossing the singular lines S as shown in Fig. 7b, then all of the vertices in \mathcal{T} are Kasteleyn-oriented, as this operation only changes the Kasteleyn property of the singular vertices in w_0 while preserving this property for all other vertices, including those in the interval of S . After completing the procedure above, we relate the vanishing of the zeroth Stiefel–Whitney homology class $[w_0]$ to the property of Kasteleyn orientation of the smallest loop around each vertex.

Note that the construction of link direction in $\tilde{\mathcal{P}}$ depends on the choice of the singular line S . On the one hand, the local shape of S is not important as long as ∂S is fixed. In fact, if we change the shape of S locally, the change in link direction in $\tilde{\mathcal{P}}$ can be obtained by several “gauge transformations” of Kasteleyn orientation, which relate two different but equivalent Kasteleyn orientations (simultaneously changing the directions of links sharing a common vertex in $\tilde{\mathcal{P}}$) [65]. An example of the basic shape changes of singular lines on \mathcal{T} and gauge transformation of Kasteleyn orientation on $\tilde{\mathcal{P}}$ is shown in Fig. 8. Note that the Majorana degrees of freedom on the vertices of $\tilde{\mathcal{P}}$ are mapped from one lattice to another according to the link direction under the gauge transformation of Kasteleyn orientation (n to n' in Fig. 8). In this way, the vacuum state without fermions (without Kitaev chain) on the left lattice is mapped to the vacuum state on the right lattice without changing the fermion parity.

On the other hand, the homology class of S matters. Different choices of topological classes of S (fixed $w_0 = \partial S$) correspond to different spin structures on M . Our constructions make sure that, for arbitrary choices of S , the *local* Kasteleyn properties along the smallest loop around every vertex is satisfied. However, the *global* Kasteleyn property along non-trivial cycles of M can be either preserved or broken. They correspond to 2^{2g} different spin structures on closed oriented surface M with genus g [65, 66]. Different choices of S induce different global Kasteleyn properties and thus correspond to different spin structures.

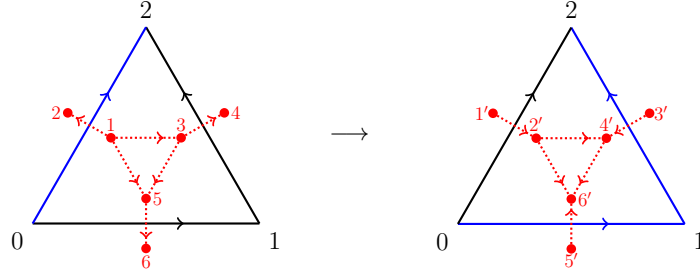


FIG. 8: Shape changing of singular lines S of \mathcal{T} and “gauge transformation” of Kasteleyn orientations of $\tilde{\mathcal{P}}$. We perform “gauge transformations” on the three red vertices inside a black triangle, which effectively change the shape of S and the directions of the three outreaching red links. The Majorana fermions are mapped from n to n' ($n = 1, 2, \dots, 6$) with respect to the directions of red links dual to black links under this FSLU.

3. Kasteleyn orientations under retriangulations

In the above, we focus only on a fixed triangulation \mathcal{T} of M and relate its discrete Stiefel–Whitney homology class $[w_0]$ to the Kasteleyn orientations and spin structures. To use FSLU transformations to classify FSPT phases, we must understand the relation of Kasteleyn orientations for different triangulations. In fact, we only have to determine the changes of Kasteleyn orientations under Pachner moves, which are basic moves of retriangulation [71].

Ordinary Pachner moves for a two-dimensional manifold consist of a (2-2) move and a (1-3) move. With branching structures, there are three types of (2-2) move and four types of (1-3) move in total. (We do not consider the mirror images of these moves; otherwise, the number of moves would double). Only two types of (2-2) move and two types of (1-3) move have branching structures that can be induced by global ordering [42]. Examples of these moves are as follows:

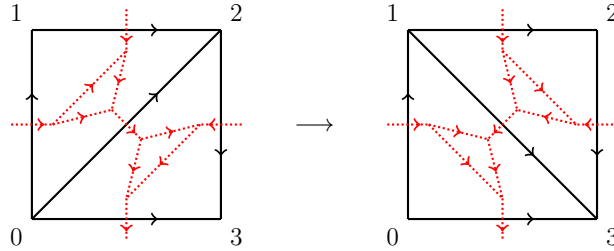


FIG. 9: Standard (2-2) move.

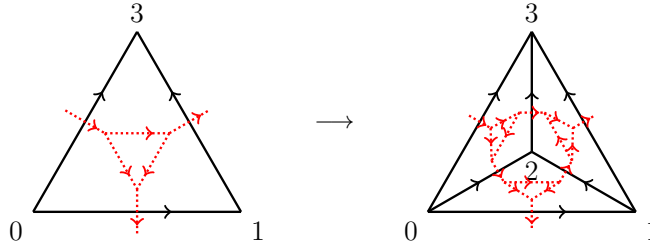


FIG. 10: One of the (1-3) moves.

Other types of (2-2) and (1-3) moves are shown in Supplementary Material. For Pachner moves that are not induced by global ordering, the representative w_0 of Stiefel–Whitney class $[w_0]$ in Eq. (19) may be changed. For Pachner moves that are induced by a global ordering, the representative w_0 of Stiefel–Whitney class $[w_0]$ is unchanged. This makes the 2D case much easier than the 3D case.

B. FSLU transformations and consistent conditions for fixed-point states

In the above subsection, we discuss discrete spin structures and Kasteleyn orientation construction on arbitrary 2D triangulation lattices. We can now decorate Kitaev's Majorana chains using these rules and systematically classify 2D FSPT states by using FSLU transformations.

1. Decoration of Kitaev's Majorana chains

As discussed in section II, our model has two types of fermionic degrees of freedom. The first type is the complex fermion $c_{\langle ijk \rangle}$, which resides at the center of triangle $\langle ijk \rangle$ of space manifold triangulation \mathcal{T} . We use $n_2(g_i, g_j, g_k) = 0, 1$ to denote the number of c fermions at triangle $\langle ijk \rangle$. In fact, the parity conservation constraint for c fermions under retriangulation is $dn_2 = 0 \pmod{2}$. Therefore n_2 is an element of $H^2(G_b, \mathbb{Z}_2)$.

The second type of (complex) fermion, $a_{\langle ij \rangle}$, resides on the link $\langle ij \rangle$ of \mathcal{T} . To describe Kitaev's Majorana chain more conveniently, we separate fermion $a_{\langle ij \rangle}$ to two Majorana fermions.

$$\gamma_{ijA} = a_{\langle ij \rangle} + a_{\langle ij \rangle}^\dagger, \quad (21)$$

$$\gamma_{ijB} = \frac{1}{i} \left(a_{\langle ij \rangle} - a_{\langle ij \rangle}^\dagger \right). \quad (22)$$

The Majorana fermions γ_{ijA} and γ_{ijB} reside on the two sides of link $\langle ij \rangle$. They also reside on the two ends of the link in $\tilde{\mathcal{P}}$ dual to link $\langle ij \rangle$. Our convention is that the dual link has direction from vertex $\langle ijA \rangle$ to vertex $\langle ijB \rangle$. The fermion parity operator of a fermions or γ fermions at link $\langle ij \rangle$ is $P_f^\gamma = -i\gamma_{ijA}\gamma_{ijB}$.

Now we decorate Kitaev's Majorana chains onto the dual lattice. We use a \mathbb{Z}_2 -valued 1-cochain $\tilde{n}_1(g_i, g_j)$ to indicate whether there is a domain wall between vertices i and j . $\tilde{n}_1 \in H^1(G_b, \mathbb{Z}_2)$ is a cocycle because we are constructing SPT states without deconfined Majorana fermions (the Kitaev chains should form closed loops). Depending on the configurations of $\{g_i\}$ and the choices of \tilde{n}_1 , the domain wall configuration in a particular lattice is different. We pair the Majorana fermions depending on the domain wall configuration as follows. If there is no domain wall on link $\langle ij \rangle$, then the Majorana fermions γ_{ijA} and γ_{ijB} on the two sides of this link are paired (vacuum pair) with respect to the direction of the dual red link (we use a solid blue line and gray ellipse to indicate this pairing). If there is a domain wall on link $\langle ij \rangle$, then the Majorana fermion of this link is paired with another Majorana fermion belonging to another link with a domain wall within the same triangle.

After fermion decoration, the (2-2) move becomes a fermionic unitary transformation between the fermionic Fock spaces on two different triangulation lattices \mathcal{T} and \mathcal{T}' . An example of this F move (the standard F move) is presented as follows (there are \mathbb{Z}_2 domain walls on links $\langle 01 \rangle$, $\langle 02 \rangle$, $\langle 03 \rangle$, and no domain wall on the other links):

$$\Psi \left(\begin{array}{c} \text{Diagram 1} \\ \text{Square lattice with diagonal } 0 \rightarrow 2 \\ \text{Links } 01, 02, 03, 12, 13, 23 \\ \text{Majorana fermions } \gamma_{ijA}, \gamma_{ijB} \\ \text{Pairings (solid blue lines, gray ellipses)} \end{array} \right) = F(g_0, g_1, g_2, g_3) \Psi \left(\begin{array}{c} \text{Diagram 2} \\ \text{Square lattice with diagonal } 1 \rightarrow 3 \\ \text{Links } 01, 02, 03, 12, 13, 23 \\ \text{Majorana fermions } \gamma_{ijA}, \gamma_{ijB} \\ \text{Pairings (solid blue lines, gray ellipses)} \end{array} \right), \quad (23)$$

where the F operator is defined as

$$F(g_0, g_1, g_2, g_3) = \nu_3(g_0, g_1, g_2, g_3) c_{(012)}^{\dagger n_2(g_0, g_1, g_2)} c_{(023)}^{\dagger n_2(g_0, g_2, g_3)} c_{(013)}^{n_2(g_0, g_1, g_3)} c_{(123)}^{n_2(g_1, g_2, g_3)} X[\tilde{n}_1(g_i, g_j)]. \quad (24)$$

Here, $\nu_3(g_0, g_1, g_2, g_3)$ is a $U_T(1)$ -valued 3-cochain and $c_{(012)}^\dagger$ is the creation operator for c fermions at triangle $\langle 012 \rangle$, etc. $X[\tilde{n}_1(g_i, g_j)]$ is a projection operator changing the Majorana fermion configurations. In the above example, the X operator has an explicit form as follows:

$$X[\tilde{n}_1] = 2^{1/2} (P_{01B,02A} P_{02B,03A}) P_{13A,13B}, \quad (25)$$

where $P_{a,b} = (1 - i\gamma_a\gamma_b)/2$ is the projection operator for Majorana pairs $\langle a, b \rangle$ (the direction is from vertex a to vertex b). The first two projection operators in the above equation project the state to the Majorana dimer configuration

in the left figure. Note that the Majorana fermions, which do not appear explicitly on one lattice, are considered to be in vacuum pairs. For example, the two Majorana fermions γ_{13A} and γ_{13B} appear only in the right figure. They are considered to be paired from γ_{13A} to γ_{13B} in the left figure. Therefore, we have a third projection operator in Eq. (25) to put the two Majorana fermions γ_{13A} and γ_{13B} into a vacuum state ($a_{(13)}^\dagger a_{(13)} = 0$) in the left figure. All other Majorana fermions that are not shown in Eq. (25) are unchanged under the aforementioned F move.

In order to make X an unitary operator acting on the Hilbert space of Majorana fermions, we introduce a normalization factor in the front of X . By directly calculating the norm of the final state after the action of X operator, we can obtain a general expression of the normalization factor

$$\prod_{\text{loop } i \text{ in } (\tilde{\mathcal{P}}, \tilde{\mathcal{P}}')} 2^{(L_i-1)/2}, \quad (26)$$

with $2L_i$ being the length of the i -th loop in the transition graph of dimer configurations in $\tilde{\mathcal{P}}$ and $\tilde{\mathcal{P}}'$. For example, the transition graph of the two states in Eq. (23) has only one loop with length bigger than two: 01B-02A-02B-03A-01B. So the factor is $2^{(4/2-1)/2} = 2^{1/2}$, according to Eq. (26).

As we are constructing FSPT states, the fermionic local unitary transformation F should be G_b symmetric in the sense that

$$F(g_0, g_1, g_2, g_3) = F(gg_0, gg_1, gg_2, gg_3), \quad (27)$$

for all $g \in G_b$ if G_b is a unitary symmetry group. That is why $\nu_3(g_0, g_1, g_2, g_3)$, $n_2(g_0, g_1, g_2)$, and $\tilde{n}_1(g_0, g_1)$ are all cochains that are invariant under unitary g action. (We note that $\nu_3(gg_0, gg_1, gg_2, gg_3) = \nu_3^*(g_0, g_1, g_2, g_3)$ for anti-unitary g action.)

In general, there are eight kinds of domain wall configuration in the above F move. One can show that for all configurations, the fermion parities of Majorana fermions are the same in the initial and final wavefunctions (this comes from the Kasteleyn orientation property of retriangulations; see section III A and Supplementary Material). Therefore, the fermion parities of c fermions and γ fermions should also be conserved separately, and both n_2 and \tilde{n}_1 are cocycles.

Similar to the 1D case, we can use FSLU to redefine the basis state $|\{g_l\}\rangle$ as

$$|\{g_l\}'\rangle = U_{\mu_2, m_1} |\{g_l\}\rangle = \prod_{\langle ij k \rangle} \mu_2(g_i, g_j, g_k)^{s_{\langle ij k \rangle}} \prod_{\langle ij \rangle} \left[f_{ijA}^{m_1(g_i, g_j)} f_{ijB}^{m_1(g_i, g_j)} \right] \prod_{\langle ij k \rangle} \left[f_{jkA}^{\dagger m_1(g_j, g_k)} f_{ijA}^{\dagger m_1(g_i, g_j)} f_{ikB}^{\dagger m_1(g_i, g_k)} \right] |\{g_l\}\rangle, \quad (28)$$

where we first create three complex fermions f_{jkA} , f_{ijA} and f_{ikB} near the three links of the triangle $\langle ij k \rangle$ ($i < j < k$), and then annihilate the two fermions f_{ijA} and f_{ijB} on the two sides of link $\langle ij \rangle$ when gluing the two triangles sharing link $\langle ij \rangle$. To preserve the fermion parity and be symmetric, m_1 should be a 1-cocycle (with \mathbb{Z}_2 coefficient): $m_1(gg_i, gg_j) = m_1(g_i, g_j)$ and $dm_1(g_i, g_j, g_k) = 0$. $\mu_2(g_i, g_j, g_k)$ is a phase factor associated with triangle $\langle ij k \rangle$, and $s_{\langle ij k \rangle} = \pm 1$ denotes the orientation of the triangle. After eliminating all f fermions in the new F move operator $F' = U_{\mu_2, m_1} F U_{\mu_2, m_1}^\dagger$ (all fermion signs are cancelled again), one find that the phase factor in Eq. (24) becomes

$$\nu_3'(g_0, g_1, g_2, g_3) = \nu_3(g_0, g_1, g_2, g_3) \frac{\mu_2(g_1, g_2, g_3) \mu_2(g_0, g_1, g_3)}{\mu_2(g_0, g_2, g_3) \mu_2(g_0, g_1, g_2)}, \quad (29)$$

So the elements ν_3 in the same group cohomology class in $H^3(G_b, U_T(1))$ correspond to the same 2D FSPT phase. This is also consistent with the general result in Eq. (14) [42], since $Sq^2(m_1)$ is also trivial in the 2D FSPT case.

Apart from the (2-2) move, there is another (2-0) move that can change the total number of vertices for triangulations. An example of domain wall configurations for the (2-0) move is

$$\Psi \left(\begin{array}{c} \text{Diagram of a diamond-shaped triangulation with vertices } g_0, g_1, g_2 \text{ and internal vertices } 01A, 01B, 01A', 01B', 12A, 12B, 12A', 12B'. \text{ Green shaded regions } C(012) \text{ and } \bar{C}(012) \text{ are shown.} \end{array} \right) = \frac{1}{|G_b|^{1/2}} c_{(012)}^{\dagger n_2(g_0, g_1, g_2)} \bar{c}_{(012)}^{\dagger n_2(g_0, g_1, g_2)} X[\tilde{n}_1(g_i, g_j)] \Psi \left(\begin{array}{c} \text{Diagram of a linear chain of vertices } g_0, g_1, g_2 \text{ with fermions } 01A, 01B, 12A, 12B \text{ on the links.} \end{array} \right), \quad (30)$$

where $c_{(012)}$ and $\bar{c}_{(012)}$ are the annihilation operators of the c fermions at the center of two triangles with opposite orientations in the left figure ($c_{(012)}$ and $\bar{c}_{(012)}$ are at the centers of the upper and lower triangles in the left figure respectively). The Hilbert dimension of the bosonic degrees of freedom on the vertices of a fixed triangulation is $|G_b|^{N_v}$, where $|G_b|$ is the order of the group G_b and N_v is the number of vertices. Therefore we add a normalization factor $|G_b|^{-1/2}$ in the front of the (2-0) move operator, for the vertex number is reduced by one from the left state to the right state. $X[\tilde{n}_1]$ is also the projection operator from the state of Majorana dimer pairs in the right figure to the state of the left figure. Note that there are six Majorana fermions ($\gamma_{02A}, \gamma_{02B}, \gamma_{01A'}, \gamma_{01B'}, \gamma_{12A'},$ and γ_{12B}') that do not appear explicitly in the right figure. Similar to the case of the (2-2) move, these fermions should also be considered to be in vacuum pairs in the right figure state, such that $-i\gamma_{02A}\gamma_{02B} = -i\gamma_{01B'}\gamma_{01A} = -i\gamma_{12B'}\gamma_{12A'} = 1$ when acting on the right figure state. This choice is possible because the dimer loop $01A-01B'-01A'-01B-01A$ is Kasteleyn oriented. Therefore, one can also use the convention that the two Majorana fermions on the two sides of a link are paired up by regarding the projection operators $-i\gamma_{01A}\gamma_{01B'}, -i\gamma_{01A'}\gamma_{01B}, -i\gamma_{12A}\gamma_{12B'},$ and $-i\gamma_{12A'}\gamma_{12B}$ as 1 when acting on the vacuum state of the left figure. The X operator then projects the state to the Majorana dimer configuration state in the left figure. The fermion parities of the left and right states are always the same. An explicit expression of X for this particular(2-0) move is

$$X[\tilde{n}_1] = 2P_{01B',02A}P_{02B,01A'}P_{12A,12B'}P_{12A',12B}. \quad (31)$$

Using the (2-0) moves, we can deduce all (3-1) moves and other (2-2) moves form the standard (2-2) F move in Eq. (23). The normalization factor is obtained from Eq. (26). there are two loops in the transition graph of the Majorana dimer states with length bigger than two: $01B'-02A-02B-01A'-01B'$ and $12A-12B'-12A'-12B-12A$. So the normalization factor is $2^{(4/2-1)/2} \times 2^{(4/2-1)/2} = 2$.

2. Fermionic pentagon equations

In the above, we discuss the FSLU moves. The most important one is the standard F move in Eq. (23). Similar to the bosonic pentagon equation for the bosonic F move, we have a fermionic pentagon equation as a consistent equation for FSLU transformations (see Fig. 11). This fermionic pentagon equation involves only the standard F move. Using the unitary conditions, one can also derive other pentagon equations, and they essentially give the same constraint for ν_3 .

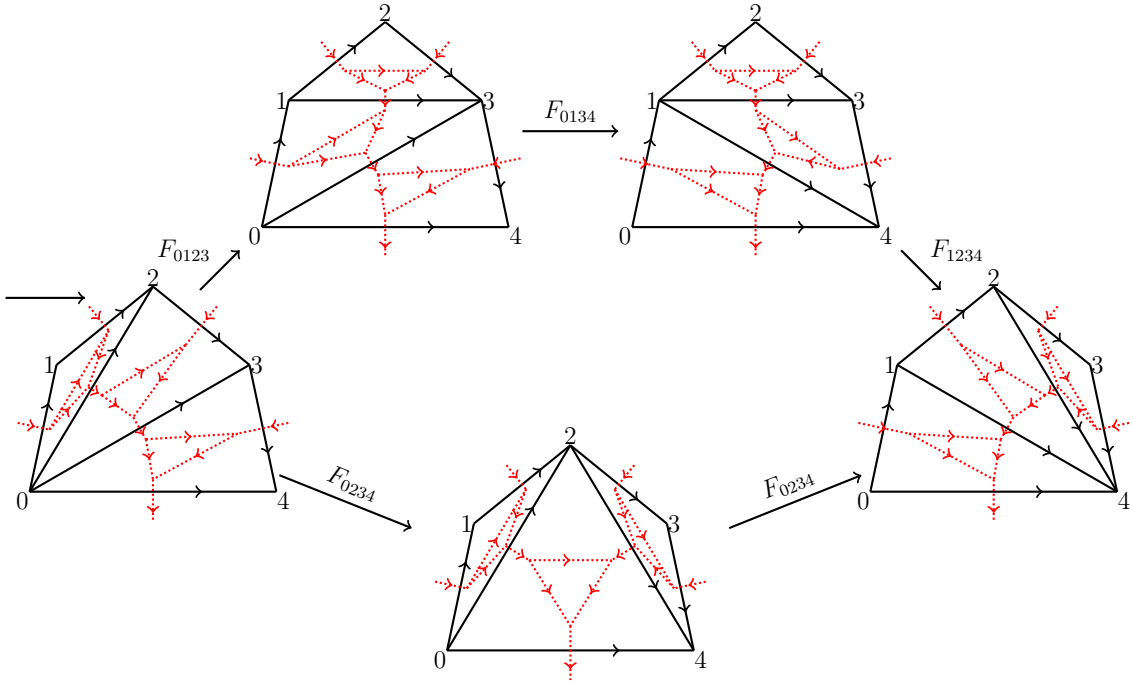


FIG. 11: Fermionic pentagon equation.

We now calculate the constraint for ν_3 from the pentagon equation in Fig. 11. As the c fermions and Majorana fermions are decoupled in the F move (the c fermion part and the Majorana fermion part of X in Eq. (24) commute),

only the c fermion twists the cocycle condition for ν_3 . The X operators are merely projection operators that do not introduce any nontrivial phases in two different paths of pentagon equation. The final result of the equation for ν_3 is the same as (special) group super-cohomology theory [42, 63], i.e.,

$$(\mathrm{d}\nu_3)(g_0, g_1, g_2, g_3, g_4) = (-1)^{Sq^2(n_2)(g_0, g_1, g_2, g_3, g_4)} = (-1)^{n_2(g_0, g_1, g_2)n_2(g_2, g_3, g_4)}. \quad (32)$$

Now, we see that only $BH^2(G_b, \mathbb{Z}_2)$, the obstruction-free subgroup of $H^2(G_b, \mathbb{Z}_2)$ formed by elements $n_2 \in H^2(G_b, \mathbb{Z}_2)$ that satisfy $Sq^2(n_2) = 0$ in $H^4(G_b, U_T(1))$, can give rise to solutions for ν_3 , and inequivalent solutions of ν_3 are still given by $H^3(G_b, U_T(1))$ according to the gauge transformations of ν_3 . Thus, the mathematical objects that classify 2D FSPT phases with a total symmetry $G_f = G_b \times \mathbb{Z}_2^f$ can be summarized as three group cohomologies of the symmetry group G_b [48, 50]: $H^1(G_b, \mathbb{Z}_2)$, $BH^2(G_b, \mathbb{Z}_2)$ and $H^3(G_b, U_T(1))$. Finally, by using the method proposed in Ref. 63, one can derive the commuting projector parent Hamiltonian of all of these FSPT states on arbitrary 2D triangulations with a branching structure.

IV. CONSTRUCTIONS AND CLASSIFICATIONS FOR FSPT STATES IN 3D

In this section, we construct and classify the 3D FSPT states parallel to the discussions of 2D FSPT states. Compared with the 2D case, the most nontrivial part of 3D phases is the fermion parity mixing of the c fermions and Majorana fermions. In section IV A, we find that there are in general no Kasteleyn orientations on a 3D lattice. The existence of a spin structure only implies *local* Kasteleyn orientations. If we decorate Kitaev's Majorana chains onto a 3D lattice, the shape-changing process of the Majorana chain may also change the fermion parity of the corresponding Majorana chain. In this case, we should use the c fermion to compensate the fermion parity changes. As a result of this fermion parity mixing, the cocycle equation for ν_4 is much more complicated than special group super-cohomology theory.

A. Discrete spin structure in 3D and local Kasteleyn orientations

In this subsection, we discuss the first Stiefel–Whitney homology class on a discrete lattice and relate it to the *local Kasteleyn orientations* on the dual lattice. The overall constructions are parallel to the 2D case. The difference is that Kasteleyn orientations are only satisfied for the smallest loops in 3D, not for the general large loops. The fermion parity of a Kitaev chain decorated onto a fluctuating loop is therefore not conserved.

1. Discrete Stiefel–Whitney homology class w_1

Similar to the oriented 2D manifolds, all oriented 3D manifolds admit spin structures. The second Stiefel–Whitney cohomology class $[w^2]$ is always trivial. We can consider the first discrete Stiefel–Whitney homology class for a triangulation \mathcal{T} with a branching structure of 3D spatial manifold M [69]:

$$w_1 = \sum_{l \in \mathcal{T}} \#\{\sigma | l \subseteq \sigma \text{ is regular}\} \cdot l. \quad (33)$$

w_1 is the summation of all links in \mathcal{T} with some \mathbb{Z}_2 coefficients. Again, $l \subseteq \sigma$ means that link l is a sub-simplex of simplex σ . $l \subseteq \sigma$ is called regular if l and σ have one of the three relative positions shown in Fig. 12. If $\#\{\sigma | l \subseteq \sigma \text{ is regular}\}$ is odd, we call the link l singular. Thus, w_1 in Eq. (33) is the formal summation of all singular lines. w_1 is a vector (1-th singular chain) in the vector space (of 1-th singular chains) spanned by formal bases of all links with \mathbb{Z}_2 coefficients.

As the second Stiefel–Whitney cohomology class $[w^2]$ of any oriented 3D manifold is trivial, we can find some surface S such that $w_1 = \partial S$. For a fixed collection of singular links (a fixed representative w_1 for $[w_1]$), different inequivalent choices of S correspond to different spin structures (see the discussions at the end of section III A 1).

2. Local Kasteleyn orientations and gauge transformations

In 3D, we also want to decorate Kitaev chains onto the intersection lines of G_b -symmetry domain walls. A natural question inherited from 2D is whether there are Kasteleyn properties for all even-link loops in 3D. This question is

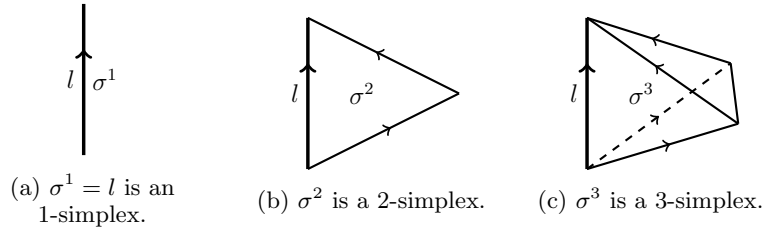


FIG. 12: Regular pairs $l \subseteq \sigma^i$ ($i = 1, 2, 3$) for link l .

related to the fermion parity of the Kitaev chain. The answer is that the existence of discrete spin structures (the vanishing of $[w_1]$) is related to the existence of *local* Kasteleyn orientations of the resolved dual lattice. In other words, Kasteleyn properties are satisfied for the smallest loops but generally broken for large loops in 3D.

We now consider the construction that is similar to the 2D case. For a fixed triangulation \mathcal{T} of 3D manifold M , the first step is to construct a polyhedral decomposition \mathcal{P} of M , which is a 4-valent graph dual to \mathcal{T} . We now add a spinless fermionic degree of freedom to every face (triangle) of \mathcal{T} and split it into two Majorana fermions on the two sides of this face for convenience. Equivalently, we resolve the triangulation \mathcal{T} by adding a new vertex to each tetrahedron center and obtain a new resolved triangulation $\tilde{\mathcal{T}}$. The Majorana fermions reside on the vertices of the resolved dual lattice $\tilde{\mathcal{P}}$, which is a 4-valent graph dual to $\tilde{\mathcal{T}}$ (see Fig. 13).

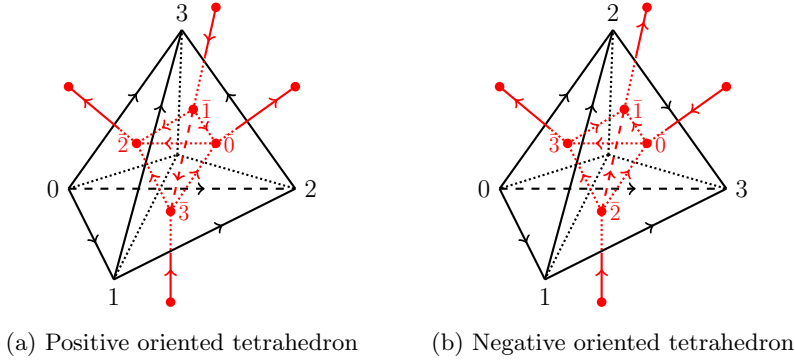


FIG. 13: Triangulation \mathcal{T} (solid black line), resolved triangulation $\tilde{\mathcal{T}}$ (solid and dashed black lines), and resolved dual lattice $\tilde{\mathcal{P}}$ (red line). The resolved triangulation $\tilde{\mathcal{T}}$ is obtained from the original \mathcal{T} by adding a new vertex to the center of each tetrahedron. The links of \mathcal{P} have orientations induced from the link orientations of \mathcal{T} according to the conventions shown in Fig. 14a. Red dots on the vertices of $\tilde{\mathcal{P}}$ represent Majorana fermions, which are split from complex fermions on each face of \mathcal{T} .

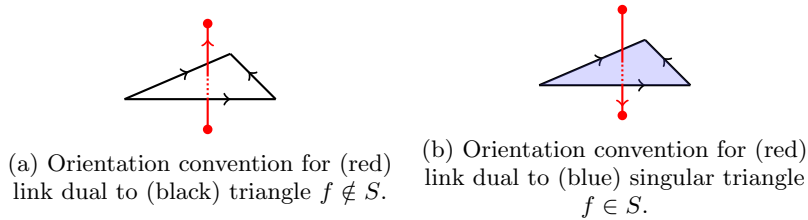


FIG. 14: Conventions for orientations of links in $\tilde{\mathcal{P}}$ (red line) from branching structure of triangulation \mathcal{T} (black line). Non-singular (singular) black (blue) triangle $f \notin S$ ($f \in S$) induces orientation for the dual link in $\tilde{\mathcal{P}}$. We introduce a spinless fermion on each (black/blue) triangle in \mathcal{T} and split it into two Majorana fermions on two sides of this triangle or vertices of $\tilde{\mathcal{P}}$ (red dots).

The second step is again adding directions to links in \mathcal{T} and $\tilde{\mathcal{P}}$. The directions of the links in \mathcal{T} are given by the branching structure. The dual link direction in \mathcal{P} is obtained from \mathcal{T} using the convention shown in Fig. 14a. The directions of the new links in $\tilde{\mathcal{P}}$ are obtained from the triangulation \mathcal{T} by using the conventions in Fig. 13.

The above link direction construction has the following properties. Consider a fixed link $l \in \mathcal{T}$. When going along the smallest red loop in $\tilde{\mathcal{P}}$ around this link l along the right-hand rule direction, we encounter an even number of red links with directions along or opposite to our direction. Using the conventions in Fig. 13, the red link direction is opposite to our direction if and only if (1) the red link is dual to a black triangle in \mathcal{T} such that the initial and final vertices of l are the first and last vertices of this black triangle (this corresponds to the case in Fig. 12b) and (2) the red link is a resolved new link inside a tetrahedron in \mathcal{T} such that the initial and final vertices of l are the first and the last vertices of this tetrahedron (this is the case in Fig. 12c). If the total number of red links with opposite directions is odd, we call the link l Kasteleyn-oriented. Under this construction, we relate the first Stiefel–Whitney homology class w_1 in Eq. (33) to the orientations of links in $\tilde{\mathcal{P}}$, i.e., w_1 is the summation of all non-Kasteleyn-oriented links.

$$\begin{aligned} w_1 &= \sum_{l \in \mathcal{T}} (1 + \#\{\sigma^2 | l \subseteq \sigma^2 \text{ is regular}\} + \#\{\sigma^3 | l \subseteq \sigma^3 \text{ is regular}\}) \cdot l \\ &= \sum_{l \in \mathcal{T}} l \text{ (} l \text{ is non-Kasteleyn-oriented)}. \end{aligned} \quad (34)$$

As discussed above, the first Stiefel–Whitney homology class $[w_1]$ for any oriented 3D manifold is trivial. Therefore, we have some singular surface S such that $w_1 = \partial S$. Now, if we reverse the direction of the links in $\tilde{\mathcal{P}}$ crossing the singular surface S , as shown in Fig. 14b, then all of the links in \mathcal{T} are Kasteleyn-oriented. After following the procedures above, we relate the vanishing of the zeroth Stiefel–Whitney homology class $[w_0]$ to the property of *local* Kasteleyn orientation of the smallest loops around all of the links in \mathcal{T} . Here, “local” means that only the smallest loops in $\tilde{\mathcal{P}}$ around links in \mathcal{T} are Kasteleyn-oriented. Larger loops with an even number of links do not have Kasteleyn properties in general.

The above construction of link directions in $\tilde{\mathcal{P}}$ depends on the choice of singular surface S . The shape of S can also be changed with fixed ∂S . If we change the shape of S locally, the changes of link directions in $\tilde{\mathcal{P}}$ can be obtained by several “gauge transformations” of Kasteleyn orientations. We define this by simultaneously changing the directions of links sharing a common vertex in $\tilde{\mathcal{P}}$, similar to the 2D case [65]. Different Kasteleyn orientations related by these “gauge transformations” are said to be equivalent. An example of shape changes of singular surfaces on \mathcal{T} and gauge transformation of Kasteleyn orientations on $\tilde{\mathcal{P}}$ are shown in Fig. 15. The Majorana degrees of freedom on the vertices of $\tilde{\mathcal{P}}$ are also mapped from one lattice to another according to the link directions (similar to the 2D case in Fig. 8). This ensures that the vacuum state (without Kitaev chain) on one lattice is mapped to the vacuum state on another lattice, without fermion parity changing (no fermion on either lattice).

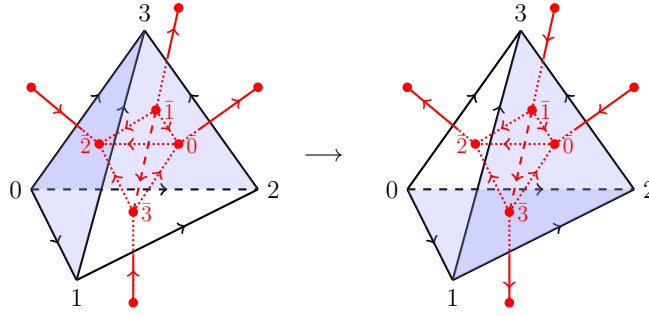


FIG. 15: Shape changing of singular surfaces S of \mathcal{T} and “gauge transformation” of Kasteleyn orientations of $\tilde{\mathcal{P}}$. We perform “gauge transformations” on the four red vertices inside a black tetrahedron, which effectively changes the shape of S and the directions of the four outreaching red links. The Majorana fermions are mapped with respect to the directions of red links dual to black triangles under this FSLU transformation.

With fixed $w_0 = \partial S$, the choices of S are not unique. Different choices of topological classes of S correspond to different spin structures on M . The global Kasteleyn properties along non-trivial cycles of M can also be either preserved or broken depending on the choices of S . Our construction generalizes the relation of Kasteleyn orientations and discrete spin structures from 2D [65] to 3D.

3. Local Kasteleyn orientations under retriangulations

To perform FSLU transformations, we now consider that the Kasteleyn orientation changes under retriangulation of M . Pachner moves for the 3D manifold consist of a (2-3) move and a (1-4) move [71]. When introducing branching

structures, there are 10 types of (2-3) move and 5 types of (1-4) move (again, we do not consider the mirror images of these moves, otherwise the number would double) [42]. Eight types of (2-3) move and three types of (1-4) move have branching structures that can be induced by global ordering [42, 72]. The standard (2-3) move is given in Fig. 16, which does not involve singular surfaces. Two examples of moves involving singular surfaces (the representative w_1 of Stiefel–Whitney class $[w_1]$ in Eq. (33) is changed) are presented in Figs. 17 and 18. Other types of (2-3) and (1-4) moves are shown in Supplementary Material.

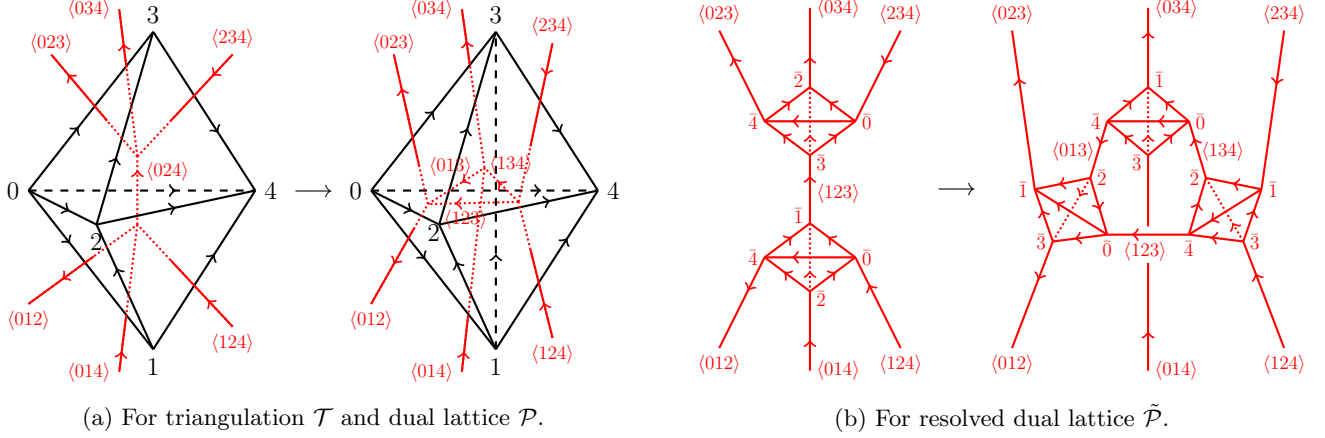


FIG. 16: Standard (2-3) move.

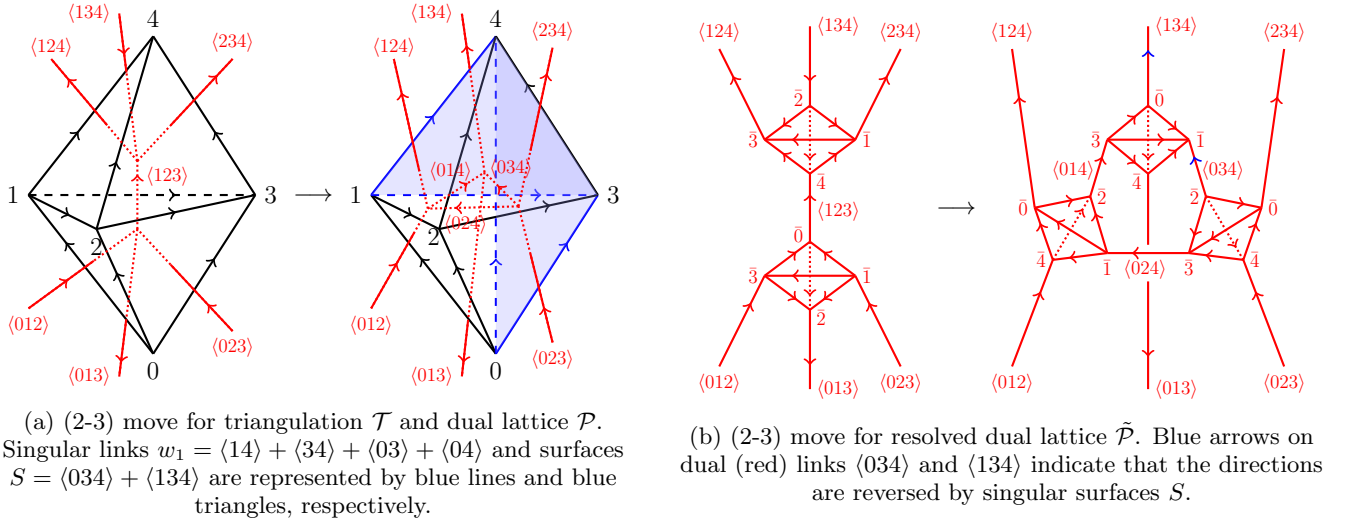


FIG. 17: A (2-3) move that involves singular surfaces.

Until now, the construction in 3D has been very similar to the 2D case. However, there is a very crucial difference. Although both the lattices before and after the Pachner move have *local* Kasteleyn properties, the Kasteleyn orientation for larger loops may be broken. Consider for example the case in Fig. 17. If we consider that the large loop consists of links $\langle 012 \rangle$, $\langle 123 \rangle$, and $\langle 124 \rangle$ (and the newly resolved links between them) on the left lattice $\tilde{\mathcal{P}}$ and links $\langle 012 \rangle$, and $\langle 124 \rangle$ (and the newly resolved links between them) on the right lattice $\tilde{\mathcal{P}}'$, the Kasteleyn properties are the same (all five links on $\tilde{\mathcal{P}}$ and three links on $\tilde{\mathcal{P}}'$ have an up direction). On the other hand, if we consider that the large loop consists of links $\langle 012 \rangle$, $\langle 123 \rangle$, and $\langle 234 \rangle$ on the left lattice $\tilde{\mathcal{P}}$ and links $\langle 012 \rangle$, $\langle 024 \rangle$, and $\langle 234 \rangle$ on the right lattice $\tilde{\mathcal{P}}'$, the Kasteleyn properties are changed (all five links on $\tilde{\mathcal{P}}$ have an up direction, but only two of five links on $\tilde{\mathcal{P}}'$ have an up direction). In the next subsection, we systematically analyze the Kasteleyn properties of loops under Pachner moves. After decorating Majorana fermions, we see that the Majorana fermion parity changes, which is crucial in constructing legitimate FSPT states.

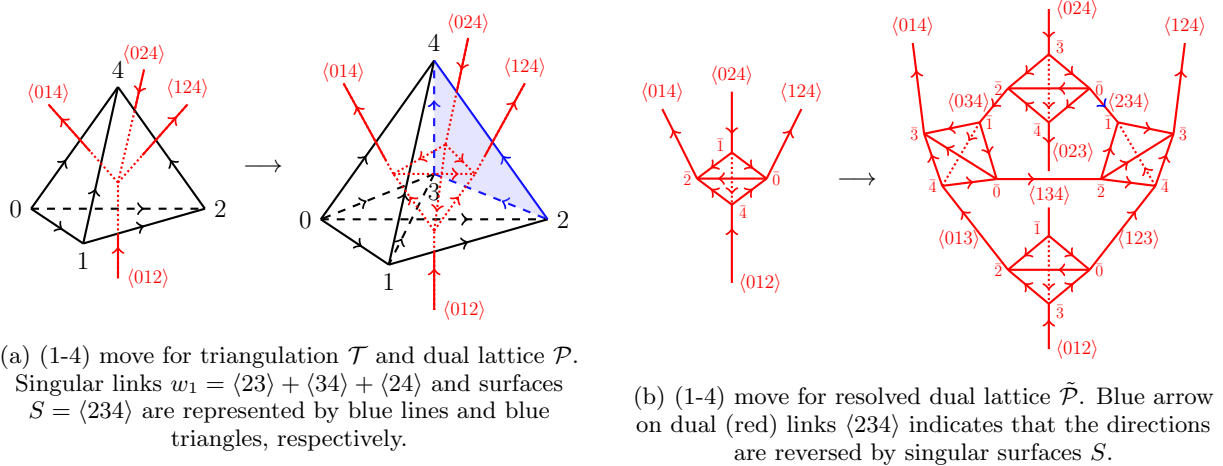


FIG. 18: A (1-4) move.

B. FSLU transformations and consistent conditions for fixed-point states

With the above setup of discrete spin structures and Kasteleyn orientation construction on a 3D lattice, we can now use the FSLU transformation to classify 3D FSPT states systematically.

1. Fermion parity conservation and the obstruction of Kitaev's Majorana chain decoration

Similar to the 2D case, our 3D model has two types of fermionic degrees of freedom. The first type is the complex fermion $c_{\langle ijkl \rangle}$, which resides at the center of tetrahedron $\langle ijkl \rangle$ of triangulation \mathcal{T} of the space manifold. In the special group super-cohomology wavefunction, the c fermion parity P_f^c is unchanged under (2-3) and (1-4) moves. If we use $n_3(g_i, g_j, g_k, g_l) = 0, 1$ to denote the number of c fermions at tetrahedron $\langle ijkl \rangle$, then the parity conserved condition becomes $dn_3 = 0 \pmod{2}$. Therefore, n_3 is an element of $H^3(G_b, \mathbb{Z}_2)$. This is not true if we introduce the second type of fermion.

The second type of fermion, complex fermion $a_{\langle ijk \rangle}$, resides on triangle $\langle ijk \rangle$ of \mathcal{T} . Similar to the 2D case, we also separate fermion $a_{\langle ijk \rangle}$ into two Majorana fermions:

$$\gamma_{ijkA} = a_{\langle ijk \rangle} + a_{\langle ijk \rangle}^\dagger, \quad (35)$$

$$\gamma_{ijkB} = \frac{1}{i} \left(a_{\langle ijk \rangle} - a_{\langle ijk \rangle}^\dagger \right). \quad (36)$$

The Majorana fermions γ_{ijkA} and γ_{ijkB} reside on the two sides of triangle $\langle ijk \rangle$, or dually, on two ends of the link in $\tilde{\mathcal{P}}$ dual to triangle $\langle ijk \rangle$. Our convention is that the dual link (we also use $\langle ijk \rangle$ to denote the dual link) has direction from vertex $\langle ijkA \rangle$ to $\langle ijkB \rangle$. As such, the fermion parity operator of a fermion or γ fermion at triangle $\langle ijk \rangle$ is $P_f^\gamma = -i\gamma_{ijkA}\gamma_{ijkB}$.

Now we decorate Kitaev's Majorana chains onto the loops in dual lattice \mathcal{P} . We introduce a \mathbb{Z}_2 cochain $\tilde{n}_2(g_i, g_j, g_k) = 0, 1$ to specify the decoration configuration of Kitaev's Majorana chain. If there is a Kitaev chain that goes through link $\langle ijk \rangle$ in \mathcal{P} (see the green links in Fig. 3 and figures in Eq. (40)), then we set $\tilde{n}_2(g_i, g_j, g_k) = 1$. On the other hand, $\tilde{n}_2(g_i, g_j, g_k) = 0$ means there is no Kitaev chain. The Kitaev chain decorations can be translated to dimer configurations of Majorana pairs in the resolved dual lattice $\tilde{\mathcal{P}}$. $\tilde{n}_2(g_i, g_j, g_k) = 0$ indicates vacuum pairing, i.e., the two Majorana fermions at triangle $\langle ijk \rangle$ are paired up from $\langle ijkA \rangle$ to $\langle ijkB \rangle$. If $\tilde{n}_2(g_i, g_j, g_k) = 1$, then γ_{ijkA} and γ_{ijkB} are paired up with other nearby Majorana fermions separately, similar to the construction of Kitaev's Majorana chain (see figures of Eq. (41), where gray ellipses indicate paired Majorana fermions).

As we are constructing an SPT state without intrinsic anyonic excitations, the decorated Kitaev chain should form a closed loop without ends. Therefore, similar to the 2D case, we have the equation $d\tilde{n}_2 = 0 \pmod{2}$, which means that the cochain \tilde{n}_2 is an element of $H^2(G_b, \mathbb{Z}_2)$. It is possible that all four faces of a tetrahedron $\langle 0123 \rangle$ in \mathcal{T} are decorated with Kitaev chains, i.e., $d\tilde{n}_2(g_0, g_1, g_2, g_3) = 4$. There are ambiguities in pairing four Majorana fermions inside the tetrahedron. For the total three possible pairings, we use the convention that the Majorana fermion $\bar{0}$ is

paired to $\bar{2}$ and $\bar{1}$ is paired to $\bar{3}$ (see Fig. 19). One can also choose other conventions which essentially produce the same results [73].

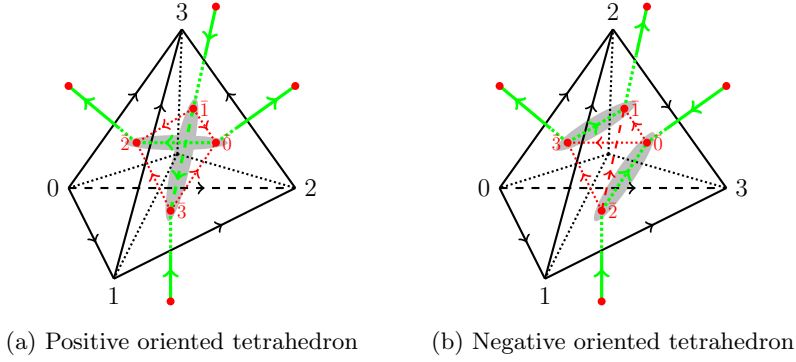


FIG. 19: Resolution of four strings of Kitaev's Majorana chains meeting at one tetrahedron. If four strings meet at one tetrahedron, we should pair the Majorana fermions $\bar{0}$ to $\bar{2}$ and $\bar{1}$ to $\bar{3}$, respectively (gray ellipses). The green lines on $\tilde{\mathcal{P}}$ indicate that these lines are decorated by Kitaev chains.

Now we turn to the Pachner moves for different triangulations. We find that the Majorana fermion parity is changed under a (2-3) move if and only if

$$Sq^2(\tilde{n}_2)(g_0, g_1, g_2, g_3, g_4) = \tilde{n}_2(g_0, g_1, g_2)\tilde{n}_2(g_2, g_3, g_4) = 1. \quad (37)$$

We use the notation $Sq^2(\tilde{n}_2) = \tilde{n}_2^2 = \tilde{n}_2 \smile \tilde{n}_2$ later. This can be obtained by directly checking the property of Kasteleyn orientation for the loops in the transition graph of two Majorana dimer states for 64 kinds of string configurations of each (2-3) move (see Supplementary Material for details). To compensate for the Majorana fermion parity changes, the fermion parity of the fermions at the center of tetrahedron should also be changed, leading to the (mod 2) equation

$$dn_3 = \tilde{n}_2 \smile \tilde{n}_2, \quad (38)$$

or more explicitly

$$n_3(g_1, g_2, g_3, g_4) + n_3(g_0, g_2, g_3, g_4) + n_3(g_0, g_1, g_3, g_4) + n_3(g_0, g_1, g_2, g_4) + n_3(g_0, g_1, g_2, g_3) = \tilde{n}_2(g_0, g_1, g_2)\tilde{n}_2(g_2, g_3, g_4). \quad (39)$$

The above equation shows that the cocycle equation of n_3 is twisted by \tilde{n}_2^2 , which is different from $dn_3 = 0$ in the special group super-cohomology model [42]. The above equation for n_3 has solutions if and only if $Sq^2(\tilde{n}_2)$ is the trivial element in $H^4(G_b, \mathbb{Z}_2)$.

2. Fermionic symmetric local unitary transformations

After fermion decoration, the standard (2-3) move Fig. 16 becomes a fermionic unitary transformation between the fermionic Fock spaces on two different triangulation lattices \mathcal{T} (left) and \mathcal{T}' (right). An example of this standard F move, which changes the fermion parity of Majorana fermions, is [on lattice \mathcal{T} , \mathcal{P} in Eq. (40) and on $\tilde{\mathcal{P}}$ in Eq. (41)]:

$$\Psi \left(\begin{array}{c} \text{tetrahedron } \mathcal{T} \\ \text{vertices } 0, 1, 2, 3, 4 \\ \text{strings } \langle 023 \rangle, \langle 034 \rangle, \langle 234 \rangle, \langle 024 \rangle, \langle 012 \rangle, \langle 014 \rangle, \langle 124 \rangle \end{array} \right) = F(g_0, g_1, g_2, g_3, g_4) \Psi \left(\begin{array}{c} \text{tetrahedron } \mathcal{T}' \\ \text{vertices } 0, 1, 2, 3, 4 \\ \text{strings } \langle 023 \rangle, \langle 034 \rangle, \langle 234 \rangle, \langle 013 \rangle, \langle 014 \rangle, \langle 124 \rangle \end{array} \right), \quad (40)$$

$$\Psi \left(\begin{array}{c} 023B \quad 034B \quad 234A \\ \text{---} \quad \text{---} \quad \text{---} \\ 023A \quad 034A \quad 234B \\ \text{---} \quad \text{---} \quad \text{---} \\ 024B \quad 024A \\ \text{---} \quad \text{---} \\ 012A \quad 124B \\ \text{---} \quad \text{---} \\ 012B \quad 014A \quad 124A \end{array} \right) = F(g_0, g_1, g_2, g_3, g_4) \Psi \left(\begin{array}{c} 023B \quad 034B \quad 234A \\ \text{---} \quad \text{---} \quad \text{---} \\ 013A \quad 034A \quad 134B \\ \text{---} \quad \text{---} \quad \text{---} \\ 011B \quad 134A \quad 234B \\ \text{---} \quad \text{---} \quad \text{---} \\ 123B \quad 123A \\ \text{---} \quad \text{---} \\ 012A \quad 124B \\ \text{---} \quad \text{---} \\ 012B \quad 014A \quad 124A \end{array} \right), \quad (41)$$

where the F operator is given by

$$F(g_0, g_1, g_2, g_3, g_4) = \nu_4(g_0, g_1, g_2, g_3, g_4) c_{(0124)}^{\dagger n_3(0124)} c_{(0234)}^{\dagger n_3(0234)} c_{(0123)}^{n_3(0123)} c_{(0134)}^{n_3(0134)} c_{(1234)}^{n_3(1234)} X[\tilde{n}_2(g_i, g_j, g_k)]. \quad (42)$$

Here, $c_{(0124)}^{\dagger n_3(0124)}$ is the abbreviation of $c_{(0124)}^{\dagger n_3(g_0, g_1, g_2, g_4)}$, which is the creation operator for c fermions at tetrahedron (0124) , etc. The $X[\tilde{n}_2]$ operator in the above F move from the resolved dual lattice $\tilde{\mathcal{P}}$ to $\tilde{\mathcal{P}}'$ has the following general expression:

$$X[\tilde{n}_2(g_i, g_j, g_k)] = P_{\tilde{\mathcal{P}}} \cdot \gamma_{012A}^{\tilde{n}_2^2(g_0, g_1, g_2, g_3, g_4)}, \quad (43)$$

$$P_{\tilde{\mathcal{P}}} = \left(\prod_{\text{loop } i \text{ in } (\tilde{\mathcal{P}}, \tilde{\mathcal{P}}')} 2^{(L_i - 1)/2} \right) \left(\prod_{\text{Majorana pairs } \langle a, b \rangle \text{ in } \tilde{\mathcal{P}}} P_{a, b} \right) \left(\prod_{\text{link } \langle ijk \rangle \notin \tilde{\mathcal{P}}} P_{ijkA, ijkB} \right),$$

where $2L_i$ is the length of the i -th loop in the transition graph of dimer configurations in $\tilde{\mathcal{P}}$ and $\tilde{\mathcal{P}}'$ and $P_{a, b} = (1 - i\gamma_a\gamma_b)/2$ is the projection operator for Majorana pairs $\langle a, b \rangle$ (from vertex a to vertex b). The projection operators in the second parenthesis project the state in the right figure to the Majorana dimer configuration states in the left figure. The projection operators in the third parenthesis are the vacuum projection operators for those Majorana fermions that do not appear in the left figure explicitly (this is similar to the projection $P_{02A, 02B}$ in Eq. (25) of the 2D case). An explicit expression of X for the Majorana pair configuration in Eqs. (40) and (41) is

$$X[\tilde{n}_2] = 2 (P_{024B, 234B} P_{012A, 024A}) (P_{013A, 013B} P_{123A, 123B} P_{134A, 134B}) \gamma_{012A}. \quad (44)$$

Note that the normalization factor in the front of a general X operator is the same as Eq. (26). For the F move in Eqs. (40) and (41), there are only one loop in the Majorana dimer transition graph with length bigger than two: $012A$ - $024A$ - $024B$ - $234B$ - $123A$ - $123B$ - $012A$. So the normalization factor is $2^{(6/2-1)/2} = 2$, as shown in Eq. (44).

When the F move changes the Majorana fermion parity, the last term of the X operator is the Majorana fermion creation or annihilation operators, which changes the fermion parity of the state. We check that, for all possible Kitaev's Majorana chain configurations, the loop-breaking Kasteleyn orientation in the transition graph of the two Majorana dimer states always contains vertex $012A$. Therefore, the X operator with γ_{012A} should indeed project the state to the desired Majorana configuration state (not 0). In fact, γ_{234B} is also an allowed choice. We calculate the consistent equation of ν_4 for both choices later.

The fermionic local unitary transformation F should also be G_b symmetric.

$$F(g_0, g_1, g_2, g_3, g_4) = F(gg_0, gg_1, gg_2, gg_3, gg_4), \quad (45)$$

for all $g \in G_b$ if G_b is a unitary symmetry group. So, $\nu_4(g_0, g_1, g_2, g_3, g_4)$, $n_3(g_0, g_1, g_2, g_3)$, and $\tilde{n}_2(g_0, g_1, g_2)$ are all cochains that are invariant under unitary g action. (We note that $\nu_4(gg_0, gg_1, gg_2, gg_3, gg_4) = \nu_4^*(g_0, g_1, g_2, g_3, g_4)$ for anti-unitary g action.)

Similar to the 1D and 2D cases, we can use FSLU to redefine the basis state $|\{g_n\}\rangle$ as

$$|\{g_n\}\rangle' = U_{\mu_3, \mu_2} |\{g_n\}\rangle = \prod_{\langle ijkl \rangle} \mu_3(g_i, g_j, g_k, g_l)^{s_{\langle ijkl \rangle}} \prod_{\langle ijk \rangle} \left[f_{ijkB}^{m_2(g_i, g_j, g_k)} f_{ijkA}^{m_2(g_i, g_j, g_k)} \right] \cdot \prod_{\langle ijkl \rangle} \left[f_{jklA}^{\dagger m_2(g_j, g_k, g_l)} f_{ijlA}^{\dagger m_2(g_i, g_j, g_l)} f_{iklB}^{\dagger m_2(g_i, g_k, g_l)} f_{ijkB}^{\dagger m_2(g_i, g_j, g_k)} \right] |\{g_n\}\rangle, \quad (46)$$

where we first create four complex fermions f_{jklA} , f_{ijlA} , f_{iklB} and f_{ijkB} near the four triangles of the tetrahedron $\langle ijkl \rangle$ ($i < j < k < l$), and then annihilate the two fermions f_{ijkA} and f_{ijkB} on the two sides of triangle $\langle ijk \rangle$ when gluing the two tetrahedra sharing triangle $\langle ijk \rangle$. To preserve the fermion parity and be symmetric, m_2 should be a 2-cocycle (with \mathbb{Z}_2 coefficient): $m_2(gg_i, gg_j, gg_k) = m_2(g_i, g_j, g_k)$ and $dm_2(g_i, g_j, g_k, g_l) = 0$. $\mu_3(g_i, g_j, g_k, g_l)$ is a phase factor associated with tetrahedron $\langle ijkl \rangle$, and $s_{\langle ijkl \rangle} = \pm 1$ denotes the orientation of the tetrahedron. After tedious calculation of eliminating all f fermions in the new F move operator $F' = U_{\mu_3, m_2} F U_{\mu_3, m_2}^\dagger$, one find that the phase factor in Eq. (42) becomes

$$\nu'_4(g_0, g_1, g_2, g_3, g_4) = \nu_4(g_0, g_1, g_2, g_3, g_4) \frac{\mu_3(g_1, g_2, g_3, g_4) \mu_3(g_0, g_1, g_3, g_4) \mu_3(g_0, g_1, g_2, g_3)}{\mu_3(g_0, g_2, g_3, g_4) \mu_3(g_0, g_1, g_2, g_4)} (-1)^{Sq^2(m_2)(g_0, g_1, g_2, g_3, g_4)}, \quad (47)$$

where $Sq^2(m_2)(g_0, g_1, g_2, g_3, g_4) = (m_2 \smile m_2)(g_0, g_1, g_2, g_3, g_4) = m_2(g_0, g_1, g_2) m_2(g_2, g_3, g_4)$ is the Steenrod square of m_2 . If ν_4 and ν'_4 can be related by the above equation, then they correspond to the same 3D FSPT phase. This is also consistent with the general result in Eq. (14) [42].

In addition to the standard (2-3) move, there are (2-0) moves as FSLU that can change the vertex number. One example of the Majorana fermion configuration for a (2-0) move is

$$\Psi \left(\begin{array}{c} \text{Diagram 1: A tetrahedron with vertices } g_0, g_1, g_2, g_3 \text{ and internal fermions } c_{(0123)}^\dagger, \bar{c}_{(0123)} \end{array} \right) = \frac{1}{|G_b|^{1/2}} c_{(0123)}^{\dagger n_3(g_0, g_1, g_2, g_3)} \bar{c}_{(0123)}^{\dagger n_3(g_0, g_1, g_2, g_3)} X[\tilde{n}_2(g_i, g_j, g_k)] \Psi \left(\begin{array}{c} \text{Diagram 2: A tetrahedron with vertices } g_0, g_1, g_2, g_3 \end{array} \right), \quad (48)$$

$$\Psi \left(\begin{array}{c} \text{Diagram 3: A complex Majorana fermion configuration with vertices } g_0, g_1, g_2, g_3 \text{ and many internal fermions } c_{(0123)}^\dagger, \bar{c}_{(0123)} \end{array} \right) = \frac{1}{|G_b|^{1/2}} c_{(0123)}^{\dagger n_3(g_0, g_1, g_2, g_3)} \bar{c}_{(0123)}^{\dagger n_3(g_0, g_1, g_2, g_3)} X[\tilde{n}_2(g_i, g_j, g_k)] \Psi \left(\begin{array}{c} \text{Diagram 4: A tetrahedron with vertices } g_0, g_1, g_2, g_3 \end{array} \right). \quad (49)$$

The notations and conventions of vacuum pairs are similar to those in the 2D case in the discussion following Eq. (30). $c_{(0123)}$ and $\bar{c}_{(0123)}$ fermions are at the centers of the lower and upper tetrahedra respectively. An explicit expression for the X operator is

$$X[\tilde{n}_2] = 2^{3/2} P_{023B, 012B'} P_{012A', 023A} P_{013A', 013B} P_{123A', 123B} P_{013A, 013B'} P_{123A, 123B'}. \quad (50)$$

Note that the normalization factor in the front of X operator is $(2^{(4/2-1)/2})^3 = 2^{3/2}$, according to Eq. (26). Because there are three loops in the Majorana dimer transition graph with length bigger than two: $012B'-023B-023A-012A'-012B'$, $013B-013A'-013B'-013A-013B$, and $123B-123A'-123B'-123A-123B$. Using two kinds of (2-0) moves (the other one is shown in Supplementary Material) and the standard (2-3) move, we can deduce all (1-4) moves and other (2-3) moves from the standard F move in Eqs. (40) and (41) (see Supplementary Material for all details).

3. Fermionic hexagon equations

The consistent equation for the moves defined in the above subsection is the fermionic hexagon equation (see Fig. 20), which is a higher dimensional version of the fermionic pentagon equation for (2+1)D fermionic topological

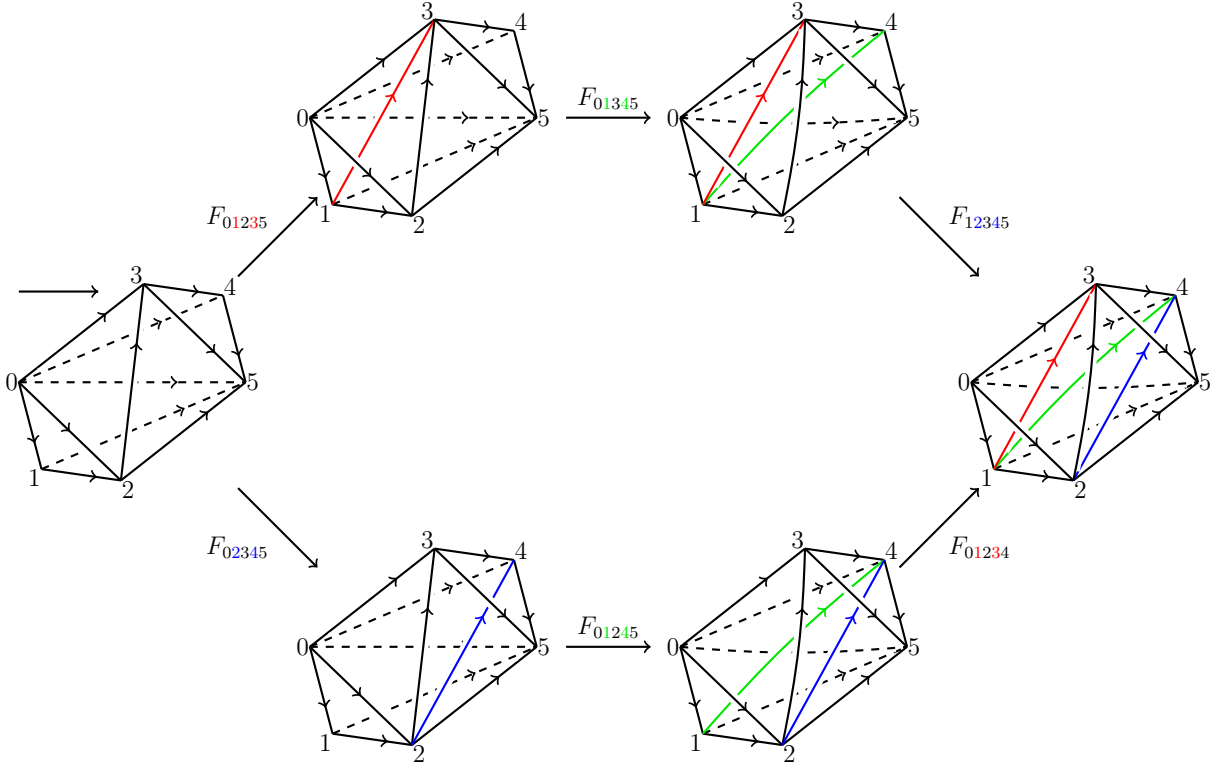


FIG. 20: Fermionic fusion hexagon equation. All of the F moves are of the standard (2-3) move (see Fig. 40 and Fig. 41). Colored numbers i and j in the subscript of F indicate that the link (ij) with the same color is added after this F move. All six F moves do not introduce new singular lines and surfaces. There is a global direction from left to right such that the vertex with the smaller number has the earlier time.

phases [63]. Reordering the fermionic operators in the fermionic hexagon equation will twist the bosonic cocycle equation for ν_4 :

$$(d\nu_4)(g_0, g_1, g_2, g_3, g_4, g_5) = \mathcal{O}(g_0, g_1, g_2, g_3, g_4, g_5). \quad (51)$$

The phase twist or obstruction on the left-hand side has three terms

$$\mathcal{O} = \mathcal{O}_c \mathcal{O}_{c\gamma} \mathcal{O}_\gamma, \quad (52)$$

resulting from three different fermion phase factors: (1) \mathcal{O}_c from reordering c fermions, (2) $\mathcal{O}_{c\gamma}$ from reordering c fermions and γ Majorana fermions, and (3) \mathcal{O}_γ from reordering γ Majorana fermions. The final result of the phase twist is

$$\begin{aligned} \mathcal{O}(012345) = & (-1)^{(n_3 \smile_1 n_3)(012345) + (n_3 \smile_2 dn_3)(012345) + dn_3(02345)dn_3(01245)dn_3(01234)} \\ & \cdot i^{dn_3(01235)dn_3(02345) + dn_3(01345)dn_3(12345)} \cdot (-i)^{dn_3(02345)dn_3(01245) + dn_3(02345)dn_3(01234)}. \end{aligned} \quad (53)$$

Here, (012345) is the abbreviation of $(g_0, g_1, g_2, g_3, g_4, g_5)$, etc. Note that the obstruction depends only on n_3 and dn_3 (or \tilde{n}_2^2 through the fermion parity equation $dn_3 = \tilde{n}_2^2$). In the following, we derive the above obstruction equation in detail.

The first part \mathcal{O}_c contains the special group super-cohomology results [42], which are obtained by reordering c fermion operators.

$$\begin{aligned} \mathcal{O}_c(012345) = & (-1)^{[Sq^2(n_3) + dn_3 \smile_2 n_3](012345)} = (-1)^{[n_3 \smile_1 n_3 + dn_3 \smile_2 n_3](012345)} \\ = & (-1)^{n_3(0345)n_3(0123) + n_3(0145)n_3(1234) + n_3(0125)n_3(2345)} \\ & \cdot (-1)^{dn_3(01234)n_3(0145) + dn_3(02345)n_3(0125) + dn_3(01234)n_3(1245) + dn_3(01345)n_3(1235) + dn_3(01234)n_3(2345) + dn_3(01245)n_3(2345)}. \end{aligned} \quad (54)$$

Here, \smile_i is Steenrod's i -th cup product [74]. Apart from the term $Sq^2(n_3)$, there is an additional term $dn_3 \smile_2 n_3$ because of $dn_3 = \tilde{n}_2^2 \neq 0$.

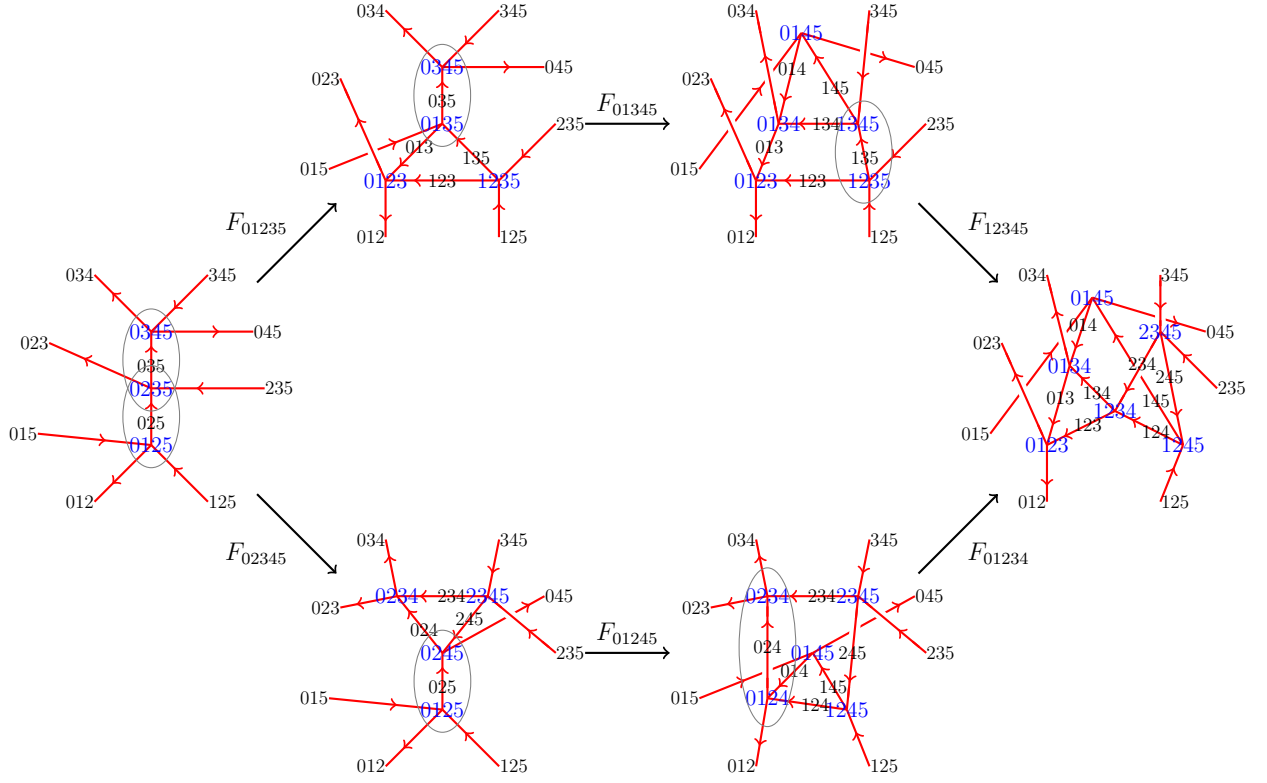


FIG. 21: Fermionic fusion hexagon equation on dual lattice \mathcal{P} .

The second part $\mathcal{O}_{c\gamma}$ comes from reordering c fermions and γ Majorana fermions (we always put c fermions in front of γ fermions). For example, the composition of F_{01345} and F_{01235} gives a sign $(-1)^{dn_3(01345)dn_3(01235)}$. In total, the upper path of three F moves gives the power $dn_3(01345)dn_3(01235) + dn_3(12345)dn_3(01345) + dn_3(12345)dn_3(01235)$, whereas the lower path gives $dn_3(01245)dn_3(01234) + dn_3(02345)dn_3(01234) + dn_3(02345)dn_3(01245)$. The final result is then

$$\begin{aligned} \mathcal{O}_{c\gamma}(012345) &= (-1)^{(dn_3 \smile_3 dn_3)(g_0, g_1, g_2, g_3, g_4, g_5)} \\ &= (-1)^{dn_3(01245)dn_3(01234) + dn_3(01235)dn_3(01345) + dn_3(02345)dn_3(01234) + dn_3(02345)dn_3(01245) + dn_3(01235)dn_3(12345) + dn_3(01345)dn_3(12345)}. \end{aligned} \quad (55)$$

After adding coboundary $(-1)^{d(n_3 \smile_3 dn_3)} = (-1)^{dn_3 \smile_3 dn_3 + n_3 \smile_2 dn_3 + dn_3 \smile_2 n_3}$ to the combination of the phase factor \mathcal{O}_c and $\mathcal{O}_{c\gamma}$, we obtain a simpler expression.

$$\mathcal{O}_c \mathcal{O}_{c\gamma} = (-1)^{n_3 \smile_1 n_3 + n_3 \smile_2 dn_3}. \quad (56)$$

Note that adding the coboundary changes the $U(1)$ -cochain $\nu_4 \rightarrow (-1)^{n_3 \smile_3 dn_3} \nu_4$.

We now turn to the subtlest part \mathcal{O}_γ coming from a decorated Majorana chain. In addition to ± 1 , \mathcal{O}_γ can take values in $\pm i$ (See Supplementary Material for the physical origin of this purely imaginary phase factor). If all six F moves do not change the Majorana fermion parity, then X_γ operators in F moves are merely projections with an even number of γ Majorana operators. The c fermions and Majorana fermions are decoupled, and both $\mathcal{O}_{c\gamma}$ and \mathcal{O}_γ are trivial. The obstruction \mathcal{O} is the same as the special group super-cohomology result. Therefore, we only need to check the case in which some of the six F moves in Fig. 20 change the Majorana fermion parity, i.e., some of $\tilde{n}_2^2(01234)$, $\tilde{n}_2^2(01245)$, $\tilde{n}_2^2(02345)$, $\tilde{n}_2^2(01345)$, $\tilde{n}_2^2(01235)$, and $\tilde{n}_2^2(12345)$ are equal to one. We denote the six X operators in F moves as $X_{01235} = P_1 \gamma_{012A}^{\tilde{n}_2^2(01235)}$, $X_{01345} = P_2 \gamma_{013A}^{\tilde{n}_2^2(01345)}$, $X_{12345} = P_3 \gamma_{123A}^{\tilde{n}_2^2(12345)}$, $X_{02345} = P_1 \gamma_{023A}^{\tilde{n}_2^2(02345)}$, $X_{01245} = P_4 \gamma_{012A}^{\tilde{n}_2^2(01245)}$, and $X_{01234} = P_5 \gamma_{012A}^{\tilde{n}_2^2(01234)}$. Here, P_i means the projection operator onto the Majorana chain configuration of the i -th figure in the hexagon equation. \mathcal{O}_γ is defined as the Majorana chain phase difference of the upper and lower paths in hexagon equation

$$X_{02345} X_{01245} X_{01234} |\text{final}\rangle = \mathcal{O}_\gamma(012345) X_{01235} X_{01345} X_{12345} |\text{final}\rangle, \quad (57)$$

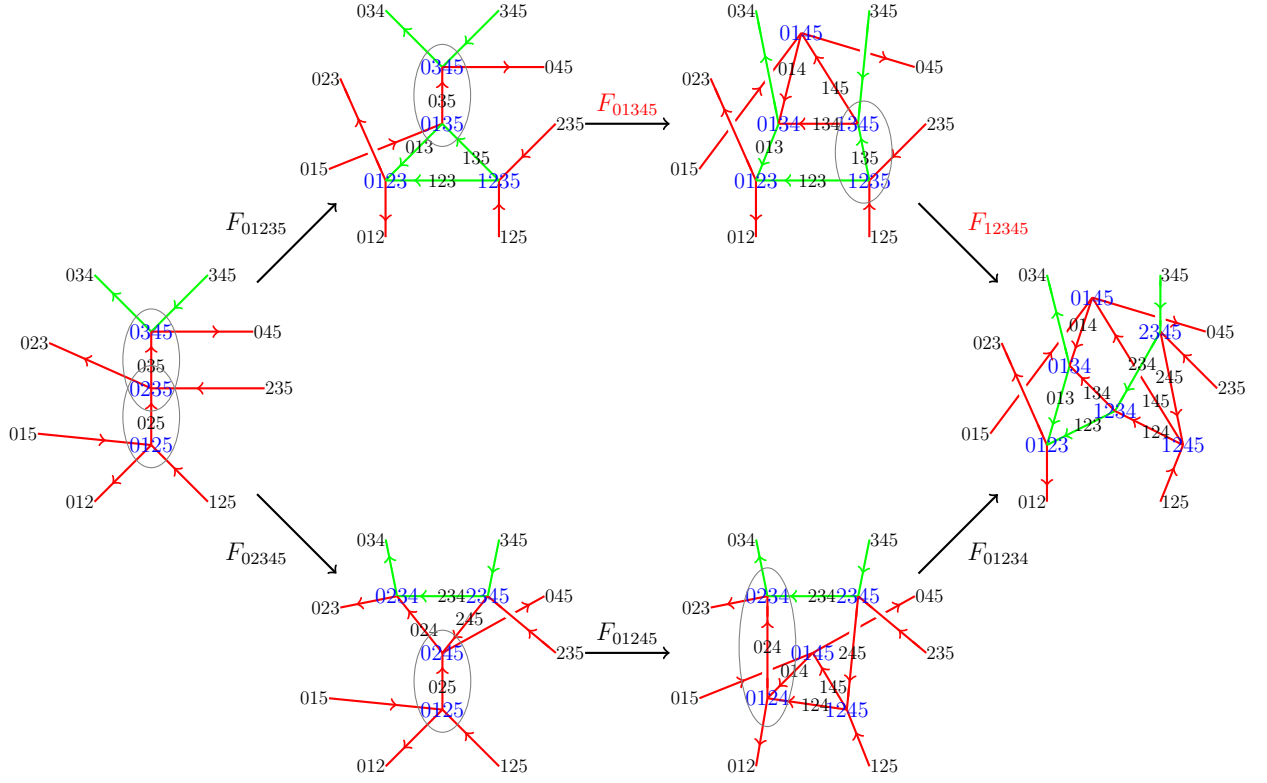


FIG. 22: One example of Kitaev's Majorana chain decoration configuration of fermionic fusion hexagon equation. Green lines indicate that these dual links are decorated by Kitaev's Majorana chains. Among the six F moves for this configuration, only F_{01345} and F_{12345} (red color in the figure) change the Majorana fermion parity. Therefore, this choice of $\tilde{n}_2(g_i, g_j, g_k)$ belongs to the $(0, 1, 1, 0, 0, 0)$ row in Table III and has obstruction $\mathcal{O}_\gamma = i$.

where $|\text{final}\rangle$ is the state of the Majorana chain configuration in the rightmost figure of the hexagon equation Fig. 21. We can calculate \mathcal{O}_γ from the expression

$$\begin{aligned} \mathcal{O}_\gamma(012345) &= \langle \text{final} | X_{12345}^\dagger X_{01345}^\dagger X_{01235}^\dagger X_{02345} X_{01245} X_{01234} | \text{final} \rangle \\ &= \langle \text{final} | \gamma_{123A}^{\tilde{n}_2^2(12345)} P_3 \gamma_{013A}^{\tilde{n}_2^2(01345)} P_2 \gamma_{012A}^{\tilde{n}_2^2(01235)} P_1 P_1 \gamma_{023A}^{\tilde{n}_2^2(02345)} P_4 \gamma_{012A}^{\tilde{n}_2^2(01245)} P_5 \gamma_{012A}^{\tilde{n}_2^2(01234)} | \text{final} \rangle. \end{aligned} \quad (58)$$

The above equation suggests that \mathcal{O}_γ depends only on the values of $\tilde{n}_2^2(01235)$, $\tilde{n}_2^2(01345)$, $\tilde{n}_2^2(12345)$, $\tilde{n}_2^2(02345)$, $\tilde{n}_2^2(01245)$, and $\tilde{n}_2^2(01234)$, i.e., the Majorana parity changes of the six F moves.

Consider, for example, the case in which only F_{01345} and F_{12345} change the Majorana fermion parity $[(0, 1, 1, 0, 0, 0)]$ in the eighth row of Table III. See Fig. 22 for an example of $\tilde{n}_2(g_i, g_j, g_k)$ satisfying this condition. We can expand projection operators P_i to Majorana fermion operators. For simplicity, we can consider the term with only contributions $-i\gamma_{013A}\gamma_{013B}$ and $-i\gamma_{123A}\gamma_{123B}$ from P_1 . We can also add $-i\gamma_{013B}\gamma_{123B}$, which equals 1 when acting on $|\text{final}\rangle$ in front of this state. The result is then

$$\begin{aligned} \mathcal{O}_\gamma(012345)|_{(0,1,1,0,0,0)} &= \langle \text{final} | \gamma_{123A} P_3 \gamma_{013A} P_2 P_1 P_4 P_5 P_6 | \text{final} \rangle \\ &= \langle \text{final} | \gamma_{123A} \gamma_{013A} (-i\gamma_{013A}\gamma_{013B}) (-i\gamma_{123A}\gamma_{123B}) (-i\gamma_{013B}\gamma_{123B}) | \text{final} \rangle \\ &= i. \end{aligned} \quad (59)$$

We assume that there are only two Kitaev strings meeting at tetrahedron $\langle 0123 \rangle$. (this is always true for all possible choices of $\tilde{n}_2(g_i, g_j, g_k)$ that belong to the eighth row of Table III.) Similarly, one can calculate other choices of \tilde{n}_2 , and at last obtain the results listed in Table III. The final results can be summarized to the expression

$$\mathcal{O}_\gamma(012345) = i \tilde{n}_2^2(01235) \tilde{n}_2^2(02345) + \tilde{n}_2^2(01345) \tilde{n}_2^2(12345) (-i) \tilde{n}_2^2(02345) \tilde{n}_2^2(01245) + \tilde{n}_2^2(02345) \tilde{n}_2^2(01234) (-1) \tilde{n}_2^2(02345) \tilde{n}_2^2(01245) \tilde{n}_2^2(01234). \quad (60)$$

Combining this \mathcal{O}_γ result with $\mathcal{O}_c \mathcal{O}_{c_\gamma}$ in Eq. (56), we obtain the obstruction claimed in Eq. (53).

TABLE III: Calculations of \mathcal{O}_γ from all possible Kitaev chain configurations in the hexagon equation. The first column has entries $(\tilde{n}_2^2(01235), \tilde{n}_2^2(01345), \tilde{n}_2^2(12345), \tilde{n}_2^2(02345), \tilde{n}_2^2(01245), \tilde{n}_2^2(01234))$, indicating whether the six F moves in the hexagon equation change the Majorana fermion parity. The second column shows the γ operators appearing in Eq. (58). The third and fourth columns are lines of Majorana dimer pairs (\emptyset means there are no $\tilde{n}_2(g_i, g_j, g_k)$ that have two or four strings at tetrahedron $\langle 0123 \rangle$). The last two columns are the values of \mathcal{O}_γ for $\tilde{n}_2(g_i, g_j, g_k)$ belonging to this row (the last column but one uses the convention γ_{012A} in Eq. (43), and the last column uses the convention γ_{234B}). Nontrivial results are labelled in red or blue. The results in this table can be summarized to the expression shown in Eq. (60) for convention γ_{012A} and in Eq. (61) for convention γ_{234B} .

fermion parity changes	γ operators in Eq. (58)	line (2 strings at $\langle 0123 \rangle$)	line (4 strings at $\langle 0123 \rangle$)	$\mathcal{O}_\gamma _{012A}$	$\mathcal{O}_\gamma _{234B}$
(0, 0, 0, 0, 0, 0)	—	—	—	1	1
(1, 1, 0, 0, 0, 0)	$\gamma_{012A}, \gamma_{013A}$	012A-013B-013A	\emptyset	1	$-i$
(1, 0, 1, 0, 0, 0)	$\gamma_{012A}, \gamma_{123A}$	012A-123B-123A	\emptyset	1	$-i$
(1, 0, 0, 1, 0, 0)	$\gamma_{012A}, \gamma_{023A}$	012A-023A	\emptyset	i	i
(1, 0, 0, 0, 1, 0)	$\gamma_{012A}^2 = 1$	—	—	1	1
(1, 0, 0, 0, 0, 1)	$\gamma_{012A}^2 = 1$	—	—	1	1
(0, 1, 1, 0, 0, 0)	$\gamma_{013A}, \gamma_{123A}$	013A-013B-123B-123A	\emptyset	i	1
(0, 1, 0, 1, 0, 0)	$\gamma_{013A}, \gamma_{023A}$	013A-013B-023A	\emptyset	1	1
(0, 1, 0, 0, 1, 0)	$\gamma_{013A}, \gamma_{012A}$	013A-013B-012A	\emptyset	1	1
(0, 1, 0, 0, 0, 1)	$\gamma_{013A}, \gamma_{012A}$	013A-013B-012A	\emptyset	1	1
(0, 0, 1, 1, 0, 0)	$\gamma_{123A}, \gamma_{023A}$	123A-123B-023A	\emptyset	1	1
(0, 0, 1, 0, 1, 0)	$\gamma_{123A}, \gamma_{012A}$	123A-123B-012A	\emptyset	1	1
(0, 0, 1, 0, 0, 1)	$\gamma_{123A}, \gamma_{012A}$	123A-123B-012A	\emptyset	1	1
(0, 0, 0, 1, 1, 0)	$\gamma_{023A}, \gamma_{012A}$	023A-012A	\emptyset	$-i$	1
(0, 0, 0, 1, 0, 1)	$\gamma_{023A}, \gamma_{012A}$	023A-012A	\emptyset	$-i$	1
(0, 0, 0, 0, 1, 1)	$\gamma_{012A}^2 = 1$	—	—	1	i
(1, 1, 0, 0, 1, 1)	$\gamma_{013A}, \gamma_{012A}^3$	012A-013B-013A, 012A	\emptyset	1	1
(1, 0, 1, 0, 1, 1)	$\gamma_{123A}, \gamma_{012A}^3$	012A-123B-123A, 012A	\emptyset	1	1
(1, 0, 0, 1, 1, 1)	$\gamma_{023A}, \gamma_{012A}^3$	012A-023A, 012A	\emptyset	i	-1
(1, 1, 1, 1, 0, 0)	$\gamma_{012A}, \gamma_{013A}, \gamma_{123A}, \gamma_{023A}$	\emptyset	$\left. \begin{array}{l} 123A-123B-013B-013A \\ 023A-012A \end{array} \right\}$	-1	i
(0, 1, 1, 1, 1, 0)	$\gamma_{013A}, \gamma_{123A}, \gamma_{023A}, \gamma_{012A}$	\emptyset	$\left. \begin{array}{l} 123A-123B-013B-013A \\ 023A-012A \end{array} \right\}$	1	1
(0, 1, 1, 1, 0, 1)	$\gamma_{013A}, \gamma_{123A}, \gamma_{023A}, \gamma_{012A}$	\emptyset	$\left. \begin{array}{l} 123A-123B-013B-013A \\ 023A-012A \end{array} \right\}$	1	1
(1, 1, 1, 1, 1, 1)	$\gamma_{013A}, \gamma_{123A}, \gamma_{023A}, \gamma_{012A}^3$	\emptyset	$\left. \begin{array}{l} 123A-123B-013B-013A \\ 023A-012A \end{array} \right\}$	-1	-1

As discussed above, we can also use the convention $X_{01234} = P_P \tilde{n}_2^2(01234)$ in the definition of a standard F move. The results using different conventions may differ from each other by some coboundaries. The obstruction from Majorana fermions in the convention γ_{234B} is

$$\mathcal{O}_\gamma(012345) = i \tilde{n}_2^2(01235) \tilde{n}_2^2(02345) + \tilde{n}_2^2(01245) \tilde{n}_2^2(01234) (-i) \tilde{n}_2^2(01235) \tilde{n}_2^2(01345) + \tilde{n}_2^2(01235) \tilde{n}_2^2(12345) (-1) \tilde{n}_2^2(01235) \tilde{n}_2^2(01345) \tilde{n}_2^2(12345). \quad (61)$$

By checking all possible choices of \tilde{n}_2 numerically, we find that the above expression of \mathcal{O}_γ equals exactly to

$$\mathcal{O}_\gamma(012345) = (-i)^{[\tilde{n}_2 \sim (\tilde{n}_2 \sim 1 \tilde{n}_2)](012345)} (-1)^{\tilde{n}_2^2(01235) \tilde{n}_2^2(02345)}. \quad (62)$$

This can be obtained from the Pontrjagin dual of the four-dimensional spin bordism [75].

We note that although \mathcal{O} takes values in \mathbb{Z}_4 , the additivity property actually requires \mathcal{O} to be a cohomology map on \mathbb{Z}_8 ; see Supplementary Material for details. Thus, to find a solution for ν_4 , we must define an obstruction-free subgroup of $H^2(G_b, \mathbb{Z}_2)$, which is formed by elements $\tilde{n}_2 \in H^2(G_b, \mathbb{Z}_2)$ that simultaneously satisfy $Sq^2(\tilde{n}_2) = 0$ in $H^4(G_b, \mathbb{Z}_2)$ and $\mathcal{O}(\tilde{n}_2) = 0$ in $H^5(G_b, U_T(1))$, where \mathcal{O} is some unknown cohomology operation (to the best of our knowledge) that maps \tilde{n}_2 satisfying $Sq^2(\tilde{n}_2) = 0$ in $H^2(G_b, \mathbb{Z}_2)$ into an element in $H^5(G_b, \mathbb{Z}_8) \subset H^5[G_b, U_T(1)]$. We note that n_3 is completely determined by \tilde{n}_2 and that any solution of $dn_3 = \tilde{n}_2^2$ can be used in the above definition. Together with the special group super-cohomology results, we conclude that the precise mathematical objects that classify 3D FSPT phases with a total symmetry $G_f = G_b \times \mathbb{Z}_2^f$ can also be summarized as three group cohomologies of the symmetry

group G_b , $\tilde{B}H^2(G_b, \mathbb{Z}_2)$, $BH^3(G_b, \mathbb{Z}_2)$, and $H_{\text{rigid}}^4(G_b, U_T(1))$. Commuting projector parent Hamiltonians for all of these FSPT states can also be constructed on arbitrary 3D triangulations with a branching structure.

Finally, let us provide some physical arguments to support our classification scheme for 3D FSPT phases with a total symmetry $G_f = G_b \times \mathbb{Z}_2^f$ when G_b is a unitary symmetry group. (a) From the concept of equivalence classes of FSLU transformations, if two fixed point wavefunctions corresponded to the same phase, there would be a finite depth FSLU circuit connecting the two. Thus, it is obvious that the fixed point wavefunctions have the same algebraic data, e.g., cocycle solutions (up to coboundary transformation) from the the above three group cohomologies of the symmetry group G_b , since these algebraic data only depends on “long distance” physics which can’t be changed by a finite depth FSLU circuit. In fact, finite depth FSLU circuit can at most generate some coboundary transformations, e.g. the transformation defined in Eq.(47). (b) Our constructions are consistent with the spin-cobordism classifications for 3D FSPT phases. (c) Similar to the bosonic 3D SPT states, if we turn on background gauge field G_b and couple it to the 3D FSPT states constructed here, the corresponding G_b flux lines will carry new types of three-loop braiding statistics. Some examples from the $BH^3(G_b, \mathbb{Z}_2)$ layer are studied in a recent work [76]. We believe that nontrivial solutions from the layer $\tilde{B}H^2(G_b, \mathbb{Z}_2)$ will give rise to non-Abelian three-loop braiding statistics, and full details will be studied in our future work.

V. DISCUSSION AND CONCLUSIONS

We have constructed fixed-point wavefunctions for FSPT phases in two and three dimensions based on the novel concept of FSLU transformations. All of these FSPT states admit parent Hamiltonians consisting of commuting projectors on arbitrary triangulations with a branching structure. We believe that our construction will give rise to a complete classification for FSPT states with total symmetry $G_f = G_b \times \mathbb{Z}_2^f$ when G_b is a unitary symmetry group. Mathematically, our constructions naturally define a general group super-cohomology theory that generalizes the so-called special group super-cohomology theory proposed in Ref. 42.

In particular, one can start with a spin manifold in an arbitrary spacial dimension d_{sp} and define the corresponding discrete spin structure via Poincare dual. Then, one can decorate Kitaev’s Majorana chain onto the intersection lines of the G_b symmetry domain walls if the first obstruction vanishes for elements $\tilde{n}_{d_{sp}-1} \in H^{d_{sp}-1}(G_b, \mathbb{Z}_2)$. That is, $Sq^2(\tilde{n}_{d_{sp}+1}) = 0$ in $H^{d_{sp}+1}(G_b, \mathbb{Z}_2)$, and the obstruction-free elements $\tilde{n}_{d_{sp}-1} \in H^{d_{sp}-1}(G_b, \mathbb{Z}_2)$ will give rise to all inequivalent patterns of Majorana chain decoration. Finally, by applying the wavefunction renormalization on arbitrary triangulations, one may derive twisted cocycle equations where the twisted factors define some unknown cohomology map \mathcal{O} that maps elements in $H^{d_{sp}-1}(G_b, \mathbb{Z}_2)$ satisfying $Sq^2(\tilde{n}_{d_{sp}-1}) = 0$ in $H^{d_{sp}+1}(G_b, \mathbb{Z}_2)$ into elements in $H^{d_{sp}+2}(G_b, \mathbb{Z}_8) \subset H^{d_{sp}+2}[G_b, U_T(1)]$, and the second obstruction-free condition requires $\mathcal{O}(\tilde{n}_{d_{sp}-1}) = 0$ in $H^{d_{sp}+2}(G_b, U_T(1))$. Elements $\tilde{n}_{d_{sp}-1} \in H^{d_{sp}-1}(G_b, \mathbb{Z}_2)$ satisfying both the first and second obstruction-free conditions may define a subgroup $\tilde{B}H^{d_{sp}-1}(G_b, \mathbb{Z}_2) \in H^{d_{sp}-1}(G_b, \mathbb{Z}_2)$, which allows us to write down another short exact sequence $0 \rightarrow \mathcal{H}^{d_{sp}+1}[G_f, U_T(1)] \rightarrow H_f^{d_{sp}+1}[G_f, U_T(1)] \rightarrow \tilde{B}H^{d_{sp}-1}(G_b, \mathbb{Z}_2) \rightarrow 0$ to define a general group super-cohomology theory. We note that here $\mathcal{H}^{d_{sp}+1}[G_f, U_T(1)]$ is the special group super-cohomology class defined by Ref. 42.

In future, it would be of great importance to understand the physical properties of 3D FSPT phases classified by general group super-cohomology theory, e.g., understanding the braiding statistics of G_b -flux lines. Of course, constructing time-reversal symmetry-protected topological states with both $T^2 = 1$ and $T^2 = P^f$ (where P^f is the total fermion parity) is another interesting direction. It should also be interesting to investigate the phase transition theory among FSPT phases in arbitrary dimensions.

ACKNOWLEDGMENTS

We thank Zheng-Xin Liu and Jianwei Li for helpful discussions on solving the system of linear Diophantine equations. We also thank Shuo Yang for helping to calculate the equations numerically. ZCG acknowledges start-up support via Direct Grant nos. 4053163 and 3132745 from The Chinese University of Hong Kong and funding from Hong Kongs Research Grants Council (ECS no.2191110, GRF no.14306714). We also would like to thank Tianhe-1A platform at the National Supercomputer Center in Tianjin and Tianhe-2 platform at the National Supercomputer Center in Guangzhou for computational support.

Note added – During the preparation of this work, we noticed a relevant work Ref. 77 considering similar problems. However, our expression for \mathcal{O}_γ is slightly different from Ref. 77.

Appendix A: Kitaev's Majorana chain, fermion parity and Kasteleyn orientation

In this Supplementary Material, we present some basic preliminaries of Kitaev's Majorana chain. The relation of fermion parity and Kasteleyn orientation will also be discussed.

For a p -wave superconductor with zero chemical potential on a chain with N sites, the BCS Hamiltonian is

$$H = - \sum_j (c_j^\dagger c_{j+1} + \text{h.c.}) - \sum_j (c_j c_{j+1} + \text{h.c.}), \quad (\text{A1})$$

where the summation is from $j = 1$ to $N - 1$ (N) for open (periodic) boundary condition. c_{N+1} is identified with c_1 in periodic boundary condition. After introducing two Majorana fermions γ_{2j-1} and γ_{2j} for each complex fermion c_j at site j , i.e.,

$$\gamma_{2j-1} = c_j + c_j^\dagger, \quad (\text{A2})$$

$$\gamma_{2j} = \frac{1}{i}(c_j - c_j^\dagger), \quad (\text{A3})$$

the BCS Hamiltonian becomes a summation of mutually commuting terms of Majorana fermion bilinear form:

$$H = i \sum_j \gamma_{2j} \gamma_{2j+1}. \quad (\text{A4})$$

Since $(i\gamma_{2j}\gamma_{2j+1})^2 = 1$, each term of the above Hamiltonian is a projection operator (up to some constant and scaling). Therefore, the full spectrum of the model can be obtained by specifying $i\gamma_{2j}\gamma_{2j+1} = \pm 1$ for all j .

1. Ground states

The ground state $|GS\rangle$ of the Kitaev chain is defined such that

$$-i\gamma_{2j}\gamma_{2j+1}|GS\rangle = |GS\rangle, \quad \forall j. \quad (\text{A5})$$

One can imagine the two Majorana fermion γ_{2j} and γ_{2j+1} are paired up from the former to the later. Graphically, we can use an oriented link from γ_{2j} to γ_{2j+1} to illustrate the pairing. If we combine these two Majorana fermions to a complex fermion

$$c_{2j,2j+1} = \frac{1}{2}(\gamma_{2j} + i\gamma_{2j+1}), \quad (\text{A6})$$

then the term in the Hamiltonian is exactly the fermion parity operator of the new complex fermion

$$P_f^{2j,2j+1} = -i\gamma_{2j}\gamma_{2j+1} = 1 - 2c_{2j,2j+1}^\dagger c_{2j,2j+1}. \quad (\text{A7})$$

In this language, the γ_{2j} and γ_{2j+1} Majorana fermion paired dimer state is the unoccupied vacuum state $|n_{c_{2j,2j+1}} = 0\rangle$ ($n_{c_{2j,2j+1}} = c_{2j,2j+1}^\dagger c_{2j,2j+1}$) for the new complex fermion $c_{2j,2j+1}$. The ground state $|GS\rangle = \otimes_j |n_{c_{2j,2j+1}} = 0\rangle$ is a Majorana fermion dimer state with γ_{2j} paired to γ_{2j+1} for all j (see Fig. 23).

In periodic boundary condition, all Majorana fermions are paired up from γ_{2j} to γ_{2j+1} (in particular, γ_{2N} is paired to γ_1). So the ground state is unique (see Fig. 23b).

In open boundary condition, however, the first and the last Majorana fermions γ_1 and γ_{2N} are dangling. We can pair them either from γ_1 to γ_{2N} , or from γ_{2N} to γ_1 . This gives rise to the two-fold-degenerate ground states (see Fig. 23c and Fig. 23d).

2. Excited states and the appearance of phase factor $\pm i$

Since the Hamiltonian Eq. (A4) is a summation of commuting projectors, we can easily construct all excited states of the model. In the Fock space of the new complex fermions $c_{2j,2j+1}$, ground state is merely $\otimes_j |n_{c_{2j,2j+1}} = 0\rangle$, and the excited states are states that some of these fermion modes are occupied.

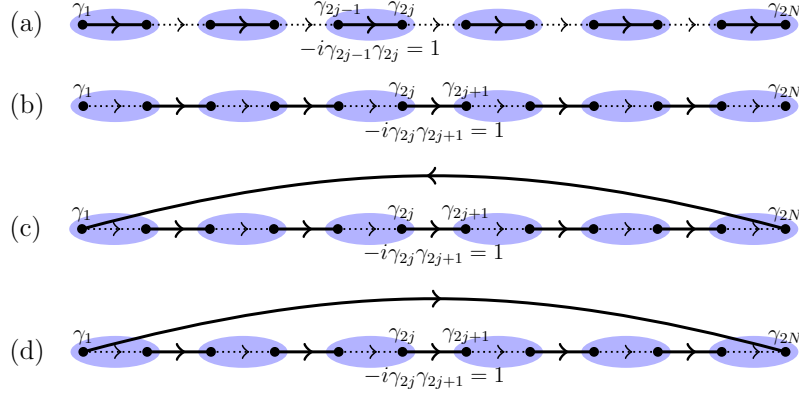


FIG. 23: Several states of the Majorana chain. Gray ellipses represent physical sites. The complex fermion c_j at site j is decomposed into two Majorana fermions as $c_j = (\gamma_{2j-1} + i\gamma_{2j})/2$. Solid oriented line from j to k indicates that γ_j is paired to γ_k , i.e., $-i\gamma_j\gamma_k = 1$ when acting on this state. (a) Trivial state $\otimes_j |n_{c_j} = 0\rangle$. In terms of Majorana fermions, γ_{2j-1} is paired to γ_{2j} ($j = 1, 2, \dots, N$), i.e., $-i\gamma_{2j-1}\gamma_{2j} = 1$ when acting on this state. (b) Ground state of the Kitaev's Majorana chain Eq. (A4) in open boundary condition. The first and the last Majorana fermions can be paired either as (c) or as (d), resulting in two fold degeneracy of the ground states. (c) Ground state of the Kitaev's Majorana chain Eq. (A4) in periodic boundary condition. The graph is not Kasteleyn oriented, and the state has odd fermion parity. (d) Ground state of the Kitaev's Majorana chain Eq. (A4) in anti-periodic boundary condition. The graph has Kasteleyn oriented, and the state has even fermion parity.

In terms of Majorana fermion operators, we can construct excited states as

$$|k\rangle = \gamma_k |GS\rangle, \quad (\text{A8})$$

where $k = 1, 2, \dots, 2N$ is some site of the Majorana fermions. Using the commutation relations of Majorana fermions, one can easily show

$$(-i\gamma_{2j}\gamma_{2j+1})|k\rangle = \begin{cases} -|k\rangle, & k = 2j, 2j+1 \\ |k\rangle, & k \neq 2j, 2j+1 \end{cases} \quad (\text{A9})$$

Therefore, $|k\rangle$ is indeed an excited state of the Kitaev chain with energy $\Delta E = 2$ above the ground state energy. All other excited states can be constructed similarly.

Since the Majorana fermion γ_k is a superposition of creation and annihilation operators of the original c_i fermions, the fermion parity of $|k\rangle$ is always different from the ground state $|GS\rangle$. Moreover, the excited states $|k\rangle$ constructed above are not linearly independent. In fact, using the definition of the ground state Eq. (A5) and the algebraic relations of Majorana fermions, we have

$$\gamma_{2j+1}|GS\rangle = i\gamma_{2j}|GS\rangle. \quad (\text{A10})$$

This equation shows that the Majorana fermion will pick up a phase factor $\pm i$ when hopping one lattice site along the chain.

Similar to Eq. (A8) to change the fermion parity, we introduced a Majorana fermion operator γ_{012A} (or γ_{234B}) in the 3D F move when the fermion parity of the Kitaev chain in this F move is changed. It indicates that the state of the final Majorana chain in the F move is the excited state of the original one with one Majorana fermion γ_{012A} (or γ_{234B}) excited. In the fermionic hexagon equation, if some of the six F moves changes Majorana fermion parity, then the excited Majorana fermion will hop along the Majorana chain. This is the reason why the obstruction \mathcal{O}_γ may have phase factor $\pm i$.

3. Fermion parity and Kasteleyn orientation

The two ground states of Kitaev chain in open boundary condition have different fermion parity (see Fig. 23c and Fig. 23d). One can check that the fermion parity of the ground state in periodic boundary condition (see Fig. 23c) is

odd:

$$\begin{aligned}
P_f|GS_{PBC}\rangle &= (-i\gamma_1\gamma_2)(-i\gamma_3\gamma_4)\cdots(-i\gamma_{2N-1}\gamma_{2N})|GS_{PBC}\rangle \\
&= (-i\gamma_2\gamma_3)(-i\gamma_4\gamma_5)\cdots(-i\gamma_{2N-2}\gamma_{2N-1})(i\gamma_{2N}\gamma_1)|GS_{PBC}\rangle \\
&= -|GS_{PBC}\rangle.
\end{aligned} \tag{A11}$$

where we have moved γ_1 from the leftmost to the rightmost position, and used the definition of ground state Eq. (A5).

Since the other ground state in Fig. 23d reverse the link direction connecting the end points of the state in Fig. 23c, their fermion parities are different. So the state in Fig. 23d has even fermion parity. When looking at the link directions of the pictures, one can easily distinguish the difference of the two states. Fig. 23d is Kasteleyn oriented in the sense that the number of arrows pointing backwards along the chain loop is odd (since the number of links is even, the walking direction is not important). Then the fermion parities for the state in Fig. 23a and Fig. 23d are the same. On the other hand, Fig. 23c is not Kasteleyn oriented. And this state has different fermion parity. For states with other choices of link orientation, one can flip the directions of several links. If we flip odd (even) number of link directions, the fermion parity is (not) changed. Therefore the Kasteleyn oriented is a necessary and sufficient condition for the fermion parity changes.

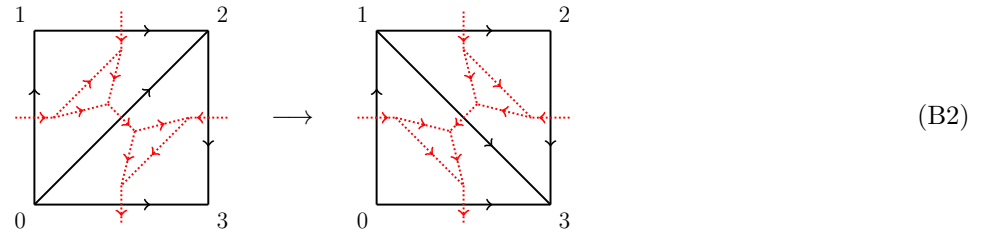
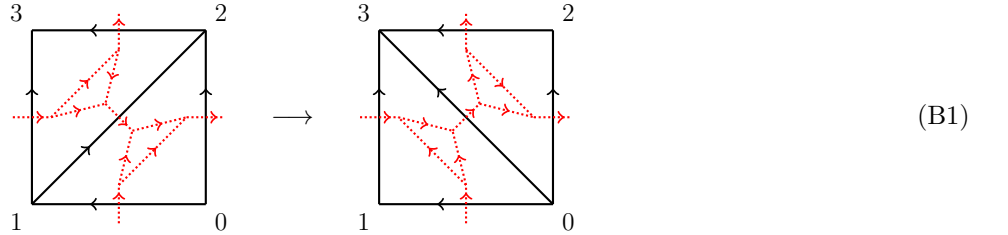
The same is true for Majorana dimer states in 2D and 3D. One can put two Majorana dimer states together. For the transition graph of the two (oriented) dimer states, if a loop is Kasteleyn oriented, then the two Majorana dimer states in this patch have the same fermion parity. If a loop is not Kasteleyn oriented, then the two states have different fermion parity in this loop.

We use this criteria for 3D lattice, and find that the Kasteleyn orientation property may change under the F move. This is why we add γ_{012A} (or γ_{234B}) to make the F operator really transform one state to another with different Majorana fermion pairty.

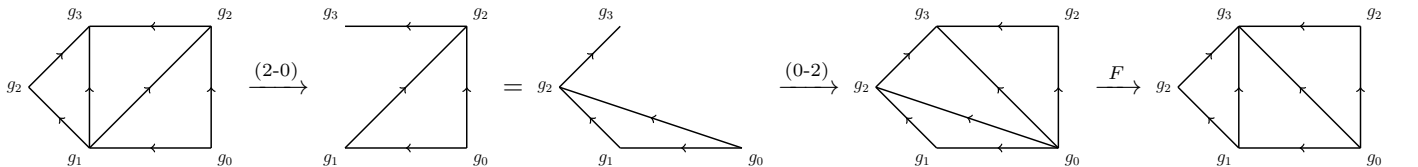
Appendix B: 2D Pachner moves

1. (2-2) moves

With a branching structure, there are three different types of (2-2) Pachner moves. Only two of them can be induced by a global ordering [see Eqs. (B1) and (B2)].



Note that the (2-2) move in Eq. (B2) is the standard move. The other (2-2) move in Eq. (B1) can be derive from a sequence of the standard move and the (2-0) moves, as shown below:



To derive the (2-2) move in Eq. (B1), we first add a vertex g_2 and a triangle labelled by g_1, g_2, g_3 on the left of the figure. After a (2-0) move, a (0-2) move and a standard (2-2) F move, we finally obtain the desired triangulation. The whole process gives the expression for the F move in Eq. (B1) as:

$$\begin{aligned}
F(0123)|_{\text{Eq. (B1)}} &= \frac{1}{|G_b|^{1/2}} c_{(123)}^{\dagger n_2(123)} \bar{c}_{(123)}^{\dagger n_2(123)} \cdot |G_b|^{1/2} \bar{c}_{(023)}^{n_2(023)} c_{(023)}^{n_2(023)} \cdot \nu_3(0123) c_{(012)}^{\dagger n_2(012)} c_{(023)}^{\dagger n_2(023)} c_{(013)}^{n_2(013)} c_{(123)}^{n_2(123)} X[\tilde{n}_1], \\
&= \nu_3(0123) (-1)^{n_2(123)} c_{(012)}^{\dagger n_2(012)} \bar{c}_{(023)}^{n_2(023)} c_{(013)}^{n_2(013)} \bar{c}_{(123)}^{\dagger n_2(123)} X[\tilde{n}_1] \\
&= \nu_3(0123) \bar{c}_{(123)}^{\dagger n_2(123)} c_{(012)}^{\dagger n_2(012)} \bar{c}_{(023)}^{n_2(023)} c_{(013)}^{n_2(013)} X[\tilde{n}_1],
\end{aligned} \tag{B3}$$

where we have used $c_{(023)}^{n_2(023)} c_{(023)}^{\dagger n_2(023)} = c_{(123)}^{\dagger n_2(123)} c_{(123)}^{n_2(123)} = 1$ when acting on appropriate states, and $dn_2(0123) = 0 \pmod{2}$. Recall that $c_{(123)}$ and $\bar{c}_{(123)}$ are annihilation operators of the c fermions at the center of triangles (123) with opposite orientations.

When decorating Kitaev's Majorana chains to the dual lattice, there are in total $2^3 = 8$ kinds of different decoration configurations (see Table IV) for each (2-2) move. One can check that, for any decoration configuration, all the loops in the transition graph of the left and right Majorana dimer states have Kasteleyn orientation property. Therefore the Majorana fermion parity is conserved in all (2-2) moves.

out-leg string #	configuration
0	
2	
4	

TABLE IV: $2^3 = 8$ kinds of configurations of Kitaev's Majorana chain decorations (green line) on the dual lattice \mathcal{P} for each (2-2) move.

2. (1-3) moves

There are in total four different types of (1-3) Pachner moves for triangulation with branching structure. Two of them have branching structure that can be induced by a global ordering [see Eqs. (B4)-(B5)]. These (1-3) moves can also be derived from a sequence of the standard (2-2) move and (2-0) moves.

(B4)

(B5)

For instance, using the standard F move and (2-0) move, we can derive the (1-3) move Eq. (B5):

(B6)

Note that we have added a triangle labelled by g_0 , g_1 and g_2 below on both figure of Eq. (B5). The above process can be summarized as a FSLU transformation:

$$\begin{aligned}
 F(0123)|_{\text{Eq. (B5)}} &= \nu_3^{-1} (0123) \bar{c}_{(012)}^{\dagger n_2(012)} \bar{c}_{(023)}^{\dagger n_2(023)} \bar{c}_{(013)}^{n_2(013)} \bar{c}_{(123)}^{n_2(123)} \cdot |G_b|^{1/2} \bar{c}_{(012)}^{n_2(012)} c_{(012)}^{n_2(012)} X[\tilde{n}_1] \\
 &= \nu_3^{-1} (0123) |G_b|^{1/2} c_{(012)}^{n_2(012)} \bar{c}_{(023)}^{\dagger n_2(023)} \bar{c}_{(013)}^{n_2(013)} \bar{c}_{(123)}^{n_2(123)} X[\tilde{n}_1].
 \end{aligned}
 \tag{B7}$$

Note that, the F move used in the above sequence is slightly different from the standard one. The differences are merely the orientations of all four triangles. There are two consequences of the orientation changes. The first one is that c 's are changed to \bar{c} 's by definition. The second consequence is that the $U(1)$ phase factor ν_2 is changed to ν_2^{-1} . This can be obtained by using several steps of (2-0) moves. It is also consistent with the path integral formalism of bosonic SPT states, for $\nu_2^{s(ijkl)}(g_i, g_j, g_k, g_l)$ is assigned to the spacetime tetrahedron $\langle ijkl \rangle$ with orientation $s(ijkl) = \pm 1$.

In total $2^3 = 8$ kinds of Kitaev's Majorana chain decoration configurations are summarized in Table V. Similar to the (2-2) moves, one can check that none of the (1-3) moves change the Majorana fermion parity for arbitrary decoration configurations.

out-leg string #	configuration-1	configuration-2
0		
2		

TABLE V: $2^3 = 8$ kinds of configurations of Kitaev's Majorana chain decorations (green line) on the dual lattice \mathcal{P} for each (1-3) move.

Appendix C: 3D Pachner moves and fermion parity changes

1. (2-0) moves

Besides the (2-0) move shown in main text, there is another (2-0) move which has a branching structure that can be induced by global ordering. This (2-0) move corresponds to the one with vertex labelled by g_2 at the center of triangle 013. The expression for this move is

$$\Psi \left(\begin{array}{c} \text{Diagram of a tetrahedron with vertices } g_1, g_2, g_3 \text{ and internal lines } \xi_{(0123)} \end{array} \right) = \frac{1}{|G_b|^{1/2}} c_{(0123)}^{\dagger n_3(g_0, g_1, g_2, g_3)} \bar{c}_{(0123)}^{\dagger n_3(g_0, g_1, g_2, g_3)} X[\tilde{n}_2(g_i, g_j, g_k)] \Psi \left(\begin{array}{c} \text{Diagram of a triangle with vertices } g_1, g_2, g_3 \text{ and a central vertex } g_0 \end{array} \right), \quad (\text{C1})$$

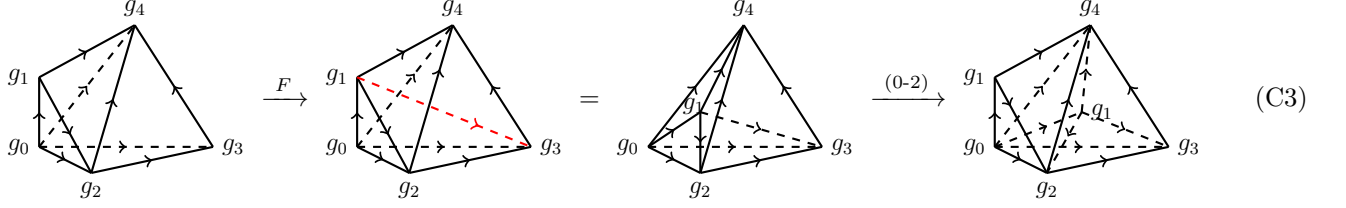
$$\Psi \left(\begin{array}{c} \text{Diagram of a tetrahedron with vertices } g_1, g_2, g_3 \text{ and internal lines } \xi_{(0123)} \end{array} \right) = \frac{1}{|G_b|^{1/2}} c_{(0123)}^{\dagger n_3(g_0, g_1, g_2, g_3)} \bar{c}_{(0123)}^{\dagger n_3(g_0, g_1, g_2, g_3)} X[\tilde{n}_2(g_i, g_j, g_k)] \Psi \left(\begin{array}{c} \text{Diagram of a triangle with vertices } g_1, g_2, g_3 \text{ and a central vertex } g_0 \end{array} \right). \quad (\text{C2})$$

Using these two (2-0) moves and the standard F move, we can deduce all (1-4) and (2-3) moves with different branching structures.

2. (1-4) moves

There are five different kinds of (1-4) 3D Pachner move. Three have branching structures that can be induced by global ordering (see Figs. 24-26). They can be obtained from a sequence of standard F moves and (2-0) moves. For

example, the move of adding vertex 1 in Fig. 25 can be obtained as follows:



We first add a tetrahedron (0124) to the left-hand-side state of Fig. 25. Then after a standard F move and a (0-2) move, we obtain the desired (1-4) move in Fig. 25. The expression for this sequence of FSLU transformation is

$$\begin{aligned} F(0123)|_{\text{Fig. (25)}} &= \nu_4^{-1}(01234)\bar{c}_{(0124)}^{\dagger n_3(0124)}\bar{c}_{(0234)}^{\dagger n_3(0234)}\bar{c}_{(0123)}^{n_3(0123)}\bar{c}_{(0134)}^{n_3(0134)}\bar{c}_{(1234)}^{n_3(1234)} \cdot |G_b|^{1/2}\bar{c}_{(0124)}^{n_3(0124)}c_{(0124)}^{n_3(0124)}X[\tilde{n}_2] \\ &= \nu_4^{-1}(01234)|G_b|^{1/2}c_{(0124)}^{n_3(0124)}\bar{c}_{(0234)}^{\dagger n_3(0234)}\bar{c}_{(0123)}^{n_3(0123)}\bar{c}_{(0134)}^{n_3(0134)}\bar{c}_{(1234)}^{n_3(1234)}X[\tilde{n}_2]. \end{aligned} \quad (\text{C4})$$

Note that we also changed c 's to \bar{c} 's and ν_3 to ν_3^{-1} in the above F move compared to the standard F move, for the orientations of the five tetrahedra are changed. The reason is exactly the same as the 2D case discussed below Eq. (B7).

For all five kinds of (1-4) moves, the move changes the Majorana fermion parity if and only if both link 012 and link 234 in lattice \mathcal{P} are decorated by Kitaev's Majorana chains. Therefore we also have $dn_3 = \tilde{n}_2 \smile \tilde{n}_2$. $2^6 = 64$ kinds of Kitaev's Majorana chain decoration configurations are summarized in Table VI.

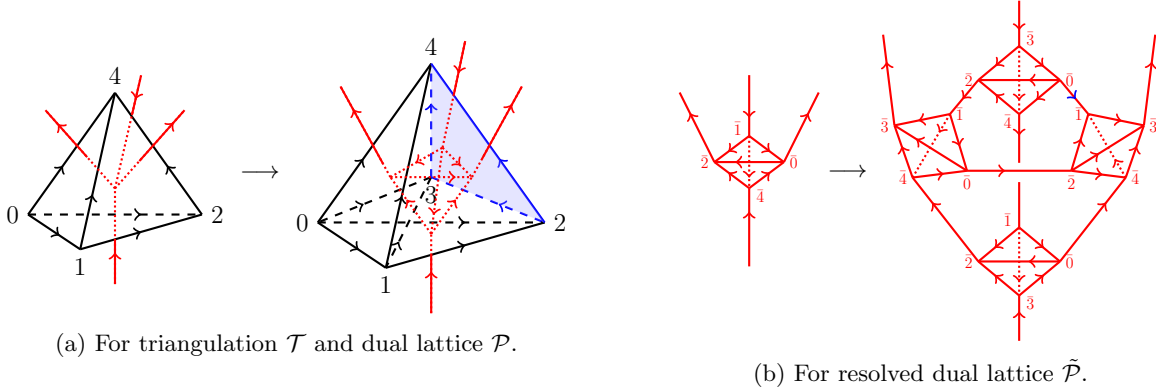


FIG. 24: (1-4)-A move.

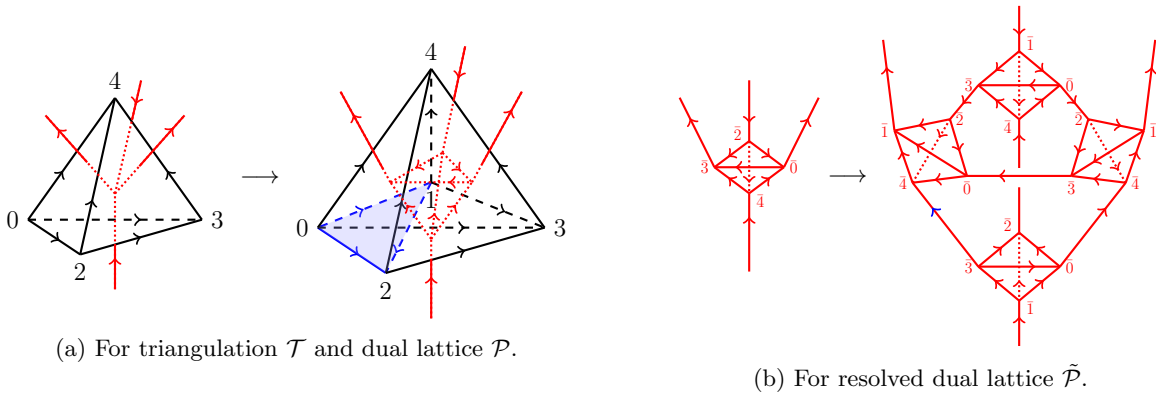


FIG. 25: (1-4)-B move.

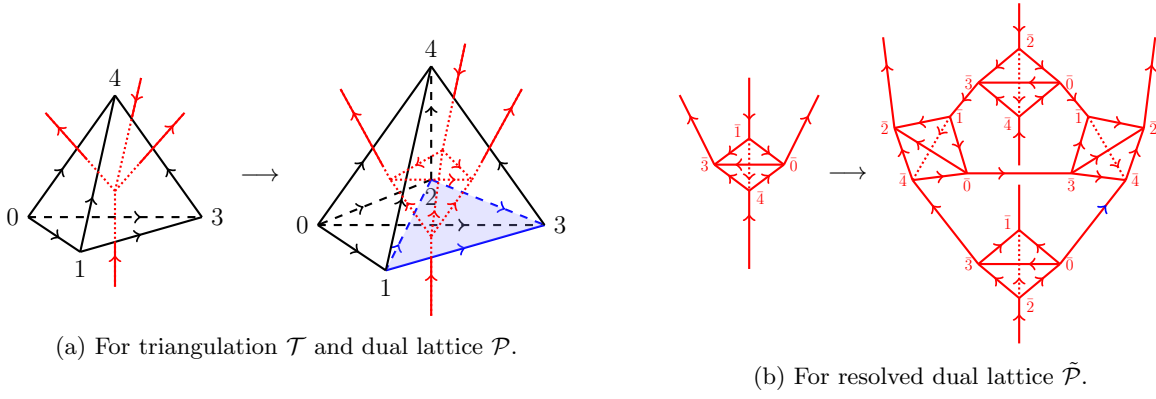


FIG. 26: (1-4)-C move.

out-leg string #	configuration #	configuration
0	1	
	4	
	3	
2	6×1	
	6×2	
	6×2	
	6×2	
	6×1	
4	3	
	4	
	1	

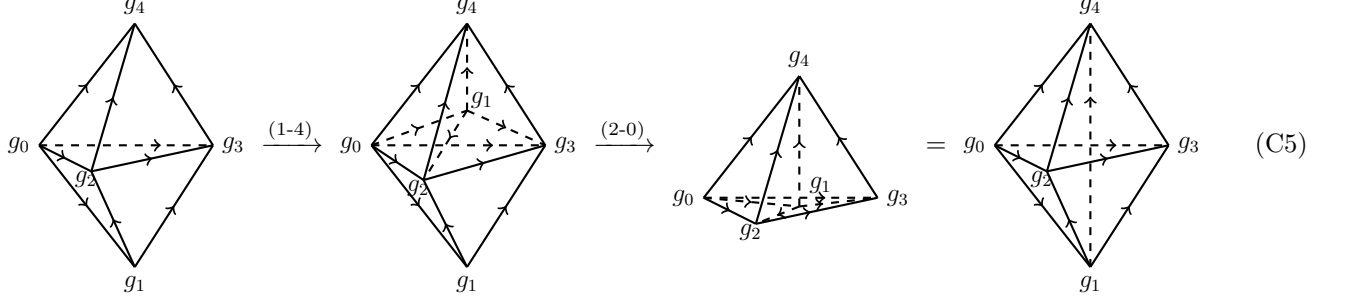
TABLE VI: $2^6 = 64$ kinds of configurations of Kitaev's Majorana chain decorations (green line) on the dual lattice \mathcal{P} for each (1-4) move. The second column counts the number of configurations of the same symmetry type. When four green lines meet at one point, we should resolve the decoration according to the conventions in main text.

3. (2-3) moves

For 3D triangulation with a branching structure, there are 10 different kinds of (2-3) Pachner move. Eight have branching structures induced by global ordering (see Figs. 27-34).

The (2-3) move in Fig. 27 is the standard move. Other (2-3) moves can be also derive from a sequence of the standard F move and the (2-0) moves. In fact, we can also use (1-4) moves since they have already been obtained from standard F moves and (2-0) moves in the last subsection. Here is an example of deriving the (2-3) move of

adding link 14 in Fig. 29:



The first step is adding a vertex labelled by g_1 at the center of the tetrahedron 0234. This is the (1-4) move in Fig. 25, which is obtained from the standard F move and (2-0) move in Fig. C3 and has expression Eq. (C4). The expression for the (2-3) FSLU transformation shown above is

$$\begin{aligned}
 F(0123)|_{\text{Fig. (29)}} &= \nu_4^{-1}(01234)|G_b|^{1/2} c_{(0124)}^{n_3(0124)} \bar{c}_{(0234)}^{\dagger n_3(0234)} \bar{c}_{(0123)}^{n_3(0123)} \bar{c}_{(0134)}^{n_3(0134)} \bar{c}_{(1234)}^{n_3(1234)} \cdot \frac{1}{|G_b|^{1/2}} c_{(0123)}^{\dagger n_3(0123)} \bar{c}_{(0123)}^{\dagger n_3(0123)} X[\tilde{n}_2] \\
 &= \nu_4^{-1}(01234)(-1)^{n_3(0123)} c_{(0124)}^{n_3(0124)} \bar{c}_{(0234)}^{\dagger n_3(0234)} c_{(0123)}^{\dagger n_3(0123)} \bar{c}_{(0134)}^{n_3(0134)} \bar{c}_{(1234)}^{n_3(1234)} X[\tilde{n}_2].
 \end{aligned} \tag{C6}$$

Different from the 2D case, when decorating Kitaev's Majorana chains to the dual lattice, the (2-3) moves may change the Majorana fermion parity. One can check the Kasteleyn orientation property for all loops in the transition graph of the left and right Majorana dimer states. A striking result is that, for all 10 kinds of (2-3) move, the move changes the Majorana fermion parity if and only if both link 012 and link 234 in lattice \mathcal{P} are decorated by Kitaev's Majorana chains. This leads to the total fermion parity conservation equation $dn_3 = \tilde{n}_2 \smile \tilde{n}_2$. $2^6 = 64$ kinds of Kitaev's Majorana chain decoration configurations are summarized in Table VII.

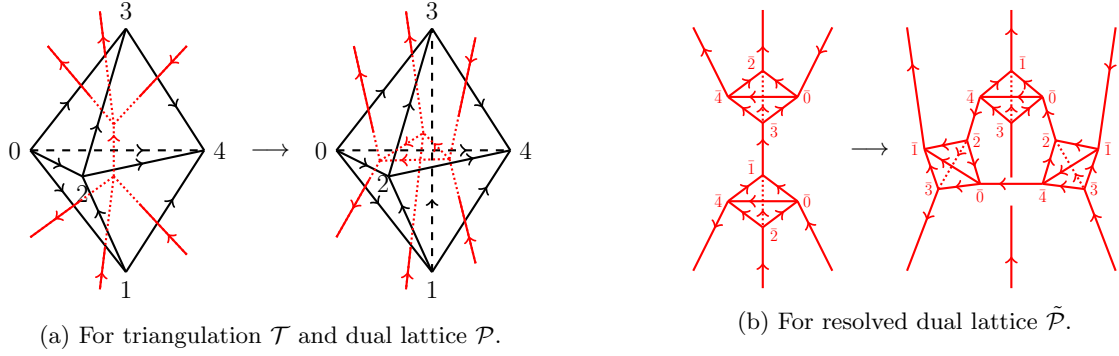


FIG. 27: (2-3)-A move.

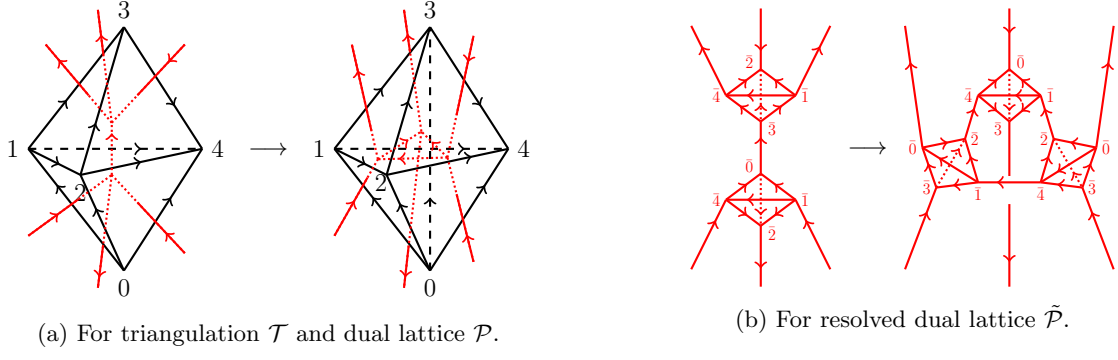


FIG. 28: (2-3)-B move.

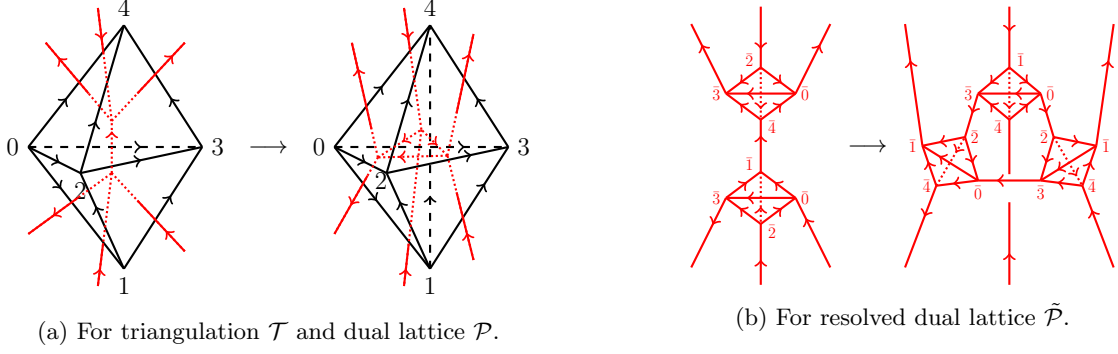


FIG. 29: (2-3)-C move.

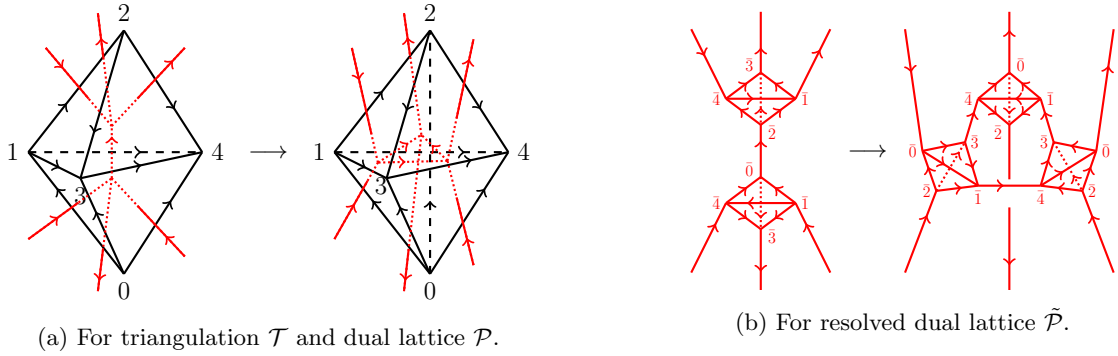


FIG. 30: (2-3)-D move.

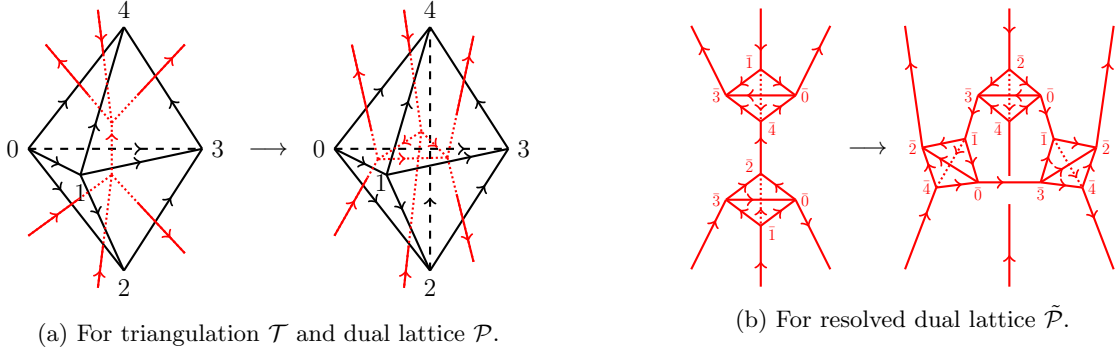


FIG. 31: (2-3)-E move.

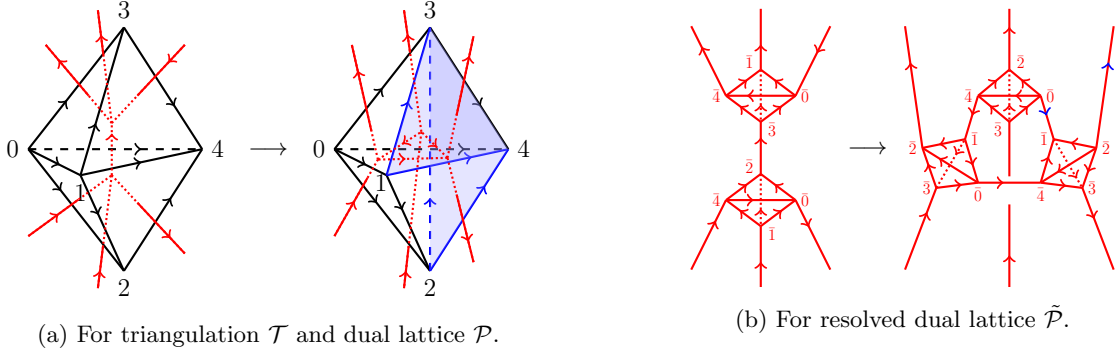


FIG. 32: (2-3)-F move.

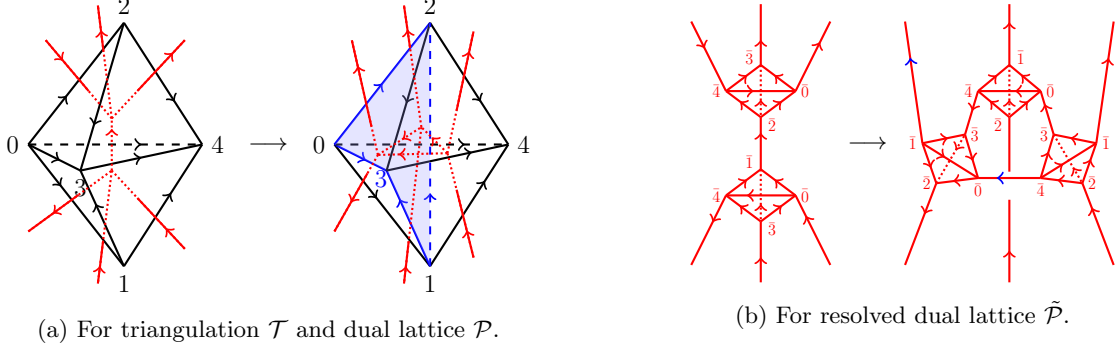


FIG. 33: (2-3)-G move.

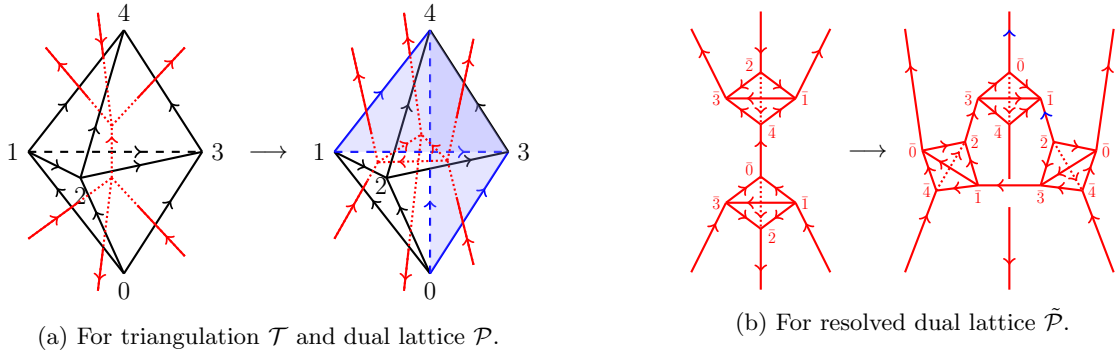


FIG. 34: (2-3)-H move.

out-leg string #	configuration #	configuration-1	configuration-2
0	1×2		
2	3×2		
	3×2		
	3×2		
	6×2		
4	3×2		
	3×2		
	3×2		
	6×2		
6	1×2		

TABLE VII: $2^6 = 64$ kinds of configurations of Kitaev's Majorana chain decorations (green line) on the dual lattice \mathcal{P} for each (2-3) move. The second column counts the number of configurations of the same symmetry type. When four green lines meet at one point, we should resolve the decoration according to the conventions in main text.

Appendix D: Abelian group structure of the general group super-cohomology solutions

Assume $(\nu_4, n_3, \tilde{n}_2)$ and $(\nu'_4, n'_3, \tilde{n}'_2)$ are two solutions of general group super-cohomology theory, i.e., they satisfy the equations

$$d\nu_4 = \mathcal{O}[n_3, \tilde{n}_2], \quad (\text{D1})$$

$$dn_3 = \tilde{n}_2^2, \quad (\text{D2})$$

$$d\tilde{n}_2 = 0, \quad (\text{D3})$$

and

$$d\nu'_4 = \mathcal{O}[n'_3, \tilde{n}'_2], \quad (\text{D4})$$

$$dn'_3 = \tilde{n}'_2{}^2, \quad (\text{D5})$$

$$d\tilde{n}'_2 = 0. \quad (\text{D6})$$

We want to construct another solution triple $(\nu_4^{\text{tot}}, n_3^{\text{tot}}, \tilde{n}_2^{\text{tot}})$ from “adding” $(\nu_4, n_3, \tilde{n}_2)$ and $(\nu'_4, n'_3, \tilde{n}'_2)$. The new solution satisfy

$$d\nu_4^{\text{tot}} = \mathcal{O}[n_3^{\text{tot}}, \tilde{n}_2^{\text{tot}}], \quad (\text{D7})$$

$$dn_3^{\text{tot}} = (\tilde{n}_2^{\text{tot}})^2, \quad (\text{D8})$$

$$d\tilde{n}_2^{\text{tot}} = 0. \quad (\text{D9})$$

If there exists such construction, then the solutions of the general group super-cohomology theory is closed under this “adding” and form an Abelian group (if the “adding” is commutative). The “adding” operation corresponds to stacking of two FSPT states physically.

The expressions of n_3^{tot} and \tilde{n}_2^{tot} are very simple. One can show that if we choose

$$n_3^{\text{tot}} = n_3 + n'_3 + \tilde{n}_2 \smile_1 \tilde{n}'_2, \quad (\text{D10})$$

$$\tilde{n}_2^{\text{tot}} = \tilde{n}_2 + \tilde{n}'_2, \quad (\text{D11})$$

then Eqs. (D8) and (D9) can be derived from Eqs. (D2), (D3), (D5) and (D6).

Assume that ν_4^{tot} has the expression

$$\nu_4^{\text{tot}} = \nu_4 \cdot \nu'_4 \cdot e^{i\pi\theta[n_3, n'_3, \tilde{n}_2, \tilde{n}'_2]}, \quad (\text{D12})$$

where $\theta[n_3, n'_3, \tilde{n}_2, \tilde{n}'_2]$ is some unknown functional of $n_3, n'_3, \tilde{n}_2, \tilde{n}'_2$. As n_3, n'_3, \tilde{n}_2 , and \tilde{n}'_2 are cochains that are invariant under G_b action, $\theta[n_3, n'_3, \tilde{n}_2, \tilde{n}'_2]$, and ν_4^{tot} are also invariant.

The obstruction in Eq. (D1) is denoted by

$$\mathcal{O}[n_3, \tilde{n}_2] = (-1)^{n_3 \smile_1 n_3 + n_3 \smile_2 dn_3 + f[\tilde{n}_2]}, \quad (\text{D13})$$

where $\mathcal{O}_\gamma = (-1)^{f[\tilde{n}_2]}$ is the obstruction coming from the Majorana fermions. From Eqs. (D1), (D4) and (D7), the equation for θ is

$$\begin{aligned} (-1)^{d\theta[n_3, n'_3, \tilde{n}_2, \tilde{n}'_2]} &= \frac{d\nu_4^{\text{tot}}}{d\nu_4 \cdot d\nu'_4} \\ &= (-1)^{(n_3^{\text{tot}} \smile_1 n_3^{\text{tot}} + n_3^{\text{tot}} \smile_2 dn_3^{\text{tot}}) - (n_3 \smile_1 n_3 + n_3 \smile_2 dn_3) - (n'_3 \smile_1 n'_3 + n'_3 \smile_2 dn'_3) + f[\tilde{n}_2^{\text{tot}}] - f[\tilde{n}_2] - f[\tilde{n}'_2]}. \end{aligned} \quad (\text{D14})$$

After substituting Eqs. (D10) and (D11) to the right hand side of the equation above, we obtain the (mod 2) linear equation

$$\begin{aligned} dy[\tilde{n}_2, \tilde{n}'_2] &\equiv (\tilde{n}_2 \smile_1 \tilde{n}'_2) \smile_1 (\tilde{n}_2 \smile_1 \tilde{n}'_2) + (\tilde{n}_2 \smile_1 \tilde{n}'_2) \smile_2 (\tilde{n}_2 \smile_1 \tilde{n}'_2 + \tilde{n}'_2 \smile_1 \tilde{n}_2) \\ &\quad + (\tilde{n}_2^2 + \tilde{n}'_2{}^2) \smile_3 (\tilde{n}_2 \smile_1 \tilde{n}'_2 + \tilde{n}'_2 \smile_1 \tilde{n}_2) + \tilde{n}_2^2 \smile_3 \tilde{n}'_2{}^2 + f[\tilde{n}_2 + \tilde{n}'_2] - f[\tilde{n}_2] - f[\tilde{n}'_2], \quad (\text{mod } 2) \end{aligned} \quad (\text{D15})$$

where $y[\tilde{n}_2, \tilde{n}'_2]$ is related to $\theta[n_3, n'_3, \tilde{n}_2, \tilde{n}'_2]$ by

$$\theta[n_3, n'_3, \tilde{n}_2, \tilde{n}'_2] = y[\tilde{n}_2, \tilde{n}'_2] + n_3 \smile_2 n'_3 + (\tilde{n}_2 \smile_1 \tilde{n}'_2) \smile_2 (n_3 + n'_3) + (n_3 + n'_3) \smile_3 (\tilde{n}_2 \smile_1 \tilde{n}'_2 + \tilde{n}'_2 \smile_1 \tilde{n}_2) + \tilde{n}_2^2 \smile_3 \tilde{n}'_2{}^2. \quad (\text{D16})$$

In summary, if $y[\tilde{n}_2, \tilde{n}'_2]$ is a solution of Eq. (D15), then the Abelian group structure of the group supercohomology solutions is

$$(\nu_4, n_3, \tilde{n}_2) + (\nu'_4, n'_3, \tilde{n}'_2) = (\nu_4 \nu'_4 e^{i\pi\theta[n_3, n'_3, \tilde{n}_2, \tilde{n}'_2]}, n_3 + n'_3 + \tilde{n}_2 \smile_1 \tilde{n}'_2, \tilde{n}_2 + \tilde{n}'_2), \quad (\text{D17})$$

where $\theta[n_3, n'_3, \tilde{n}_2, \tilde{n}'_2]$ is defined by Eq. (D16).

1. Explicit construction of $\theta[n_3, n'_3, \tilde{n}_2, \tilde{n}'_2]$

To construct $\theta[n_3, n'_3, \tilde{n}_2, \tilde{n}'_2]$ in the Eq. (D17), we need only to find a solution $y[\tilde{n}_2, \tilde{n}'_2]$ of Eq. (D15). Note that Eq. (D15) is a mod 2 equation when evaluating for arbitrary $(g_0, g_1, g_2, g_3, g_4, g_5) \in G_b^6$. $y[\tilde{n}_2, \tilde{n}'_2](g_0, g_1, g_2, g_3, g_4)$ is automatically symmetric under G_b because it depends on g_i through \tilde{n}_2 and \tilde{n}'_2 .

As defined previously, $y[\tilde{n}_2, \tilde{n}'_2]$ is a functional of \tilde{n}_2 and \tilde{n}'_2 . When evaluating at $(g_0, g_1, g_2, g_3, g_4)$, it is a function $y[\{\tilde{n}_2(g_i, g_j, g_k)\}, \{\tilde{n}'_2(g_i, g_j, g_k)\}]$ ($0 \leq i < j < k \leq 4$). It seems that y has $2 \times C_5^3 = 20$ arguments. However, as \tilde{n}_2 is a cocycle with equation $d\tilde{n}_2 = 0 \pmod{2}$, $\{\tilde{n}_2(g_i, g_j, g_k)\}$ ($0 \leq i < j < k \leq 4$) are not fully independent. After solving the equations $d\tilde{n}_2(g_i, g_j, g_k, g_l) = 0$ ($0 \leq i < j < k < l \leq 4$) explicitly, we find that the number of independent cocycles $\tilde{n}_2(g_i, g_j, g_k)$ ($0 \leq i < j < k \leq 4$) is six. In fact, 2^6 is exactly the number of Kitaev chain decoration configurations of a 4-simplex or a (2-3) Pachner move (see Table VII). We can choose the six independent cocycles to be $\tilde{n}_2(012), \tilde{n}_2(013), \tilde{n}_2(014), \tilde{n}_2(023), \tilde{n}_2(024),$ and $\tilde{n}_2(034)$ [again, (012) means (g_0, g_1, g_2) , etc.], respectively. The other four cocycles, including $\{\tilde{n}_2(123), \tilde{n}_2(124), \tilde{n}_2(134),$ and $\tilde{n}_2(234)\}$, respectively, can be derived from the previous six. Therefore, $y[\{\tilde{n}_2(g_i, g_j, g_k)\}, \{\tilde{n}'_2(g_i, g_j, g_k)\}]$ ($0 \leq i < j < k \leq 4$) has only 12 independent arguments and can thus be written as

$$y[\tilde{n}_2(012), \tilde{n}_2(013), \tilde{n}_2(014), \tilde{n}_2(023), \tilde{n}_2(024), \tilde{n}_2(034), \tilde{n}'_2(012), \tilde{n}'_2(013), \tilde{n}'_2(014), \tilde{n}'_2(023), \tilde{n}'_2(024), \tilde{n}'_2(034)]. \quad (\text{D18})$$

Each \tilde{n}_2 or \tilde{n}'_2 can take two values, and so the number of unknown variables of y is $q = 2^{12} = 4096$.

The number of equations in Eq. (D15) is the number of all possible cocycles \tilde{n}_2 and \tilde{n}'_2 , i.e., the number of different cochain patterns \tilde{n}_2 and \tilde{n}'_2 satisfying $d\tilde{n}_2(g_i, g_j, g_k, g_l) = d\tilde{n}'_2(g_i, g_j, g_k, g_l) = 0$ ($0 \leq i < j < k < l \leq 5$). One can solve the cocycle equation and find that the number of different $\tilde{n}_2(g_i, g_j, g_k)$ ($0 \leq i < j < k \leq 5$) patterns is 2^{10} . This is the number of Kitaev chain decoration configurations of a 5-simplex or the hexagon equation. Thus, the number of equations is $p = 2^{20} = 1048576$.

The right-hand side of Eq. (D15) involves $f(\tilde{n}_2)$. As $\mathcal{O}_\gamma = (-1)^{f[\tilde{n}_2]}$ can be ± 1 or $\pm i$, $f(\tilde{n}_2)$ takes value in $\{0, \frac{1}{2}, 1, \frac{3}{2}\}$. To make the right-hand side of Eq. (D15) integers, we can multiply Eq. (D15) by 2, and scale y by

$$y = \frac{x}{2}. \quad (\text{D19})$$

The final equation for x in the matrix form is

$$Ax \equiv b, \quad \text{mod } 4. \quad (\text{D20})$$

This is an overdetermined system of linear equations with $p = 2^{20}$ equations and $q = 2^{12}$ unknowns.

Using the procedure list in the next subsection, we find that the above linear equation indeed has solutions. We can use the solution x to construct θ . And the group structure of the general super-cohomology solutions is given by Eq. (D17).

2. Solving system of linear equations in $\mathbb{R}/4\mathbb{Z}$

In this subsection, we discuss how to solve equations of the form

$$Ax \equiv b, \quad \text{mod } 4. \quad (\text{D21})$$

Here, $A \in M_{p,q}(\mathbb{Z})$ is a $p \times q$ ($p = 2^{20}, q = 2^{12}$) matrix with elements in \mathbb{Z} (the matrix form of coboundary operator “d” has elements in \mathbb{Z}). On the right hand side, $b \in \mathbb{Z}^p$ is a \mathbb{Z} -valued vector with length p . However, $x \in \mathbb{R}^q$ is a \mathbb{R} -valued vector with length q . All the equations hold modulo 4. Note that this equation is not a system of linear equations in ring $\mathbb{Z}/4\mathbb{Z}$ because elements of x can take value in $\mathbb{R}/4\mathbb{Z}$, not merely in $\mathbb{Z}/4\mathbb{Z}$. In fact, we find that the above equation in our case has no solution of x in $\mathbb{Z}/4\mathbb{Z}$, but it does have a solution in $\mathbb{R}/4\mathbb{Z}$.

To solve the mod 4 equation, we introduce an integer variable n such that Eq. (D21) becomes an equation in \mathbb{R} without modulo 4.

$$Ax = b + 4n. \quad (\text{D22})$$

Now the equation holds in \mathbb{R} and the unknowns are $x \in \mathbb{R}^q$ and $n \in \mathbb{Z}^p$.

The basic idea to solving Eq. (D22) is Gaussian elimination. As x takes value in \mathbb{R} , we can use the usual Gaussian elimination (column reduction) in field \mathbb{R} . However, as n takes value in \mathbb{Z} , the row reduction of Gaussian elimination can only be performed in ring \mathbb{Z} (the invertible scalars are only ± 1). Performing Gaussian elimination in \mathbb{Z} to solve

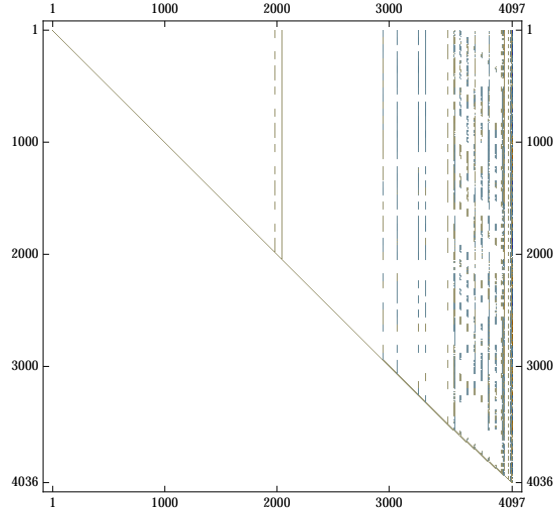


FIG. 35: Graphic display of the unique Hermite normal form of the augmented matrix (A, b) . We omit all the zero rows below the nonzero ones (the number of zero rows is $p - r - 1 = 1044540$). White represents zero matrix elements. The last element at $(r + 1, q + 1) = (4036, 4097)$ is 4, indicating the existence of solutions for Eq. (D20). The first nonzero element in each row of the Hermite normal form of A is either 1 or 2. Thus, the Abelian group structure of the general group super-cohomology solutions takes value in \mathbb{Z}_8 rather than in \mathbb{Z}_4 .

linear equations is actually a way of finding the Hermite normal form of A , which is the standard technique in solving systems of linear Diophantine equations. The detailed procedures for solving Eq. (D22) are as follows.

We first find the Hermite normal form of A :

$$UA = H, \quad (\text{D23})$$

where $U \in M_{p,p}(\mathbb{Z})$ is a unimodular matrix with elements in \mathbb{Z} . As an upper triangular integer matrix, H is the Hermite normal form of A . The equation becomes

$$Hx = b' + 4n' \quad (\text{D24})$$

where

$$b' = Ub, \quad (\text{D25})$$

$$n' = Un. \quad (\text{D26})$$

As U is a unimodular matrix that is invertible in \mathbb{Z} , we can construct a unique solution (x, n) of the original equation Eq. (D22) from a solution (x, n') of the new equation Eq. (D24), and vice versa.

Now we perform column Gaussian elimination for H in \mathbb{R} , such that

$$HV = \begin{pmatrix} I_r & 0 \\ 0 & 0 \end{pmatrix}, \quad (\text{D27})$$

where V is an invertible matrix in \mathbb{R} , and I_r is the identity matrix with size $r \times r$. The equation becomes

$$\begin{pmatrix} I_r & 0 \\ 0 & 0 \end{pmatrix} x' = b' + 4n' \quad (\text{D28})$$

where

$$x' = V^{-1}x \quad (\text{D29})$$

The solution (x', n') of the new equation Eq. (D28) can be also used to construct a unique solution (x, n') of Eq. (D24) because V is invertible in \mathbb{R} (recall that x has elements in \mathbb{R}).

Eq. (D28) has solution (x', n') ($x' \in \mathbb{R}^q, n' \in \mathbb{Z}^p$) if and only if the last $p - r$ elements of b' are all 0 (mod 4), i.e.,

$$b'_{p-r} \in (4\mathbb{Z})^{p-r}, \quad (\text{D30})$$

where we have used the notation $b' = \begin{pmatrix} b'_r \\ b'_{q-r} \end{pmatrix}$. If it is true, one can construct all of the solutions of x' in Eq. (D28) and use them to obtain all x by using Eq. (D29).

In summary, to know whether Eq. (D21) has solution (x, n) ($x \in \mathbb{R}^p, n \in \mathbb{Z}^p$), we need to find the Hermite normal H of A ($UA = H$). First, denote the number of nonzero rows of H by r . The next step is to check whether the last $p - r$ elements of Ub are all 0 (mod 4). In practice, calculating the unimodular matrix U is very time consuming. We only need to find the Hermite normal form of the augmented matrix (A, b) . The original equation (D21) has the solution if and only if the element in the $(r + 1)$ -th row and $(q + 1)$ -th column of the Hermite normal form is 0 (mod 4).

We use SageMath [?] to calculate the Hermite normal form of the augmented matrix (A, b) with size $p \times (q + 1) = 2^{20} \times (2^{12} + 1)$. The rank of A is $r = 4035$, and the matrix element at the place $(r + 1, q + 1) = (4036, 4097)$ of the Hermite normal form is 4 (see Fig. 35). Therefore, the highly overdetermined Eq. (D20) indeed has solutions. We can use the solutions to construct the group structure of the general group super-cohomology solutions by Eq. (D17).

We further check to see that the first nonzero element in each row of the Hermite normal form of A is either 1 or 2. Thus, the solution x can be chosen to have elements in $\frac{1}{2}\mathbb{Z}$ (the equation has no solution if we restrict x in \mathbb{Z}^q). Also, the phase factor $e^{i\pi\theta}$ in ν_4^{tot} takes values in $\mathbb{Z}_8 \cong \{e^{in\pi/4} | n \in \mathbb{Z}\}$. This implies that the cohomology operation defined by the obstruction is in fact in \mathbb{Z}_8 rather than \mathbb{Z}_4 . This is a very interesting hierarchical structure: the obstruction in the special group super-cohomology has a \mathbb{Z}_2 phase factor that is the fermion sign, the Majorana fermion decoration gives a \mathbb{Z}_4 phase factor obstruction from the Kitaev chain (p -wave superconductor), and the Abelian group structure of general group super-cohomology theory takes value in \mathbb{Z}_8 .

- [1] Z.-C. Gu and X.-G. Wen, “Tensor-entanglement-filtering renormalization approach and symmetry-protected topological order,” *Phys. Rev. B* **80**, 155131 (2009).
- [2] Xie Chen, Zheng-Cheng Gu, Zheng-Xin Liu, and Xiao-Gang Wen, “Symmetry-protected topological orders in interacting bosonic systems,” *Science* **338**, 1604–1606 (2012).
- [3] X. Chen, Z.-C. Gu, Z.-X. Liu, and X.-G. Wen, “Symmetry protected topological orders and the group cohomology of their symmetry group,” *Phys. Rev. B* **87**, 155114 (2013).
- [4] M. Z. Hasan and C. L. Kane, “*Colloquium* : Topological insulators,” *Rev. Mod. Phys.* **82**, 3045–3067 (2010).
- [5] X.-L. Qi and S.-C. Zhang, “Topological insulators and superconductors,” *Rev. Mod. Phys.* **83**, 1057–1110 (2011).
- [6] Edward Witten, “Fermion path integrals and topological phases,” *Rev. Mod. Phys.* **88**, 035001 (2016).
- [7] F. D. M. Haldane, “Nonlinear field theory of large-spin heisenberg antiferromagnets: Semiclassically quantized solitons of the one-dimensional easy-axis néel state,” *Phys. Rev. Lett.* **50**, 1153–1156 (1983).
- [8] Xiao-Gang Wen, “Construction of bosonic symmetry-protected-trivial states and their topological invariants via $g \times so(\infty)$ nonlinear σ models,” *Phys. Rev. B* **91**, 205101 (2015).
- [9] A. Kapustin, “Symmetry Protected Topological Phases, Anomalies, and Cobordisms: Beyond Group Cohomology,” ArXiv e-prints (2014), [arXiv:1403.1467](https://arxiv.org/abs/1403.1467).
- [10] M. Levin and Z.-C. Gu, “Braiding statistics approach to symmetry-protected topological phases,” *Phys. Rev. B* **86**, 115109 (2012).
- [11] Meng Cheng and Zheng-Cheng Gu, “Topological response theory of abelian symmetry-protected topological phases in two dimensions,” *Phys. Rev. Lett.* **112**, 141602 (2014), [arXiv:1302.4803](https://arxiv.org/abs/1302.4803).
- [12] Chenjie Wang, Chien-Hung Lin, and Zheng-Cheng Gu, “Interacting fermionic symmetry-protected topological phases in two dimensions,” arXiv e-prints (2016), [arXiv:1610.08478](https://arxiv.org/abs/1610.08478).
- [13] C. Wang and M. Levin, “Braiding statistics of loop excitations in three dimensions,” *Phys. Rev. Lett.* **113**, 080403 (2014).
- [14] S. Jiang, A. Mesaros, and Y. Ran, “Generalized modular transformations in (3 + 1)D topologically ordered phases and triple linking invariant of loop braiding,” *Phys. Rev. X* **4**, 031048 (2014).
- [15] C. Wang and M. Levin, “Topological invariants for gauge theories and symmetry-protected topological phases,” *Phys. Rev. B* **91**, 165119 (2015).
- [16] J. C. Wang and X.-G. Wen, “Non-abelian string and particle braiding in topological order: Modular $SL(3, \mathbb{Z})$ representation and (3 + 1)-dimensional twisted gauge theory,” *Phys. Rev. B* **91**, 035134 (2015).
- [17] C.-H. Lin and M. Levin, “Loop braiding statistics in exactly soluble three-dimensional lattice models,” *Phys. Rev. B* **92**, 035115 (2015).
- [18] A. Vishwanath and T. Senthil, “Physics of three-dimensional bosonic topological insulators: Surface-deconfined criticality and quantized magnetoelectric effect,” *Phys. Rev. X* **3**, 011016 (2013).
- [19] C. Wang and T. Senthil, “Boson topological insulators: A window into highly entangled quantum phases,” *Phys. Rev. B* **87**, 235122 (2013).
- [20] X. Chen, F. J. Burnell, A. Vishwanath, and L. Fidkowski, “Anomalous symmetry fractionalization and surface topological order,” *Phys. Rev. X* **5**, 041013 (2015).
- [21] Chenjie Wang, Chien-Hung Lin, and Michael Levin, “Bulk-boundary correspondence for three-dimensional symmetry-

- protected topological phases,” *Phys. Rev. X* **6**, 021015 (2016).
- [22] P. Bonderson, C. Nayak, and X.-L. Qi, “A time-reversal invariant topological phase at the surface of a 3d topological insulator,” *Journal of Statistical Mechanics: Theory and Experiment* **2013**, P09016 (2013).
- [23] C. Wang, A. C. Potter, and T. Senthil, “Gapped symmetry preserving surface state for the electron topological insulator,” *Phys. Rev. B* **88**, 115137 (2013).
- [24] L. Fidkowski, X. Chen, and A. Vishwanath, “Non-abelian topological order on the surface of a 3d topological superconductor from an exactly solved model,” *Phys. Rev. X* **3**, 041016 (2013).
- [25] X. Chen, L. Fidkowski, and A. Vishwanath, “Symmetry enforced non-abelian topological order at the surface of a topological insulator,” *Phys. Rev. B* **89**, 165132 (2014).
- [26] Chong Wang and T. Senthil, “Interacting fermionic topological insulators/superconductors in three dimensions,” *Phys. Rev. B* **89**, 195124 (2014).
- [27] M. A. Metlitski, C. L. Kane, and M. P. A. Fisher, “Symmetry-respecting topologically ordered surface phase of three-dimensional electron topological insulators,” *Phys. Rev. B* **92**, 125111 (2015).
- [28] Xie Chen, Zheng-Cheng Gu, and Xiao-Gang Wen, “Local unitary transformation, long-range quantum entanglement, wave function renormalization, and topological order,” *Phys. Rev. B* **82**, 155138 (2010).
- [29] K. Walker and Z. Wang, “(3+1)-tqfts and topological insulators,” *Front. Phys.* **7**, 150 (2012).
- [30] F. J. Burnell, X. Chen, L. Fidkowski, and A. Vishwanath, “Exactly soluble model of a three-dimensional symmetry-protected topological phase of bosons with surface topological order,” *Phys. Rev. B* **90**, 245122 (2014).
- [31] A. P. Schnyder, S. Ryu, A. Furusaki, and A. W. W. Ludwig, “Classification of topological insulators and superconductors in three spatial dimensions,” *Phys. Rev. B* **78**, 195125 (2008).
- [32] A. Kitaev, “Periodic table for topological insulators and superconductors,” *AIP Conference Proceedings* **1134**, 22 (2009).
- [33] Lukasz Fidkowski and Alexei Kitaev, “Effects of interactions on the topological classification of free fermion systems,” *Phys. Rev. B* **81**, 134509 (2010).
- [34] X.-L. Qi, “A new class of (2+1)-dimensional topological superconductors with \mathbb{Z}_8 topological classification,” *New Journal of Physics* **15**, 065002 (2013).
- [35] H. Yao and S. Ryu, “Interaction effect on topological classification of superconductors in two dimensions,” *Phys. Rev. B* **88**, 064507 (2013).
- [36] S. Ryu and S.-C. Zhang, “Interacting topological phases and modular invariance,” *Phys. Rev. B* **85**, 245132 (2012).
- [37] Z.-C. Gu and M. Levin, “Effect of interactions on two-dimensional fermionic symmetry-protected topological phases with \mathbb{Z}_2 symmetry,” *Phys. Rev. B* **89**, 201113 (2014).
- [38] Yi-Zhuang You and Cenke Xu, “Symmetry-protected topological states of interacting fermions and bosons,” *Phys. Rev. B* **90**, 245120 (2014).
- [39] T. Morimoto, A. Furusaki, and C. Mudry, “Breakdown of the topological classification \mathbb{Z} for gapped phases of noninteracting fermions by quartic interactions,” *Phys. Rev. B* **92**, 125104 (2015).
- [40] Titus Neupert, Claudio Chamon, Christopher Mudry, and Ronny Thomale, “Wire deconstructionism of two-dimensional topological phases,” *Phys. Rev. B* **90**, 205101 (2014).
- [41] C. Wang, A. C. Potter, and T. Senthil, “Classification of Interacting Electronic Topological Insulators in Three Dimensions,” *Science* **343**, 629–631 (2014), arXiv:1306.3238.
- [42] Zheng-Cheng Gu and Xiao-Gang Wen, “Symmetry-protected topological orders for interacting fermions: Fermionic topological nonlinear σ models and a special group supercohomology theory,” *Phys. Rev. B* **90**, 115141 (2014).
- [43] X. Chen, Z.-C. Gu, and X.-G. Wen, “Classification of gapped symmetric phases in one-dimensional spin systems,” *Phys. Rev. B* **83**, 035107 (2011).
- [44] L. Fidkowski and A. Kitaev, “Topological phases of fermions in one dimension,” *Phys. Rev. B* **83**, 075103 (2011).
- [45] A. Kapustin, R. Thorngren, A. Turzillo, and Z. Wang, “Fermionic Symmetry Protected Topological Phases and Cobordisms,” arXiv e-prints (2014), arXiv:1406.7329.
- [46] D. S. Freed, “Short-range entanglement and invertible field theories,” arXiv e-prints (2014), arXiv:1406.7278.
- [47] Davide Gaiotto and Anton Kapustin, “Spin tqfts and fermionic phases of matter,” *International Journal of Modern Physics A* **31**, 1645044 (2016).
- [48] L. Bhardwaj, D. Gaiotto, and A. Kapustin, “State sum constructions of spin-TFTs and string net constructions of fermionic phases of matter,” ArXiv e-prints (2016), arXiv:1605.01640.
- [49] M. Barkeshli, P. Bonderson, M. Cheng, and Z. Wang, “Symmetry, Defects, and Gauging of Topological Phases,” ArXiv e-prints (2014), arXiv:1410.4540.
- [50] M. Cheng, Z. Bi, Y.-Z. You, and Z.-C. Gu, “Towards a Complete Classification of Symmetry-Protected Phases for Interacting Fermions in Two Dimensions,” arXiv e-prints (2015), arXiv:1501.01313.
- [51] Chenjie Wang, “Braiding statistics and classification of two-dimensional charge- $2m$ superconductors,” *Phys. Rev. B* **94**, 085130 (2016).
- [52] T. Lan, L. Kong, and X.-G. Wen, “Classification of 2+1D topological orders and SPT orders for bosonic and fermionic systems with on-site symmetries,” ArXiv e-prints (2016), arXiv:1602.05946.
- [53] Daniel S. Freed and Michael J. Hopkins, “Reflection positivity and invertible topological phases,” arXiv e-prints (2016), arXiv:1604.06527.
- [54] Greg Brumfiel and John Morgan, “The Pontrjagin Dual of 3-Dimensional Spin Bordism,” arXiv e-prints (2016), arXiv:1612.02860.
- [55] A Yu Kitaev, “Unpaired majorana fermions in quantum wires,” *Physics-Uspekhi* **44**, 131 (2001).
- [56] The fermion parity symmetry is gauged in such constructions.

- [57] M. A. Metlitski, L. Fidkowski, X. Chen, and A. Vishwanath, “Interaction effects on 3D topological superconductors: surface topological order from vortex condensation, the 16 fold way and fermionic Kramers doublets,” ArXiv e-prints (2014), [arXiv:1406.3032](https://arxiv.org/abs/1406.3032).
- [58] A. Kitaev, <http://www.ipam.ucla.edu/abstract/?tid=12389&pcode=STQ2015>.
- [59] R. Queiroz, E. Khalaf, and A. Stern, “Classification of interacting fermionic phases by dimensional reduction,” ArXiv e-prints (2016), [arXiv:1601.01596](https://arxiv.org/abs/1601.01596).
- [60] Pavel Putrov, Juven Wang, and Shing-Tung Yau, “Braiding Statistics and Link Invariants of Bosonic/Fermionic Topological Quantum Matter in 2+1 and 3+1 dimensions,” arXiv e-prints (2016), [arXiv:1612.09298](https://arxiv.org/abs/1612.09298).
- [61] M. Cheng, Z.-C. Gu, S. Jiang, and Y. Qi, “Exactly Solvable Models for Symmetry-Enriched Topological Phases,” ArXiv e-prints (2016), [arXiv:1606.08482](https://arxiv.org/abs/1606.08482).
- [62] C. Heinrich, F. Burnell, L. Fidkowski, and M. Levin, “Symmetry enriched string-nets: Exactly solvable models for SET phases,” ArXiv e-prints (2016), [arXiv:1606.07816](https://arxiv.org/abs/1606.07816).
- [63] Zheng-Cheng Gu, Zhenghan Wang, and Xiao-Gang Wen, “Classification of two-dimensional fermionic and bosonic topological orders,” *Phys. Rev. B* **91**, 125149 (2015).
- [64] P. W. Kasteleyn, “Dimer statistics and phase transitions,” *Journal of Mathematical Physics* **4**, 287–293 (1963).
- [65] David Cimasoni and Nicolai Reshetikhin, “Dimers on surface graphs and spin structures. i,” *Communications in Mathematical Physics* **275**, 187–208 (2007).
- [66] David Cimasoni and Nicolai Reshetikhin, “Dimers on Surface Graphs and Spin Structures. II,” *Communications in Mathematical Physics* **281**, 445–468 (2008).
- [67] Nicolas Tarantino and Lukasz Fidkowski, “Discrete spin structures and commuting projector models for two-dimensional fermionic symmetry-protected topological phases,” *Phys. Rev. B* **94**, 115115 (2016).
- [68] Brayden Ware, Jun Ho Son, Meng Cheng, Ryan V. Mishmash, Jason Alicea, and Bela Bauer, “Ising anyons in frustration-free majorana-dimer models,” *Phys. Rev. B* **94**, 115127 (2016).
- [69] Richard Z Goldstein and Edward C Turner, “A formula for Stiefel-Whitney homology classes,” *Proceedings of the American Mathematical Society* **58**, 339–339 (1976).
- [70] Note that the barycentric subdivision triangulation illustrated in Ref. 47 is a special case of this general construction of the Stiefel–Whitney homology class [69].
- [71] Udo Pachner, “P.l. homeomorphic manifolds are equivalent by elementary shellings,” *European Journal of Combinatorics* **12**, 129 – 145 (1991).
- [72] Francesco Costantino, “A calculus for branched spines of 3-manifolds,” *Mathematische Zeitschrift* **251**, 427–442 (2005).
- [73] If we choose the convention of pairing $\langle \bar{0}\bar{3} \rangle$ and $\langle \bar{1}\bar{2} \rangle$ of the four Majorana fermions at the center of tetrahedron $\langle 0123 \rangle$, all of the results are the same as those of the conventional $\langle \bar{0}\bar{2} \rangle$ and $\langle \bar{1}\bar{3} \rangle$ used in the main text of our paper. γ_{012A} and γ_{234B} can also be chosen consistently in the definition of X operators (see the discussion below Eq. (44)). The last choice of pairing $\langle \bar{0}\bar{1} \rangle$ and $\langle \bar{2}\bar{3} \rangle$ is different from the above two conventions because the Majorana fermion parity is changed when four Kitaev strings meet at one tetrahedron. However, we can shift the c fermion number $n_3(g_0, g_1, g_2, g_3)$ by one (mod 2) to absorb this fermion parity change and then obtain the same obstruction results.
- [74] N. E. Steenrod, “Products of cocycles and extensions of mappings,” *Annals of Mathematics* **48**, 290–320 (1947).
- [75] G. Brumfiel and J. Morgan, Unpublished.
- [76] Meng Cheng, Nathanan Tantivasadakarn, and Chenjie Wang, “Loop Braiding Statistics and Interacting Fermionic Symmetry-Protected Topological Phases in Three Dimensions,” ArXiv e-prints (2017), [arXiv:1705.08911](https://arxiv.org/abs/1705.08911).
- [77] A. Kapustin and R. Thorngren, “Fermionic SPT phases in higher dimensions and bosonization,” ArXiv e-prints (2017), [arXiv:1701.08264](https://arxiv.org/abs/1701.08264) [cond-mat.str-el].